

EXPERIMENTAL VERIFICATION OF  
BUILDUP REGION DOSE CALCULATION FOR  
A COMMERCIAL TREATMENT PLANNING SYSTEM

A Thesis Submitted to the College of  
Graduate Studies and Research  
In Partial Fulfillment of the Requirements  
For the Degree of Master of Science  
In the Department of Physics and Engineering Physics  
University of Saskatchewan  
Saskatoon

By

Bassey Ekpenyong Bassey

Keywords: Buildup region dose, Pinnacle<sup>3</sup>, Attix parallel plate ionization chamber

© Copyright Bassey Ekpenyong Bassey, June 2011. All rights reserved.

## **Permission to Use**

In presenting this thesis in partial fulfilment of the requirements for a Postgraduate degree from the University of Saskatchewan, I agree that the Libraries of this University may make it freely available for inspection. I further agree that permission for copying of this thesis in any manner, in whole or in part, for scholarly purposes may be granted by Dr. Narinder Sidhu or, in his absence, by the Head of the Department or the Dean of the College in which my thesis work was done. It is understood that any copying or publication or use of this thesis or parts thereof for financial gain shall not be allowed without my written permission. It is also understood that due recognition shall be given to me and to the University of Saskatchewan in any scholarly use which may be made of any material in my thesis.

Requests for permission to copy or to make other use of material in this thesis in whole or part should be addressed to:

Head of the Department of Physics and Engineering Physics

116 Science Place

University of Saskatchewan

Saskatoon, Saskatchewan

Canada

S7N 5E2

## **Abstract**

The purpose of this research was to verify experimentally the buildup region dose calculation for Pinnacle<sup>3</sup> (version 9.0), a commercial treatment planning system, commissioned and in use at the Saskatoon Cancer Center. To achieve this, buildup dose measurements using Attix parallel-plate ionization chamber and calculations by Pinnacle<sup>3</sup>, for a variety of clinical setups, were compared. The clinical setups involved 6 MV and 15 MV photon beams, open fields, enhanced dynamic wedges, physical wedges, block tray, 85, 100 and 120 cm source-to-surface distances (SSDs), and field sizes 3 x 3, 4 x 4, 5 x 5, 8 x 8, 10 x 10, 12 x 12, 15 x 15, 20 x 20, 30 x 30 cm<sup>2</sup>. The dose difference (DD) and distance-to-agreement (DTA) were used to evaluate the discrepancy between measured and calculated dose values. Significant discrepancies between measured and calculated buildup dose values were observed because the modeling in Pinnacle<sup>3</sup> is based on measurements made using a cylindrical ionization chamber. Based on the criteria of DD less than 2% or DTA less than 2 mm, 93.7% of 1,710 dose points for the 6 MV photon beam passed while for the 15 MV photon beam, 96.1% of the 2,244 dose points passed. The dose points that did not pass these criteria were mostly for open fields, block tray fields, fields with physical wedges of 15 degrees and 30 degrees and for fields with shorter source-to-surface distances. This is attributed to the high electron contamination associated with these fields. The low levels of discrepancies between measured and calculated dose values for the 15 MV beam as compared to those of the 6 MV beam need further investigations. The good agreement between measured and calculated dose values after remodeling the Electron Contamination in Pinnacle<sup>3</sup> based on Attix chamber measurements is an indication that the Electron Contamination equation in Pinnacle<sup>3</sup> may be adequate for modeling of electron contamination in the buildup dose region. The disagreement between Attix chamber and EBT 2 film measured buildup dose values was less than 3% for 89.9% of the buildup dose measurements compared. It is recommended to use a good parallel plate ionization chamber, such as the Attix chamber, for measurements in the buildup region.

## **Acknowledgements**

I am most thankful to my supervisor Dr. Narinder Sidhu, my sponsor Akwa Ibom State University, Nigeria, and the Department of Physics and Engineering Physics at the University of Saskatchewan, not just for the various forms of support offered to me, but also for offering me a second chance to pursue a postgraduate degree in Canada. I acknowledge Patrick Cadman of the Saskatoon Cancer for proof reading my thesis and for other forms of contribution of his to this research. For the help I got from Gavin Crammer-Sargison, Deluan Tu, Tracy Custer, Eileen Park-Sommers and other staff at the Saskatoon Cancer Center during the period of this research, I am thankful.

I appreciate Dr. Rob Pywell, a member of my Academic Advisory Committee for his contributions. I appreciate my friends Dr. Kerry Babcock, Samuel Udofia, Wilson Ogoh, Toks Bakinson, and Blessing Iserhienrhien for their supports to me. Also appreciated for their help are the Department Secretaries, Debbie Parker and Marj Granrude.

I acknowledge my academic father and mentor, Professor David Eka of the University of Uyo, Nigeria, for his supports. I acknowledge the encouragements and supports of my fellow Akwa Ibom State University colleagues, Samuel Hanson, Cletus Asuquo, Aniekan Williams and Ubong Peters.

I am very grateful to my mother and siblings for their prayers and financial supports. And lastly, I appreciate my wife Iniobong, and two daughters, Blessing and Ubokobong, without them, the completion of this research would not have been possible.

## Contents

Permission to Use .....	i
Abstract .....	ii
Acknowledgements .....	iii
Contents .....	iv
List of Tables .....	vi
List of Figures .....	x
List of Abbreviations .....	xiv
<b>1 Introduction</b>	<b>1</b>
1.1 Radiation Treatment Planning Process .....	1
1.2 Dose Buildup Region .....	2
1.3 Treatment Planning Systems .....	5
1.3.1 Pinnacle <sup>3</sup> Treatment Planning System .....	7
1.3.1.1 Collapsed Cone Convolution/Superposition Dose Algorithm ..	7
1.3.1.2 Pinnacle <sup>3</sup> Photon Beam Model Parameters .....	9
1.4 Radiation Treatment Accuracy .....	11
1.5 Motivation/Objectives .....	12
<b>2 Materials and Methods</b>	<b>14</b>
2.1 Linear Accelerator .....	14
2.2 Plane-Parallel Plate Ionization Chamber/Electrometer .....	16
2.3 GafChromic EBT 2 Film/EPSON Expression 10000 XL Colour Scanner ...	21
2.4 Solid Water Phantom .....	25
2.5 Clinical Setups .....	27

2.6	Measurements with Attix Plane Parallel-Parallel Ionization Chamber . . . . .	32
2.6.1	Corrections Applied to Readings . . . . .	35
2.6.1.1	Polarity Effect Correction . . . . .	35
2.6.1.2	Temperature and Pressure Corrections . . . . .	35
2.7	Measurements with GafChromic EBT 2 Film . . . . .	36
2.8	Remodeling of Electron Contamination Models in Pinnacle <sup>3</sup> . . . . .	41
2.9	Pinnacle <sup>3</sup> Treatment Planning System Calculations . . . . .	41
<b>3</b>	<b>Results and Discussions</b>	<b>42</b>
3.1	Results . . . . .	43
3.1.1	Validation Measurements using GafChromic EBT 2 Film . . . . .	43
3.1.2	Measured and Calculated Buildup Doses . . . . .	50
3.1.3	Analysis of Measured and Calculated Buildup Doses . . . . .	61
3.2	Discussions. . . . .	86
<b>4</b>	<b>Conclusions</b>	<b>90</b>
	<b>References</b>	<b>92</b>

## List of Tables

2.1	Specifications of Slabs of CTG Gammex Model 457 Solid Water Phantom . . . . .	27
2.2	Open Fields Clinical Setups . . . . .	29
2.3	Enhanced Dynamic Wedges Fields Clinical Setups . . . . .	29
2.4	Physical Wedges Fields Clinical Setups. . . . .	30
2.5	Block Tray Fields Clinical Setups . . . . .	31
3.1	Summary of the analysis of the results based on Venselaar et al. (2001) criteria for 6 MV x Open Fields . . . . .	62
3.2	Summary of the analysis of the results based on Venselaar et al. (2001) criteria for 6 MV x EDW (15°) Fields . . . . .	62
3.3	Summary of the analysis of the results based on Venselaar et al. (2001) criteria for 6 MV x EDW (60°) Fields . . . . .	62
3.4	Summary of the analysis of the results based on Venselaar et al. (2001) criteria for 6 MV x PW (15°) Fields . . . . .	63
3.5	Summary of the analysis of the results based on Venselaar et al. (2001) criteria for 6 MV x PW (30°) Fields . . . . .	63
3.6	Summary of the analysis of the results based on Venselaar et al. (2001) criteria for 6 MV x PW (45°) Fields . . . . .	63
3.7	Summary of the analysis of the results based on Venselaar et al. (2001) criteria for 6 MV x PW (60°) Fields . . . . .	63
3.8	Summary of the analysis of the results based on Venselaar et al. (2001) criteria for 6 MV x Block Tray Fields . . . . .	64
3.9	Summary of the analysis of the results based on Venselaar et al. (2001) criteria for 15 MV x Open Fields . . . . .	64
3.10	Summary of the analysis of the results based on Venselaar et al. (2001) criteria for 15 MV x EDW (15°) Fields . . . . .	64
3.11	Summary of the analysis of the results based on Venselaar et al. (2001) criteria for 15 MV x EDW (60°) Fields . . . . .	64

3.12	Summary of the analysis of the results based on Venselaar et al. (2001) criteria for 15 MV x PW (15°) Fields . . . . .	65
3.13	Summary of the analysis of the results based on Venselaar et al. (2001) criteria for 15 MV x PW (30°) Fields . . . . .	65
3.14	Summary of the analysis of the results based on Venselaar et al. (2001) criteria for 15 MV x PW (45°) Fields . . . . .	65
3.15	Summary of the analysis of the results based on Venselaar et al. (2001) criteria for 15 MV x PW (60°) Fields . . . . .	65
3.16	Summary of the analysis of the results based on Venselaar et al. (2001) criteria for 15 MV x Block Tray Fields . . . . .	66
3.17	Summary of the analysis of the results based on criteria of less than 2% or 2 mm for 6 MV x Open Fields . . . . .	67
3.18	Summary of the analysis of the results based on criteria of less than 2% or 2 mm for 6 MV x EDW (15°) Fields . . . . .	67
3.19	Summary of the analysis of the results based on criteria of less than 2% or 2 mm for 6 MV x EDW (60°) Fields . . . . .	68
3.20	Summary of the analysis of the results based on criteria of less than 2% or 2 mm for 6 MV x PW (15°) Fields . . . . .	68
3.21	Summary of the analysis of the results based on criteria of less than 2% or 2 mm for 6 MV x PW (30°) Fields . . . . .	68
3.22	Summary of the analysis of the results based on criteria of less than 2% or 2 mm for 6 MV x PW (45°) Fields . . . . .	68
3.23	Summary of the analysis of the results based on criteria of less than 2% or 2 mm for 6 MV x PW (60°) Fields . . . . .	69
3.24	Summary of the analysis of the results based on criteria of less than 2% or 2 mm for 6 MV x Block Tray Fields . . . . .	69
3.25	Summary of the analysis of the results based on criteria of less than 2% or 2 mm for 15 MV x Open Fields . . . . .	69
3.26	Summary of the analysis of the results based on criteria of less than 2% or 2 mm for 15 MV x EDW (15°) Fields . . . . .	69

3.27	Summary of the analysis of the results based on criteria of less than 2% or 2 mm for 15 MV x EDW (60°) Fields . . . . .	70
3.28	Summary of the analysis of the results based on criteria of less than 2% or 2 mm for 15 MV x PW (15°) Fields . . . . .	70
3.29	Summary of the analysis of the results based on criteria of less than 2% or 2 mm for 15 MV x PW (30°) Fields . . . . .	70
3.30	Summary of the analysis of the results based on criteria of less than 2% or 2 mm for 15 MV x PW (45°) Fields . . . . .	70
3.31	Summary of the analysis of the results based on criteria of less than 2% or 2 mm for 15 MV x PW (60°) Fields . . . . .	71
3.32	Summary of the analysis of the results based on criteria of less than 2% or 2 mm for 15 MV x Block Tray Fields . . . . .	71
3.33	Summary of the analysis of the results based on criteria of less than 2% or 2 mm for 6 MV x Open Fields after EC remodeling . . . . .	82
3.34	Summary of the analysis of the results based on criteria of less than 2% or 2 mm for 6 MV x EDW (15°) Fields after EC remodeling . . . . .	82
3.35	Summary of the analysis of the results based on criteria of less than 2% or 2 mm for 6 MV x EDW (60°) Fields after EC remodeling . . . . .	82
3.36	Summary of the analysis of the results based on criteria of less than 2% or 2 mm for 6 MV x PW (15°) Fields after EC remodeling . . . . .	82
3.37	Summary of the analysis of the results based on criteria of less than 2% or 2 mm for 6 MV x PW (30°) Fields after EC remodeling . . . . .	83
3.38	Summary of the analysis of the results based on criteria of less than 2% or 2 mm for 6 MV x PW (45°) Fields after EC remodeling . . . . .	83
3.39	Summary of the analysis of the results based on criteria of less than 2% or 2 mm for 6 MV x PW (60°) Fields after EC remodeling . . . . .	83
3.40	Summary of the analysis of the results based on criteria of less than 2% or 2 mm for 15 MV x Open Fields after EC remodeling . . . . .	83
3.41	Summary of the analysis of the results based on criteria of less than 2% or 2 mm for 15 MV x EDW (15°) Fields after EC remodeling . . . . .	84

3.42	Summary of the analysis of the results based on criteria of less than 2% or 2 mm for 15 MV x EDW (60°) Fields after EC remodeling . . . . .	84
3.43	Summary of the analysis of the results based on criteria of less than 2% or 2 mm for 15 MV x PW (15°) Fields after EC remodeling . . . . .	84
3.44	Summary of the analysis of the results based on criteria of less than 2% or 2 mm for 15 MV x PW (30°) Fields after EC remodeling . . . . .	84
3.45	Summary of the analysis of the results based on criteria of less than 2% or 2 mm for 15 MV x PW (45°) Fields after EC remodeling . . . . .	85
3.46	Summary of the analysis of the results based on criteria of less than 2% or 2 mm for 15 MV x PW (60°) Fields after EC remodeling . . . . .	85
3.47	Comparison of the analysis of the results based on criteria of less than 2% or 2 mm for 6 MV photon beam (simple geometry) before and after EC remodeling . . . . .	85
3.48	Comparison of the analysis of the results based on criteria of less than 2% or 2 mm for 6 MV photon beam (complex geometries) before and after EC remodeling . . . .	86
3.49	Comparison of the analysis of the results based on criteria of less than 2% or 2 mm for 15 MV photon beam (simple geometry) before and after EC remodeling . . . . .	86
3.50	Comparison of the analysis of the results based on criteria of less than 2% or 2 mm for 15 MV photon beam (complex geometries) before and after EC remodeling . . . .	86

## List of Figures

1.1	Megavoltage beam incident on a patient and dose distribution on the central axis of a megavoltage beam striking a patient . . . . .	4
2.1	Block diagram of the components of a clinical linac . . . . .	15
2.2	Cross-section showing the major components of Attix ionization chamber, Model RMI 449 . . . . .	20
2.3	Attix plane-parallel plate ion chamber fitted into the RMI 457 . . . . .	20
2.4	Configuration of GafChromic EBT 2 film . . . . .	23
2.5	Slabs of CTG Gammex Model 457 solid water phantom . . . . .	26
2.6	Physical wedges (Steel-angle 30° and Lead-angle 45°) . . . . .	28
2.7	Varian photon block tray . . . . .	29
2.8	Experimental setup for measurements using Attix plane-parallel plate ion chamber .	34
2.9	EBT 2 film calibration curve obtained using 6 MV photon beam . . . . .	39
2.10	EBT 2 film calibration curve obtained using 15 MV photon beam . . . . .	40
3.1	A comparison of EBT 2 film and Attix pp ion chamber RD graphs for 6 MV x 100 cm SSD x Open Field (10 x 10 cm <sup>2</sup> FS) . . . . .	44
3.2	A comparison of EBT 2 film and Attix pp ion chamber RD graphs for 6 MV x 100 cm SSD x EDW (15°) Field (15 x 15 cm <sup>2</sup> FS) . . . . .	45
3.3	A comparison of EBT 2 film and Attix pp ion chamber RD graphs for 6 MV x 100 cm SSD x EDW (60°) Field (15 x 15 cm <sup>2</sup> FS) . . . . .	45
3.4	A comparison of EBT 2 film and Attix pp ion chamber RD graphs for 6 MV x 100 cm SSD x PW (15°) Field (10 x 10 cm <sup>2</sup> FS) . . . . .	46
3.5	A comparison of EBT 2 film and Attix pp ion chamber RD graphs for 6 MV x 100 cm SSD x PW (60°) Field (10 x 10 cm <sup>2</sup> FS) . . . . .	46
3.6	A comparison of EBT 2 film and Attix pp ion chamber RD graphs for 6 MV x 100 cm SSD x Block Tray Field (10 x 10 cm <sup>2</sup> FS) . . . . .	47

3.7	A comparison of EBT 2 film and Attix pp ion chamber RD graphs for 15 MV x 100 cm SSD x Open Field (20 x 20 cm <sup>2</sup> FS) . . . . .	47
3.8	A comparison of EBT 2 film and Attix pp ion chamber RD graphs for 15 MV x 100 cm SSD x EDW (15°) Field (5 x 5 cm <sup>2</sup> FS) . . . . .	48
3.9	A comparison of EBT 2 film and Attix pp ion chamber RD graphs for 15 MV x 100 cm SSD x EDW (60°) Field (10 x 10 cm <sup>2</sup> FS) . . . . .	48
3.10	A comparison of EBT 2 film and Attix pp ion chamber RD graphs for 15 MV x 100 cm SSD x PW (15°) Field (15 x 15 cm <sup>2</sup> FS) . . . . .	49
3.11	A comparison of EBT 2 film and Attix pp ion chamber RD graphs for 15 MV x 100 cm SSD x PW (60°) Field (15 x 15 cm <sup>2</sup> FS) . . . . .	49
3.12	A comparison of EBT 2 film and Attix pp ion chamber RD graphs for 15 MV x 100 cm SSD x Block Tray Field (10 x 10 cm <sup>2</sup> FS) . . . . .	50
3.13	RD graphs for 6 MV x 85 cm SSD x Open Field (10 x 10 cm <sup>2</sup> FS) . . . . .	51
3.14	RD graphs for 6 MV x 100 cm SSD x Open Field (10 x 10 cm <sup>2</sup> FS) . . . . .	52
3.15	RD graphs for 6 MV x 120 cm SSD x Open Field (10 x 10 cm <sup>2</sup> FS) . . . . .	52
3.16	RD graphs for 6 MV x 100 cm SSD x EDW (15°) Field (15 x 15 cm <sup>2</sup> FS) . . . . .	53
3.17	RD graphs for 6 MV x 100 cm SSD x EDW (60°) Field (10 x 10 cm <sup>2</sup> FS) . . . . .	53
3.18	RD graphs for 6 MV x 100 cm SSD x PW (15°) Field (10 x 10 cm <sup>2</sup> FS) . . . . .	54
3.19	RD graphs for 6 MV x 100 cm SSD x PW (30°) Field (5 x 5 cm <sup>2</sup> FS) . . . . .	54
3.20	RD graphs for 6 MV x 100 cm SSD x PW (45°) Field (12 x 12 cm <sup>2</sup> FS) . . . . .	55
3.21	RD graphs for 6 MV x 100 cm SSD x PW (60°) Field (10 x 10 cm <sup>2</sup> FS) . . . . .	55
3.22	RD graphs for 6 MV x 100 cm SSD x Block Tray Field (10 x 10 cm <sup>2</sup> FS) . . . . .	56
3.23	RD graphs for 15 MV x 85 cm SSD x Open Field (10 x 10 cm <sup>2</sup> FS) . . . . .	56
3.24	RD graphs for 15 MV x 100 cm SSD x Open Field (10 x 10 cm <sup>2</sup> FS) . . . . .	57
3.25	RD graphs for 15 MV x 120 cm SSD x Open Field (10 x 10 cm <sup>2</sup> FS) . . . . .	57

3.26	RD graphs for 15 MV x 100 cm SSD x EDW (15°) Field (15 x 15 cm <sup>2</sup> FS) . . . . .	58
3.27	RD graphs for 15 MV x 100 cm SSD x EDW (60°) Field (10 x 10 cm <sup>2</sup> FS) . . . . .	58
3.28	RD graphs for 15 MV x 100 cm SSD x PW (15°) Field (10 x 10 cm <sup>2</sup> FS) . . . . .	59
3.29	RD graphs for 15 MV x 100 cm SSD x PW (30°) Field (5 x 5 cm <sup>2</sup> FS) . . . . .	59
3.30	RD graphs for 15 MV x 100 cm SSD x PW (45°) Field (12 x 12 cm <sup>2</sup> FS) . . . . .	60
3.31	RD graphs for 15 MV x 100 cm SSD x PW (60°) Field (10 x 10 cm <sup>2</sup> FS) . . . . .	60
3.32	RD graphs for 15 MV x 100 cm SSD x Block Tray Field (10 x 10 cm <sup>2</sup> FS) . . . . .	61
3.33	RD graphs for 6 MV x 85 cm SSD x Open Field (10 x 10 cm <sup>2</sup> FS) after EC remodeling . . . . .	73
3.34	RD graphs for 6 MV x 100 cm SSD x Open Field (10 x 10 cm <sup>2</sup> FS) after EC remodeling . . . . .	73
3.35	RD graphs for 6 MV x 120 cm SSD x Open Field (10 x 10 cm <sup>2</sup> FS) after EC remodeling . . . . .	74
3.36	RD graphs for 6 MV x 100 cm SSD x EDW (15°) Field (15 x 15 cm <sup>2</sup> FS) after EC remodeling . . . . .	74
3.37	RD graphs for 6 MV x 100 cm SSD x EDW (60°) Field (10 x 10 cm <sup>2</sup> FS) after EC remodeling . . . . .	75
3.38	RD graphs for 6 MV x 100 cm SSD x PW (15°) Field (10 x 10 cm <sup>2</sup> FS) after EC remodeling . . . . .	75
3.39	RD graphs for 6 MV x 100 cm SSD x PW (30°) Field (5 x 5 cm <sup>2</sup> FS) after EC remodeling . . . . .	76
3.40	RD graphs for 6 MV x 100 cm SSD x PW (45°) Field (12 x 12 cm <sup>2</sup> FS) after EC remodeling . . . . .	76
3.41	RD graphs for 6 MV x 100 cm SSD x PW (60°) Field (10 x 10 cm <sup>2</sup> FS) after EC remodeling . . . . .	77
3.42	RD graphs for 15 MV x 85 cm SSD x Open Field (10 x 10 cm <sup>2</sup> FS) after EC remodeling . . . . .	77

3.43	RD graphs for 15 MV x 100 cm SSD x Open Field (10 x 10 cm <sup>2</sup> FS) after EC remodeling . . . . .	78
3.44	RD graphs for 15 MV x 120 cm SSD x Open Field (10 x 10 cm <sup>2</sup> FS) after EC remodeling . . . . .	78
3.45	RD graphs for 15 MV x 100 cm SSD x EDW (15°) Field (15 x 15 cm <sup>2</sup> FS) after EC remodeling . . . . .	79
3.46	RD graphs for 15 MV x 100 cm SSD x EDW (60°) Field (10 x 10 cm <sup>2</sup> FS) after EC remodeling . . . . .	79
3.47	RD graphs for 15 MV x 100 cm SSD x PW (15°) Field (10 x 10 cm <sup>2</sup> FS) after EC remodeling . . . . .	80
3.48	RD graphs for 15 MV x 100 cm SSD x PW (30°) Field (5 x 5 cm <sup>2</sup> FS) after EC remodeling . . . . .	80
3.49	RD graphs for 15 MV x 100 cm SSD x PW (45°) Field (12 x 12 cm <sup>2</sup> FS) after EC remodeling . . . . .	81
3.50	RD graphs for 15 MV x 100 cm SSD x PW (60°) Field (10 x 10 cm <sup>2</sup> FS) after EC remodeling . . . . .	81

## List of Abbreviations

AAPM	The American Association of Physicists in Medicine
CT	Computed Tomography
CTG	Certified Therapy Grade
DC	Direct Current
DD	Dose-Difference
$D_{\max}$	Depth of maximum dose
DTA	Distance-To-Agreement
EC	Electron Contamination
EDW	Enhanced Dynamic Wedge
Exp	Experiment
FS	Field Size
ICRU	International Commission on Radiation Units and Measurements
ISP	International Specialty Products
MRI	Magnetic Resonance Imaging
MU	Monitor Units
MV	Megavoltage
OD	Optical Density
P3	Pinnacle <sup>3</sup>
PET	Positron Emission Tomography
PP	Parallel Plate
PW	Physical Wedge
RD	Relative Dose
RMI	Radiation Measurement Instrument
ROI	Region of Interest
SD	Standard Deviation
SSD	Source to Surface Distance
TERMA	Total Energy Released per unit Mass
TPS	Treatment Planning System

# Chapter 1

## Introduction

### 1.1 Radiation Treatment Planning Process

The radiation treatment planning process, a complex series of interwoven procedures involving the efforts of many departmental personnel, is instrumental in accomplishing the goal of radiation therapy treatment of cancer - to cure, locally control, or palliate the disease while minimizing complications in normal tissues (Fraass et al., 1998). The treatment planning process encompasses all of the steps involved in planning a patient's treatment (Fraass et al., 1998).

1. *First Step-Patient positioning and immobilization:* This involves the determination of optimum patient position for treatment and the construction of immobilization devices necessary to maintain the patient in that position during treatment.
2. *Second Step-Localization or Simulation:* This involves the use of special equipment [e.g., simulators, computed tomography (CT) simulators or positron emission tomography (PET)/magnetic resonance imaging (MRI) scanners] to determine the size, extent, and location of the patient's tumor (target volume), and its relationship with normal organs and external surface anatomy.
3. *Third Step-Dose Planning:* This step begins only at the completion of the first and second steps; it is performed using a treatment planning system (TPS). This step involves entering of the patient's anatomical information and any treatment field information obtained during simulation into the TPS, performing of the field design, calculation and optimization of the dose distribution within the patient by the treatment planner, evaluation of the final treatment plan by a radiation oncology physicist, and approval of the evaluated treatment plan by the radiation oncologist.

4. *Fourth /Last Step-Plan Verification:* This involves checking the accuracy of the planned treatment before treatment delivery. During this step, the patient may be required to undergo additional procedures including a “plan verification” simulation or “setup” (treatment simulation on the treatment machine).

## **1.2 Dose Buildup Region**

In radiation therapy, high-energy photon (megavoltage photon) beams are used. When photons interact with atoms in the patient or phantom, the energy of the photons is transferred to the patient or phantom. There are two steps involved in the energy transfer (Khan, 2010):

1. high-speed electrons, termed secondary electrons, are liberated from the atoms in the patient or phantom;
2. liberated high-speed secondary electrons transfer their energy to the patient by ionizing and exciting atoms along their path in the patient. The energy transferred to the patient through the ionization and excitation of atoms in the patient is called the absorbed dose.

As the photon beam travels through the patient, it is being attenuated and thus, the number of secondary electrons set into motion in the patient, that is, charged particle fluence and hence the absorbed dose, first increases and then decreases with depth. The secondary electrons set into motion travel a definite distance (range) before transferring all their energy to the patient; the range of the secondary electrons set into motion by high energy photon beams does not change appreciably with depth in the patient (Podgorsak, 2005). At a certain depth in the patient, the number of secondary electrons stopping per unit mass equals the number of secondary electrons set into motion by photons; this condition is termed electronic equilibrium (charged particle

equilibrium). The maximum energy transferred by the secondary electrons to the patient (maximum dose) occurs at this depth, the depth at which charged particle equilibrium is reached; this depth is referred to as depth of maximum dose,  $z_{\max}$  (or  $D_{\max}$ ). Beyond  $z_{\max}$ , the energy transferred decreases gradually as the effects of attenuation and increased distance reduce the supply of photons that set the secondary electrons in motion (Bentel, 1996). The region between the surface of the patient and  $z_{\max}$  is known as the dose buildup region. Charged particle equilibrium does not exist in this region (Podgorsak, 2005). The dose buildup effect of the high energy photon beams (megavoltage photon beams) give rise to what is clinically known as the skin-sparing-effect because the surface dose (i.e., dose to the skin surface) is generally much lower than the maximum dose, which is beneath the skin surface (Podgorsak, 2005; Khan, 2010).

The sources of the buildup dose are complex and machine configuration dependent, they include the primary photon beam, backscattered radiation from the patient, and contaminating electrons, which are primarily derived from the electrons originating from interactions between the primary photons and parts of the accelerator head and the air volume downstream to the patient (Hsu et al., 2010). The contaminating electrons reduce the skin-sparing-effect (Adams & Hounsell, 1995).

A typical dose distribution (energy distribution) on the central axis of a megavoltage photon beam striking a patient is as shown on Fig. 1.1. The beam enters the patient on the surface, where it delivers a certain surface dose  $D_s$ . Beneath the surface the dose first rises rapidly, reaches a maximum value at depth  $z_{\max}$  and then decreases exponentially until it reaches a value  $D_{\text{ex}}$  at the patient's exit point; the slight downwards curving of the dose distribution close to the beam exit

point is attributed to the missing scatter contribution at the exit point from points beyond the exit dose point (Podgorsak, 2005).

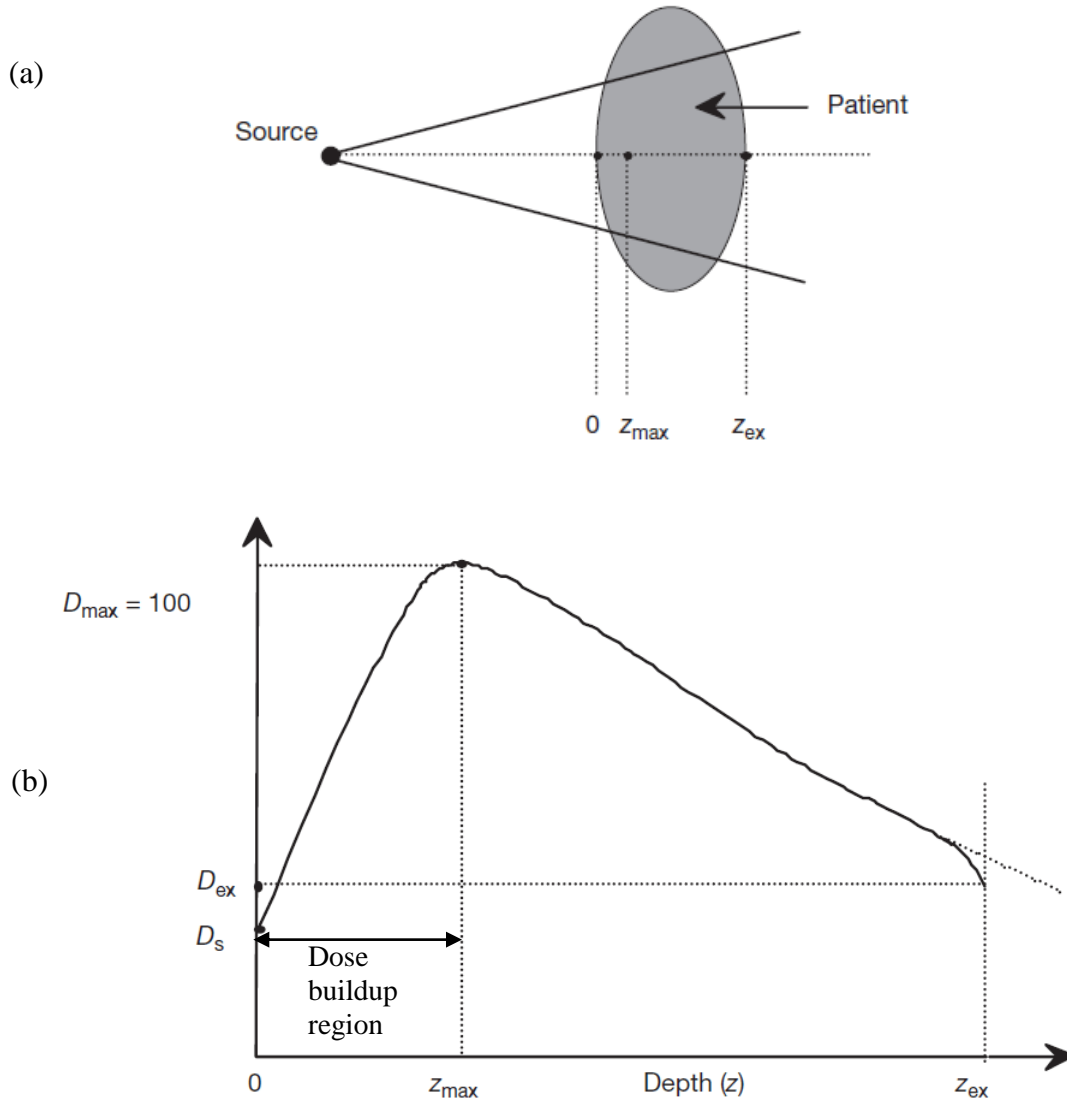


Figure 1.1: (a) Megavoltage beam incident on a patient, (b) Dose distribution on the central axis of a megavoltage beam striking a patient.

As shown in Fig. 1.1, the dose at the surface of the patient (i.e., skin surface),  $D_s$  is not zero.

What contributes dose to the surface of the patient are: photons scattered from the collimators,

flattening filter and air; photons backscattered from the patient; high energy electrons produced by photon interactions in the air and any shielding structures in the vicinity of the patient.

Accurate calculation of the absorbed dose in the buildup region is of major importance in radiation therapy, particularly when the target volume has superficial extension close to the skin as in the case of breast or head and neck cancer treatments. In these treatments, the accuracy of dose distributions calculated by a TPS in the buildup region has to be assessed in order to provide adequate superficial tumour coverage and to avoid potential skin toxicity (Panettieri et al., 2009). It is important to verify dose calculations in order to carry out optimal radiation therapy (Bäck et al., 1998).

### **1.3 Treatment Planning Systems**

Treatment planning systems (TPSs), which are considered as an indispensable tool for radiation treatment planning (IAEA, 2007) , are used in external beam radiation therapy to generate beam shapes and dose distribution with the intent to maximize tumour control and minimize normal tissue complications (Podgorsak, 2005). A TPS is made up of a computer, input and output devices, and software. The functionality and quality of any TPS is dependent on the type of algorithms used in the different steps of the treatment planning process (IAEA, 2004). Dose calculation algorithms play a crucial role in modern TPSs (Hasenbalg et al., 2007).

Commercially available TPSs employ different dose calculations algorithms, such as the pencil beam convolution/superposition, the collapsed cone convolution/superposition and the anisotropic analytical algorithm. Some examples of TPS that are available commercially are: Oncentra MasterPlan (Nucletron BV, Veenendal, Netherlands), PrecisePlan (Elekta AB,

Stockholm, Sweden), CORVUS (Nomos Corp., Pittsburg, Pennsylvania, USA), Eclipse 1 and 2 (Varian Medical Systems Inc., Palo Alto, California, USA), and Pinnacle<sup>3</sup> (Philips Radiation Oncology Systems, Milpitas, California, USA). This study involves version 9.0 of Pinnacle<sup>3</sup>.

Early TPSs dose calculation algorithms were based on a simple tabular representation of the dose distribution that was obtained directly from beam measurements but most calculation models now in use are physically based models rather than measurement based, with the most advanced current physically based models based on the Monte Carlo approach, in which the histories of many millions of particles are traced as they interact with matter using basic physics interactions (Animesh, 2005). Due to limitations of computer speed, the Monte Carlo based algorithms are not yet practical for clinical treatment planning systems.

A TPS has to be commissioned before it is put into use clinically. The commissioning process is the preparation of TPS for clinical use and generally involves (Venselaar & Welleweerd, 2001):

1. entering basic beam data (for modeling of the beam) into the TPS according to the methods and requirements described in the user's manual of the TPS; and
2. comparing the results of dose calculations with the entered basic beam data that were measured specifically for this purpose and adjusting modeling parameters if necessary.

The differences between calculated and actual dose values that may exist are attributed partly to the uncertainties in the measured data, and partly to imperfect beam modeling. Criteria for acceptability have to be applied before accepting a TPS for clinical use.

### **1.3.1 Pinnacle<sup>3</sup> Treatment Planning System**

Pinnacle<sup>3</sup> TPS (Philips Radiation Oncology Systems, Milpitas, California) is a commercially available TPS that uses the collapsed cone convolution/superposition dose algorithm (a photon dose algorithm) to determine the dose distribution in patients from external photon beams (Cadman et al., 2005; Starkschall et al., 2000). The dose algorithm used by Pinnacle<sup>3</sup> has undergone several studies (Cadman et al., 2005; Lydon, 1998; Ramsey et al., 1999; Guan et al., 2010; Baird et al., 2001).

#### **1.3.1.1 Collapsed Cone Convolution/Superposition Dose Algorithm**

The collapsed cone convolution/superposition photon dose algorithm is based on the convolution algorithm, which was introduced by Makie et al., and extended by Papanikolaou et al. to polyenergetic spectra (Starkschall et al., 2000). The convolution is facilitated by the introduction of the collapsed cone approximation. In this approximation, all energy released into coaxial cones of equal solid angle, from volume elements on the cone axis, is rectilinearly transported, attenuated, and deposited in elements of the axis (Ahnesjö, 1989). This algorithm accomplishes the dose computation process by first computing the distribution of the total energy released per unit mass (TERMA) in the patient due to photons generated in the accelerator and then convolving the TERMA distribution with energy deposition kernels (convolution kernels) that account for transportation of charged particles and scattered photons generated in the patient. This TERMA includes contributions from primary photons coming out of the target as well as scattered photons from the field flattening filter and primary collimator (Ramsey et al., 1999).

The energy deposition kernels, which describe the distribution of dose around a single photon site in a homogenous medium, are obtained using Monte Carlo methods that model primary

photon interactions and subsequent secondary photons as well as the resulting charged particles. The energy deposition kernels also take into account charged particle transport that allows accumulation and storage information used to compute dose in electronic disequilibrium regions. For heterogeneous calculations, superposition is used to approximate the true kernels by scaling the homogeneous kernels according to the radiological path length between the primary interaction site and the dose deposition site (Ramsey et al., 1999).

Accordingly, the dose that is absorbed at a point  $\mathbf{r}$  in a homogeneous medium, denoted as  $D(\mathbf{r})$ , is given by:

$$D(\mathbf{r}) = \int \frac{\mu}{\rho}(\mathbf{r}') \cdot \Psi(\mathbf{r}') \cdot K(\mathbf{r} - \mathbf{r}') d^3\mathbf{r}' \quad (1.1)$$

where  $\mu/\rho$  is the mass attenuation coefficient (fraction of energy removed from primary photon energy fluence per unit mass) at position  $\mathbf{r}'$ ,  $\Psi(\mathbf{r}')$  is the energy fluence spectrum at position  $\mathbf{r}'$ , and  $K(\mathbf{r} - \mathbf{r}')$  is the convolution kernel, which gives the fraction of TERMA from a primary interaction point that is deposited to surrounding points. In equation (1.1) above, TERMA, denoted as  $T(\mathbf{r}')$  is:

$$T(\mathbf{r}') = \frac{\mu}{\rho}(\mathbf{r}') \cdot \Psi(\mathbf{r}') \quad (1.2)$$

In a heterogeneous medium, the convolution equation, that is, equation (1.1) above is modified for actual radiological path length to account for heterogeneities. In this case, the dose  $D(\mathbf{r})$  is given by:

$$D(\mathbf{r}) = \int \frac{\mu}{\rho}(\rho_{\mathbf{r}'} \cdot \mathbf{r}') \cdot \Psi(\rho_{\mathbf{r}'} \cdot \mathbf{r}') \cdot K(\rho_{\mathbf{r}-\mathbf{r}'} \cdot (\mathbf{r} - \mathbf{r}')) d^3\mathbf{r}' \quad (1.3)$$

In a summary, the collapsed cone convolution/superposition algorithm used in Pinnacle<sup>3</sup> TPS consists of three parts (Cadman et al., 2005):

1. creation of an incident energy fluence map for a beam,
2. computation of a 3D (3 dimensional) total energy released per unit mass (TERMA) grid by projecting the incident energy fluence through the patient representation, and
3. superposition of the TERMA with a dose deposition kernel to compute dose in the patient.

### **1.3.1.2 Pinnacle<sup>3</sup> Photon Beam Model Parameters**

The Pinnacle<sup>3</sup> photon beam model parameters characterize the radiation exiting the head of the linear accelerator. These parameters, which are as summarized as follows (Starkschall et al., 2000), are generated from measured data using either Monte Carlo techniques combined with manual adjustments or using the automatic modeling procedure included with Pinnacle<sup>3</sup> (Bedford et al., 2003):

1. a discrete energy spectrum consisting of a set of energies and corresponding relative photon fluences, which are described by relative weights at each energy;
2. a factor,  $S$ , that models off-axis beam softening;
3. a cone angle and a cone radius for modeling off-axis changes in the in-air photon fluence;
4. a transmission factor for photon fluence through the collimators;
5. the height and width of the Gaussian distribution of scatter from the flattening filter;
6. a measure, MSF(Modifier Scatter Factor), of the scatter from the beam modifiers;
7. the dimensions of the photon source; and
8. a set of parameters ( $d_m$ ,  $K$ ,  $SF$ ,  $DF$ ,  $A$ ,  $C_1$ ,  $C_2$ , and  $C_3$ ) that model the electron contamination using the following equation:

$$D_e(r, d; fs) = F_D(d; fs)F_{OA}(r) \quad (1.4)$$

where  $F_D(d; fs)$  is the depth-dependent factor and  $F_{OA}(r)$  is the off-axis factor. The depth-dependent factor is given by

$$\begin{aligned} F_D(d; fs) &= \frac{F_{fs}(fs)}{SF} \frac{e^{-Kd} - e^{-Kd_m}}{1 - e^{-Kd_m}}, \quad d > DFd_m \\ &= F_{fs}(fs) \left[ 1 + \frac{SF - e^{-KDFd_m} + (1-SF)e^{-Kd_m}}{SF(1 - e^{-Kd_m})DFd_m} d \right], \quad d < DFd_m \\ &= 0, \quad d > d_m \end{aligned} \quad (1.5)$$

The off-axis factor is given by

$$F_{OA}(r) = e^{-A\theta^2} \quad (1.6)$$

where  $\theta$  is the angle defined by the central axis and the ray line passing through the point at off-axis distance  $r$ . In Eq. (1.5), the field-size dependent dose  $F_{fs}(fs)$  is given by the expression

$$F_{fs}(fs) = F(10 \times 10) + C_1(fs - 10) + C_2(e^{-10C_3} - e^{-fsC_3}) \quad (1.7)$$

where  $F(10 \times 10)$  is the surface dose for a 10 cm x 10 cm field.

$d_m$ , a maximum depth of electron contamination [Eq. (1.5)],

$K$ , a factor that describes steepness of the exponential depth dose of electron contamination [Eq. (1.5)],

$SF$ , a factor modifying the surface dose [Eq. (1.5)],

$DF$ , a depth at which the electron contamination curve becomes linear [Eq. (1.5)],

$A$ , a factor that measures the rapidity at which the off-axis component of the electron contamination goes to zero [Eq. (1.6)],

$C_1$ ,  $C_2$ , and  $C_3$  are parameters that alter the field-size dependence of the electron contamination [Eq. (1.7)].

## 1.4 Radiation Treatment Accuracy

It is the recommendation of the International Commission on Radiation Units and Measurements (ICRU) that radiation dose be delivered to within 5% of the prescribed dose. This requires that the uncertainty in each individual step in the treatment process (including treatment planning) be significantly less than the quoted 5% (Fraass et al., 1998). In the buildup region, the criteria for acceptability of photon beam dose calculation of TPS, as proposed by Venselaar et al. (analogous to that of Van Dyk et al. and the report of AAPM Task Group 53) are (Venselaar et al., 2001):

1. For homogeneous, simple geometry: 2 mm or 10%
2. For complex geometry (wedge, inhomogeneity, asymmetry): 3 mm or 15%
3. For more complex geometries, i.e., combinations of (2): 3 mm or 15%

The criteria above are based on the deviations,  $\delta$ , between results of TPS calculations and measurements. Deviations expressed in percent (%) are based on the dose-difference technique:

$$\delta = \frac{D_{\text{calculated}} - D_{\text{measured}}}{D_{\text{measured}}} \times 100\% \quad (1.4)$$

Deviations expressed in millimeters (mm) are based on the distance-to-agreement (DTA) distribution technique. The DTA is the distance between a measured data point and the nearest point in the calculated dose distribution that exhibits the same dose (Low et al., 1998).

The requirements for achieving accurate dose calculations have resulted in TPSs utilizing dose calculations based on convolution techniques (Weber & Nilsson, 2002) where the deposition of primary energy is convolved with a poly-energetic point spread function or kernel that describes the energy spread of secondary particles and accounts for the lateral transport of energy in the

medium (Hasenbalg et al., 2007). The accuracy of TPS dose calculations for external beam photon therapy has been the subject of extensive review (Gershkevitch et al., 2009).

Due to the complex nature of dose distribution in the buildup region (partly due to electron contamination and low-energy scattered photons from the treatment head of the accelerator), most dose calculation algorithms are not able to predict the dose in the buildup region accurately. Convolution based models are used to calculate the dose in the buildup region but the predicting power of the convolution based models is limited when predicting dose in the buildup region accurately for a wide variety of clinical situations such as variation in source to surface distance (SSD), beam shape, wedge filter and tray. It has been reported that dose computation algorithms of commercial TPS are not able to predict buildup dose to a high degree of accuracy and even Monte Carlo algorithms may fail to determine the dose in the buildup region correctly (Paelinck et al., 2005). It is the responsibility of the radiation oncology physicist to determine the accuracy of the institution's TPS for a range of clinical situations; and how the expectation of the accuracy must be modified to account for any particular clinical situations, the kinds of treatment plans that are created, and other aspects of the local situation (Fraass et al., 1998).

## **1.5 Motivation/Objectives**

Pinnacle<sup>3</sup> TPS is the TPS that is currently used at the Saskatoon Cancer Center. Court et al. (2008) in their research reported that the skin dose calculated by one of the known available commercial TPS, Eclipse, and those measured experimentally by Metal-Oxide-Semiconductor Field-Effect Transistor (MOSFET) in hemispheric phantoms was within  $\pm 20\%$  for 95% of all measured points. According to Roland et al. (2008), the inaccuracy of TPS in estimating the dose to the skin or surface dose region has been the subject of several studies. Since the skin

constitutes a part of dose buildup region, the above two reports motivated the undertaking of this research with the following objectives:

1. Verifying experimentally the buildup region dose calculation for Pinnacle<sup>3</sup> TPS for a variety of clinical setups. These clinical setups involve:
  - (a) 6 Megavoltage (MV) and 15 Megavoltage (MV) photon beams
  - (b) Source to surface distance-SSD (cm): 85, 100 and 120
  - (c) Square field size (cm<sup>2</sup>): 3 x 3, 4 x 4, 5 x 5, 8 x 8, 10 x 10, 12 x 12, 15 x 15, 20 x 20, and 30 x 30
  - (d) Open field
  - (e) Block tray
  - (f) Physical wedge-PW (degrees): 15, 30, 45 and 60
  - (g) Enhanced dynamic wedge-EDW (degrees): 15 and 60
2. Deciding whether or not the modeling in Pinnacle<sup>3</sup> should be improved upon. This will depend on the level of the discrepancies between the measured and the calculated dose in the buildup region.

## Chapter 2

### Materials and Methods

#### 2.1 Linear Accelerator

A linear accelerator (linac) is a machine in which charged particles (electrons, protons or heavy ions) are accelerated to high energies through a linear tube using high-frequency (radio frequency-RF) electromagnetic waves (Khan, 2010). In a linac, the accelerated charged particles travel along a straight line; hence the use of the word “linear” to describe the accelerator (Jayaraman & Lanzl, 2004).

There are different types of accelerator designs, but the ones used in radiation therapy (Clinical or Medical linac) accelerate electrons to kinetic energies from 4 to 25 MeV using either traveling or stationary electromagnetic waves of frequency in the microwave region, that is, microwave RF fields in the frequency range from  $10^3$  MHz to  $10^4$  MHz (Khan, 2010; Podgorsak, 2005). The difference between traveling wave and stationary wave accelerators is attributed to the design of the accelerator structure (Khan, 2010).

A block diagram of the various sections of a clinical linac is as shown in Figure 2.1 (Jayaraman & Lanzl, 2004). A power supply provides the required direct current (DC) power to the modulator. High-voltage pulses generated by the modulator then trigger both the electron gun (source of electrons) and a microwave oscillator (magnetron or klystron). Pulsed microwaves from the microwave oscillator are injected into the accelerator tube through a waveguide system. The pulsed microwaves injected to the accelerator tube create electromagnetic fields, which interact with the electrons that are also injected (with an initial energy of about 50 keV) into the

accelerator tube (Khan, 2010). The electrons are then accelerated through the accelerator tube as a result of energy transfer from the electromagnetic fields of the microwaves to the electrons. The high energy electron beam produced, which is in the form of a pencil beam, can either be allowed to proceed straight on and strike a target or bent through a suitable angle (usually about 90 or 270 degrees) to strike a target for x-ray production. The high energy electron beam produced, instead of being made to strike a target for production of x-rays, can be spread out using either a scattering foil or a magnetic field to produce a clinically useful electron beam. Some clinical linacs provide x-rays only in the low megavoltage range (4 or 6 MV), while others provide both x-rays and electrons at various megavoltage energies (Podgorsak, 2005).

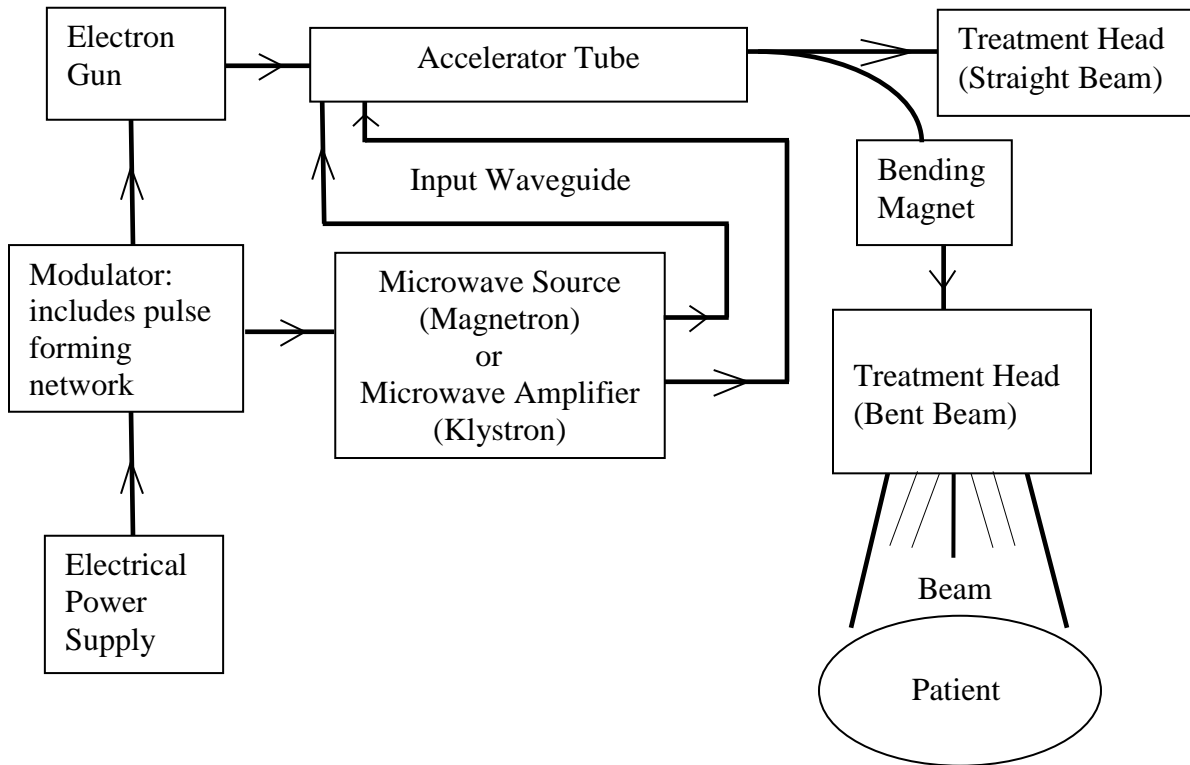


Figure 2.1: Block diagram of the components of a clinical linac.

In this research, 6 Megavoltage (6 MV) and 15 Megavoltage (15 MV) photon beams are used. These beams are produced by the dual energy (6 MV and 15 MV) Clinac 21 EX (Varian Medical Systems Inc., Palo Alto, California) linear accelerator.

## **2.2 Plane-Parallel Plate Ionization Chamber/Electrometer**

Generally, an ionization chamber (ion chamber) is a gas-filled detector used for the detection or measurement of ionizing radiation. It contains two conducting electrodes-positive and negative electrodes. The electrodes may be in the form of parallel plates (Parallel Plate Ion Chamber) or coaxial cylinders (Cylindrical Ion Chamber); in some ion chambers the walls of the chambers serve as one of the electrodes.

When an ionizing radiation is incident on an ion chamber, the gas between the electrodes becomes ionized. The resulting ions and dissociated electrons move to the electrodes of opposite polarity creating ionization current, which may be measured by an electrometer. An electrometer (a device for measuring small currents, of the order of  $10^{-9}$  Amperes or less) when used in conjunction with an ionization chamber is a high gain, negative feedback, operational amplifier with a standard resistor or a standard capacitor in the feedback path to measure the chamber current or charge collected over a fixed time interval Podgorsak, 2005).

Ionization chambers are used in radiation therapy and diagnostic radiology for radiation dose determination. The charge,  $Q$  detected from an ionization chamber is correlated to the energy imparted to it by the ionizing radiation incident on it, and is related to the dose absorbed ( $D_{det}$ ) in the ion chamber by (Zhu, 1999):

$$D_{\text{det}} = \left(\frac{W}{e}\right)_{\text{air}} \cdot \left(\frac{Q}{m}\right) \cdot \beta \quad (2.1)$$

where  $(W/e)_{\text{air}}$  is the average energy required to produce an ion pair in air = 33.85 eV/ion pair or 3.85J/C,  $Q$  is the charge (in Coulomb, C) detected,  $m$  is the mass (in kilogram, kg) of the gas in the ion chamber, and  $\beta$  (has no unit) is a proportionality constant between the dose and the kinetic energy released per unit mass (kerma) in air (i.e., ratio of dose to kerma in air). The unit of absorbed dose ( $D_{\text{det}}$ ) is Gray (Gy), where 1 Gy equals 1 J kg<sup>-1</sup>.

The non-existence of charge particle equilibrium in the buildup region and in all transition zones between different media (such as the surface of a phantom), which results in a rapid variation of dose with depth (steep dose gradient), causes perturbation effects in ionization chambers when used for these measurements; this also makes accurate measurement of dose at the surface a phantom and in the buildup region a difficult task (Gerbi & Khan, 1990; O'Shea & McCavana, 2003). The recommended and generally accepted instrument for accurate measurement of dose at the surface of a phantom and in the buildup region of megavoltage photon beams is the extrapolation ion chamber because of its high accuracy in the non-charge particle equilibrium region (O'Shea & McCavana, 2003; Rawlinson et al., 1992). But because extrapolation ion chambers are very expensive, not available in most institutions, tedious and time-consuming to use (Rawlinson et al., 1992; Tannous et al., 1981), plane-parallel plate ion chambers are most commonly used (Gerbi & Khan, 1990; Rawlinson et al., 1992; Nilsson & Montelius, 1986; Wickman & Holmström, 1992; Gerbi & Khan, 1997).

A plane-parallel plate ion chamber is made up of two plane walls, one serving as an entry window and polarizing electrode and the other as the back wall and collecting electrode, as well

as a guard ring system (Podgorsak, 2005). Extrapolation ion chambers are also parallel plate chambers. The difference between extrapolation ion chambers and plane-parallel plate ion chambers is that, in plane-parallel plate ion chambers, the distance separating the parallel plate is fixed and hence a fixed sensitive volume, whereas in extrapolation ion chambers, the distance between the parallel plate can be varied and hence a variable sensitive volume.

Extrapolation ion chambers (variable sensitive volume) are preferred to plane-parallel plate ion chambers with fixed sensitive volume in measuring dose at the surface of a phantom and buildup region because perturbation effects in extrapolation chambers can be eliminated. This is done by making measurements as a function of the cavity thickness (sensitive volume) and then extrapolating to zero thickness (zero volume) (Podgorsak, 2005). Perturbation effects in fixed sensitive volume plane-parallel plate ion chambers cause an overestimation of the dose measured in non-charged particle equilibrium region mainly due to secondary electrons that are scattered into the chamber volume from the wall of the chamber (O'Shea & McCavana, 2003). Appropriate corrections are applied to measurements made with fixed sensitive volume parallel plate ion chambers in the buildup region and at the surface of a phantom because of these perturbation effects.

In this research, the fixed-separation (fixed sensitive volume) plane-parallel plate ionization chamber used is the Attix plane-parallel ionization chamber model RMI 449 (RMI, Radiation Measurements, Inc., Middleton, WI). This chamber is used in conjunction with a SPTW-PTW Unidos 10002 (SN: 20121) electrometer [Physikalisch-Technische Werkstätten (PTW), Freiburg, Germany]. Figure 2.2 is a cross section showing major components of the Attix plane-parallel

plate ion chamber, while Figure 2.3 shows the Attix ion chamber fitted into the RMI 457 solid water that accompanies it.

According to the manufacturer, the Attix plane-parallel plate ion chamber is made almost completely of solid water, RMI 457, and meets the American Association of Physicists in Medicine Task Group 21 (AAPM TG-21, 1983) performance. It has the following physical characteristics:

1. Chamber window material: Kapton Conductive Film
2. Chamber window thickness: 0.0025 cm, 4.8 mg/cm<sup>2</sup>
3. Ion collecting volume (Sensitive volume): approximately 0.125 cm<sup>3</sup> vented to atmosphere. Its vented design ensures that the chamber volume remains at atmospheric pressure even when the device is placed in a solid water phantom.
4. Collecting Electrode Diameter: 1.27 cm
5. Collecting Electrode Insulator: 1.3 cm thick polyethylene
6. Guard Ring Outer Diameter: 4.0 cm
7. Guard Ring Width (Collecting Electrode edge to side wall distance):  $\approx$ 1.35 cm
8. Electrode Separation (Cavity thickness or air gap): 0.1 cm
9. Chamber Body: Solid water, RMI 457, and nylon screws
10. Overall Dimensions: 6.0 cm diameter x 1.5 cm thick
11. Overall Dimensions: 30 x 20 x 2.5 cm (assembled)

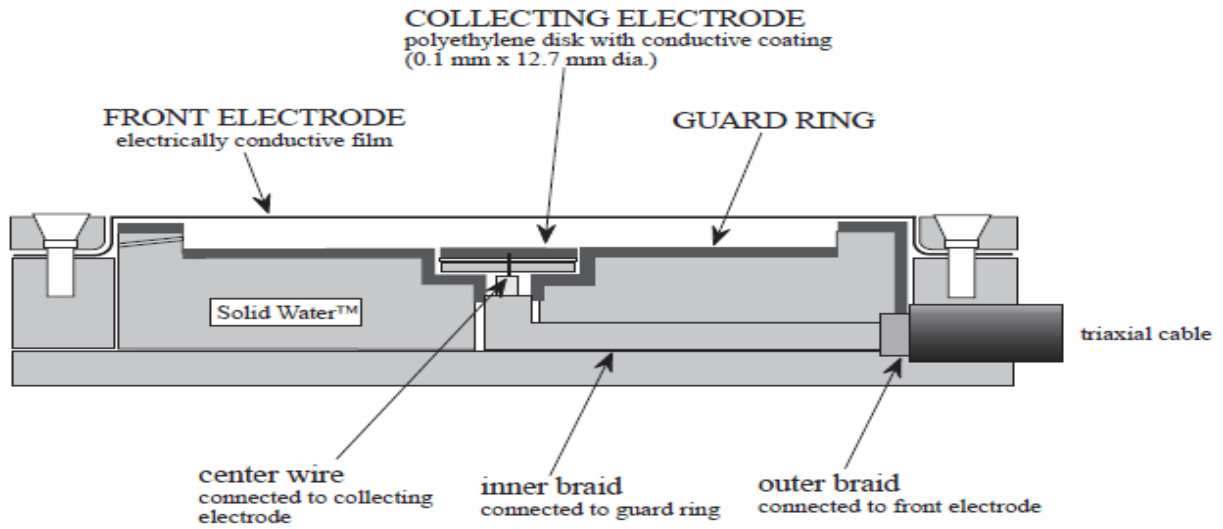


Figure 2.2: Cross - section showing major components of Attix Ionization chamber, Model RMI 449 (449-92-US10 Attix Plane-Parallel Plate Ionization Chamber 449 USER’S GUIDE).

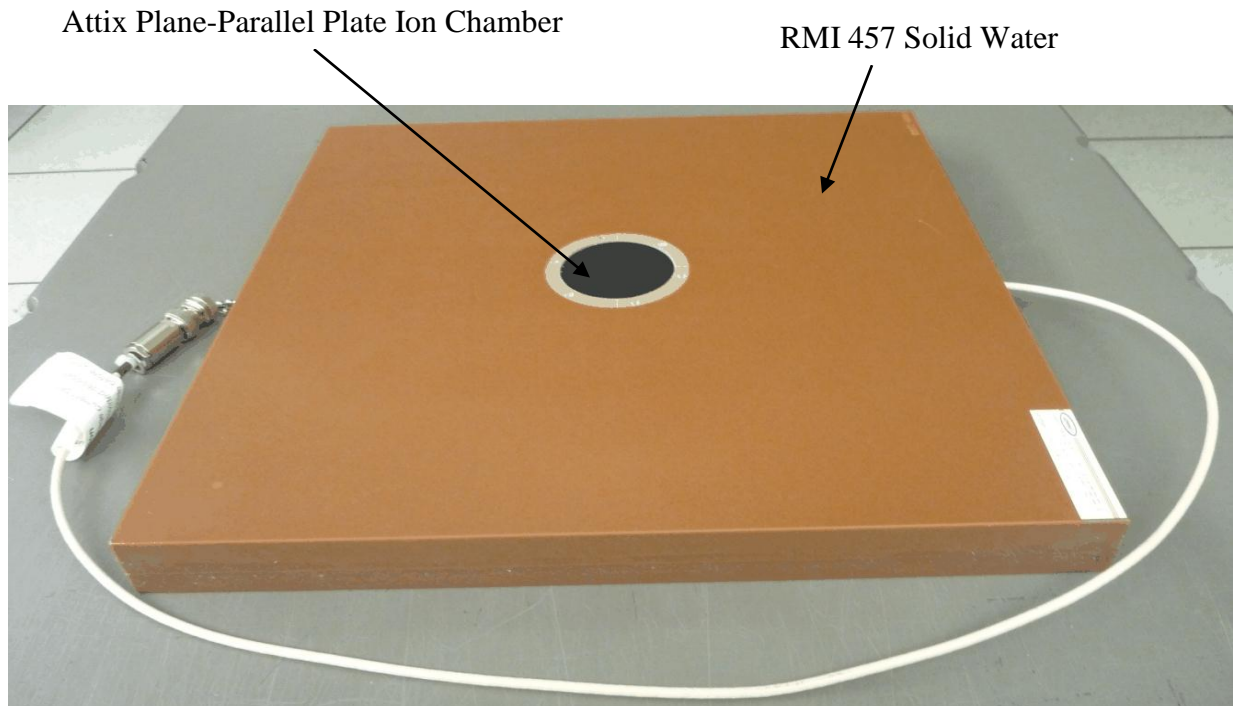


Figure 2.3: Attix plane-parallel plate ion chamber fitted into the RMI 457 solid water that accompanies it.

Rawlinson et al. (1992) showed that, the overestimation of dose measurements in the buildup region of megavoltage photon beams by fixed-separation parallel plate ion chamber due to secondary electrons scattered into the chamber volume from the wall of the chamber, is primarily dependent on the ratio of the electrode separation ( $s$ ) to the wall diameter ( $w$ ) as well as on the wall density and wall angle. They reported that, for fixed-separation parallel ion chambers to measure doses in the buildup region of megavoltage photon beams without the need for correction factors to account for the effect of the side wall, a design criterion of  $w/s \geq 25$  is required. The Attix plane-parallel plate ion chamber, with a wall diameter ( $w$ ) of 40 mm and a plate separation ( $s$ ) of 1 mm, has  $w/s$  of 40. This exceeds the design criterion of  $w/s \geq 25$  reported (Gerbi, 1993). It has also been reported that the Attix plane-parallel plate ionization chamber has a good depth resolution and requires little empirical correction ( $<1\%$  of dose at maximum depth,  $D_{\max}$  due to ‘in scatter’) because of its guard ring geometry and casing material (Yokoyama et al., 2004). The overestimation of surface dose by the Attix plane-parallel plate chamber is the smallest among all the commercially available chambers (Zhu, 1999).

### **2.3 Gafchromic EBT 2 Film/EPSON Expression 10000 XL Colour Scanner**

GafChromic EBT 2 [International Specialty Products (ISP), Wayne, NJ, USA], a radiochromic film released in early 2009, is a self developing film. Self-developing radiochromic films offer high spatial resolution dose measurements and since these films are self-developing, the uncertainties associated with the developing conditions are ruled out (Sankar et al., 2006). The chemical compositions of radiochromic films are nearly tissue equivalent (Todorovic et al., 2006). EBT 2 film has undergone several studies since it was released (Buston et al., 2009;

Richley et al., 2010; Hartmann et al., 2010; Arjomandy et al., 2010; Desroches et al., 2010; Lindsay et al., 2010; Andrés et al., 2010).

According to ISP (ISP, 2009a), EBT 2 has several improved features in their radiochromic film technology, that is, in terms of their previously produced radiochromic films: HD-810, XR-T, HS and EBT. Some of these features are:

1. Incorporation of a yellow “marker” dye; a feature that minimizes response differences caused by coating anomalies, protects the active layer from exposure by ultraviolet and visible light and can be used to improve dose accuracy by adjusting for small differences over the area of the film.
2. Formulated to be energy independent from 50 keV into the MeV range.
3. More tolerant of light exposure: can be handled in room light and thus the need for a darkroom is eliminated.
4. The binder component used is synthetic polymer instead of Gelatin so as to improve composition and performance stability between lots.
5. Less prone to damaged edges when cut.

EBT 2 films are marked with a small slit to distinguish the sides. When a sheet of EBT 2 film is held in landscape orientation such that the slit is at the right side of the top edge of the film, the side facing up is the side with the 50 microns polyester laminate. EBT 2 has a nominal thickness of 285  $\mu\text{m}$  and an effective atomic number,  $Z_{\text{eff}}$ , of 6.84. The configuration of EBT 2 film is as shown in Figure 2.4.

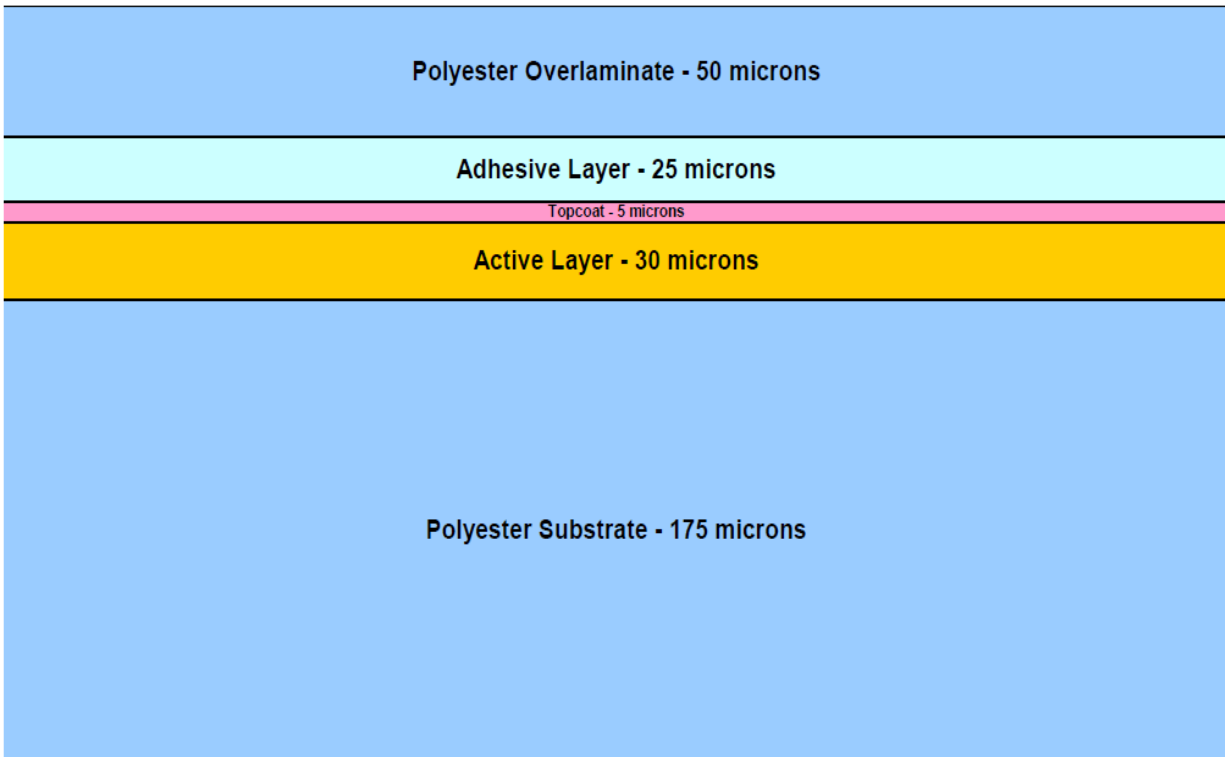


Figure 2.4: Configuration of Gafchromic EBT 2 film (ISP, 2009a).

A given type of radiochromic film responds to ionizing radiation uniquely, resulting in an absorption spectrum that is characterized by one or more maxima. This spectrum, and the wavelength(s) at which the maxima occur, can be dependent upon the absorbed dose and the post-irradiation read-out time (Richley et al., 2010). When EBT 2 film is exposed to radiation, its active component reacts to form a blue coloured polymer (i.e., undergoes a polymerization reaction) with absorption maxima (absorption peaks) at wavelengths of about 636 nm and 585 nm (Buston et al., 2009; ISP, 2009a). The absorption peak at a wavelength of about 636 nm is considered as the primary peak while that at about 585 nm is considered as the secondary peak. Hence the response of EBT 2 upon irradiation is enhanced by measurement with red light (red light has a wavelength of about 650 nm) (ISP, 2009a).

The reacting of the active component of EBT 2 film to form a blue coloured polymer upon exposure to radiation results in the darkening of the film. But to the human eye, the exposed film appears green due to the presence of the yellow marker dye in its active layer (ISP, 2009a). The degree of film darkening, which is a measure of the energy absorbed by the film, is quantified in terms of optical density, a logarithmic ratio of incident to transmitted light intensity (Richley et al., 2010). That is:

$$\text{Optical Density of exposed film (OD}_{\text{exp}}) = \log_{10} \frac{I_0}{I_{\text{exp}}} \quad (2.2)$$

where  $I_0$  is the intensity of light incident on the film and  $I_{\text{exp}}$  is the intensity of light transmitted by the film. If a film scanner is used,  $I_0$  and  $I_{\text{exp}}$  are expressed in terms of the pixel value of blank scan-without the exposed film ( $PV_{\text{blank}}$ ) and pixel value of the scan of exposed film ( $PV_{\text{exp}}$ ) respectively. Thus,  $OD_{\text{exp}}$  is expressed as:

$$\text{Optical Density of exposed film (OD}_{\text{exp}}) = \log_{10} \frac{PV_{\text{blank}}}{PV_{\text{exp}}} \quad (2.3)$$

When the optical density of unexposed film ( $OD_{\text{unexp}}$ ), that is,

$$\text{Optical Density of unexposed film (OD}_{\text{unexp}}) = \log_{10} \frac{I_0}{I_{\text{unexp}}} = \log_{10} \frac{PV_{\text{blank}}}{PV_{\text{unexp}}} \quad (2.4)$$

is subtracted from  $OD_{\text{exp}}$ , the term net optical density (net OD) is used. On combining equations (2.3) and (2.4) give:

$$\text{net OD} = OD_{\text{exp}} - OD_{\text{unexp}} = \log_{10} \frac{PV_{\text{unexp}}}{PV_{\text{exp}}} \quad (2.5)$$

Optical density of radiochromic film with respect to dose can be determined by digitizing the film using a scanner. The digitization also enables film images to be analyzed for absorbed dose (Andrés et al, 2010). In this research, the optical density of EBT 2 is analyzed using an EPSON Expression 10000 XL rgb (red, green, blue) flatbed color scanner (Epson America Inc., Long Beach, California, USA) and version 2.2.0113 of FILM QA™ Verification Software [3cognition

LLC (a division of ISP), Wayne, NJ, USA]. Epson Expression 10000XL scanner is an A3-size flatbed colour image scanner with the capability of generating scan images in 48-bit rgb mode, 16 bits per colour channel mode. Its optical resolution is 2,400 dots per inch (dpi). It uses an extended light source-xenon gas fluorescent lamp and has a charge coupled device chamber of six lines (94,500 pixels) as its image sensor. EBT 2 is best analyzed using FILM QA™ Verification Software and Epson flatbed colour scanner (e.g. EPSON Expression 10000XL colour scanner) (ISP, 2009b).

## **2.4 Solid Water Phantom**

In the studies of radiation interactions in patients, certain materials are used in place of patients. These materials are commonly called phantoms. Water is the standard and most universally used phantom material for dose measurements of photon and electron beams because (Khan, 2010; Podgorsak, 2005):

1. it closely approximates the radiation absorption and scattering properties of muscle and other soft tissues;
2. it is universally available with reproducible radiation properties.

But since some ionization radiation detectors cannot be used in water phantom, such as the Attix plane-parallel plate ion chamber used in this research, solid phantom materials that are tissue or water equivalent have been developed as substitutes for water. Examples of solid phantom materials are: Polystyrene, Plexiglas (Perspex, Lucite), Polyethylene, Paraffin, Mix D, M 3 and Solid water (Khan, 2010).

For a given material to be considered tissue or water equivalent, it must have the same effective atomic number, number of electrons per gram, and mass density as tissue or water. But the

Compton Effect, the predominant mode of interaction for megavoltage photon beams used in radiation therapy, is almost independent of atomic number. Because of this, the necessary condition for water equivalence of solid water phantom materials for such beams is the same electron density (number of electrons per cubic centimeter) as that of water (Khan, 2010).

A Certified Therapy Grade (CTG) Solid Water Phantom Set (30 x30 x4.5 cm), Gammex Model 457-CTG-KIT-4.5 (Gammex Inc., Middleton, Wisconsin, USA), is used in this research. This is because the Attix plane-parallel plate ion chamber, one of the dosimeters used in this research, cannot be used in water phantom. The set includes 7 slabs shown in Figure 2.5; their specifications are as shown in Table 2.1.



Figure 2.5: Slabs of CTG Gammex Model 457 solid water phantom.

Table 2.1: Specifications of Slabs of CTG Gammex Model 457 Solid Water Phantom.

Slab No.	1	2	3	4	5	6	7
Physical Density (g/cm <sup>3</sup> )	1.0435	1.0412	1.0423	1.0429	1.0435	1.0412	1.0423
Thickness (cm)	0.2 (±0.0015)	0.2 (±0.0015)	0.3 (±0.0015)	0.3 (±0.0015)	0.5 (±0.0015)	1.0 (±0.0015)	2.0 (±0.0015)
Length (cm)	30 (±0.0015)	30 (±0.0015)	30 (±0.0015)	30 (±0.0015)	30 (±0.0015)	30 (±0.0015)	30 (±0.0015)
Width (cm)	30 (±0.0015)	30 (±0.0015)	30 (±0.0015)	30 (±0.0015)	30 (±0.0015)	30 (±0.0015)	30 (±0.0015)
Effective Atomic Number	8.111	8.111	8.111	8.111	8.112	8.111	8.111
Mass Electron Density (e <sup>-</sup> /g)	0.539xN <sub>A</sub> *	0.539xN <sub>A</sub>					
Electron Density (e <sup>-</sup> /cm <sup>3</sup> )	0.563xN <sub>A</sub>	0.562xN <sub>A</sub>	0.562xN <sub>A</sub>	0.563xN <sub>A</sub>	0.563xN <sub>A</sub>	0.562xN <sub>A</sub>	0.562xN <sub>A</sub>
Electron Density Relative to Water	1.014	1.012	1.013	1.014	1.014	1.012	1.013
Flatness within (cm)	0.015	0.015	0.015	0.015	0.015	0.015	0.015

\* N<sub>A</sub> is Avogadro's number.

## 2.5 Clinical Setups

The various clinical setups or clinical irradiation conditions for which measurements were made are some of the common clinical setups of patients for radiation therapy treatment. These setups include open fields, physical wedge (fixed wedge) fields, enhanced dynamic wedge fields, and block tray fields.

The photon beam field that gets to the patient or phantom after the beam has traversed a physical wedge or a block tray placed in the path of the beam is referred to as physical wedge field (a wedge-shaped dose field) or block tray field respectively. Enhanced dynamic wedge field is a wedge-shaped dose field produced without the use of external beam modifiers (e.g. a physical wedge) but through computer-controlled collimator jaw motion on a linac (Fontanarosa et al, 2009; Zhu, 2005). Wedge-shaped dose fields are routinely used in photon beam radiation therapy to improve the dose distribution (Shih et al., 2000). A block tray is a tray on which blocks (e.g. lead or Cerrobend) used for shaping of treatment fields are placed on. The shaping of treatment field is primarily dictated by tumor distribution (Khan 2010).

Four physical wedges (angles  $15^\circ$ ,  $30^\circ$ ,  $45^\circ$  and  $60^\circ$ ), made of lead and steel were used in this research. Two of these physical wedges and the block tray (Varian photon block tray-0.5 cm thick) used in this research are as shown in Figures 2.6 and 2.7 respectively. The various clinical setups for which measurements were made are as given in Tables 2.2 to 2.5.



(a)

(b)

Figure 2.6: Physical wedges: (a) Steel-angle  $30^\circ$  and (b) Lead-angle  $45^\circ$ .



Figure 2.7: Varian photon block tray (0.5 cm thick).

Table 2.2: Open Fields Clinical Setups.

Open Field x 6 MV x 85 cm SSD: Field sizes (cm <sup>2</sup> ): 3 x 3, 5 x 5, 8 x 8, 10 x 10, 12 x 12, 15 x 15, 20 x 20, 30 x 30
Open Field x 6 MV x 100 cm SSD: Field sizes (cm <sup>2</sup> ): 3 x 3, 5 x 5, 8 x 8, 10 x 10, 12 x 12, 15 x 15, 20 x 20, 30 x 30
Open Field x 6 MV x 120 cm SSD: Field sizes (cm <sup>2</sup> ): 3 x 3, 5 x 5, 8 x 8, 10 x 10, 12 x 12, 15 x 15, 20 x 20, 30 x 30
Open Field x 15 MV x 85 cm SSD: Field sizes (cm <sup>2</sup> ): 3 x 3, 5 x 5, 8 x 8, 10 x 10, 12 x 12, 15 x 15, 20 x 20, 30 x 30
Open Field x 15 MV x 100 cm SSD: Field sizes (cm <sup>2</sup> ): 3 x 3, 5 x 5, 8 x 8, 10 x 10, 12 x 12, 15 x 15, 20 x 20, 30 x 30
Open Field x 15 MV x 120 cm SSD: Field sizes (cm <sup>2</sup> ): 3 x 3, 5 x 5, 8 x 8, 10 x 10, 12 x 12, 15 x 15, 20 x 20, 30 x 30

Table 2.3: Enhanced Dynamic Wedges (EDW) Fields Clinical Setups.

EDW Field x 6 MV x 15 Degrees x 85 cm SSD: Field sizes (cm <sup>2</sup> ): 4 x 4, 5 x 5, 8 x 8, 10 x 10, 12 x 12, 15 x 15, 20 x 20
EDW Field x 6 MV x 60 Degrees x 85 cm SSD: Field sizes (cm <sup>2</sup> ): 4 x 4, 5 x 5, 8 x 8, 10 x 10, 12 x 12, 15 x 15, 20 x 20
EDW Field x 6 MV x 15 Degrees x 100 cm SSD: Field sizes (cm <sup>2</sup> ): 4 x 4, 5 x 5, 8 x 8, 10 x 10, 12 x 12, 15 x 15, 20 x 20
EDW Field x 6 MV x 60 Degrees x 100 cm SSD: Field sizes (cm <sup>2</sup> ): 4 x 4, 5 x 5, 8 x 8, 10 x 10, 12 x 12, 15 x 15, 20 x 20

EDW Field x 6 MV x 15 Degrees x 120 cm SSD: Field sizes (cm <sup>2</sup> ): 4 x 4, 5 x 5, 8 x 8, 10 x 10, 12 x 12, 15 x 15, 20 x 20
EDW Field x 6 MV x 60 Degrees x 120 cm SSD: Field sizes (cm <sup>2</sup> ): 4 x 4, 5 x 5, 8 x 8, 10 x 10, 12 x 12, 15 x 15, 20 x 20
EDW Field x 15 MV x 15 Degrees x 85 cm SSD: Field sizes (cm <sup>2</sup> ): 4 x 4, 5 x 5, 8 x 8, 10 x 10, 12 x 12, 15 x 15, 20 x 20
EDW Field x 15 MV x 60 Degrees x 85 cm SSD: Field sizes (cm <sup>2</sup> ): 4 x 4, 5 x 5, 8 x 8, 10 x 10, 12 x 12, 15 x 15, 20 x 20
EDW Field x 15 MV x 15 Degrees x 100 cm SSD: Field sizes (cm <sup>2</sup> ): 4 x 4, 5 x 5, 8 x 8, 10 x 10, 12 x 12, 15 x 15, 20 x 20
EDW Field x 15 MV x 60 Degrees x 100 cm SSD: Field sizes (cm <sup>2</sup> ): 4 x 4, 5 x 5, 8 x 8, 10 x 10, 12 x 12, 15 x 15, 20 x 20
EDW Field x 15 MV x 15 Degrees x 120 cm SSD: Field sizes (cm <sup>2</sup> ): 4 x 4, 5 x 5, 8 x 8, 10 x 10, 12 x 12, 15 x 15, 20 x 20
EDW Field x 15 MV x 60 Degrees x 120 cm SSD: Field sizes (cm <sup>2</sup> ): 4 x 4, 5 x 5, 8 x 8, 10 x 10, 12 x 12, 15 x 15, 20 x 20

Table 2.4: Physical Wedges (Fixed Wedges) Fields Clinical Setups.

Fixed Wedge Field x 6 MV x 15 Degrees x 85 cm SSD: Field sizes (cm <sup>2</sup> ): 4 x 4, 5 x 5, 8 x 8, 10 x 10, 12 x 12, 15 x 15, 20 x 20
Fixed Wedge Field x 6 MV x 30 Degrees x 85 cm SSD: Field sizes (cm <sup>2</sup> ): 4 x 4, 5 x 5, 8 x 8, 10 x 10, 12 x 12, 15 x 15, 20 x 20
Fixed Wedge Field x 6 MV x 45 Degrees x 85 cm SSD: Field sizes (cm <sup>2</sup> ): 4 x 4, 5 x 5, 8 x 8, 10 x 10, 12 x 12, 15 x 15, 20 x 20
Fixed Wedge Field x 6 MV x 60 Degrees x 85 cm SSD: Field sizes (cm <sup>2</sup> ): 4 x 4, 5 x 5, 8 x 8, 10 x 10, 12 x 12, 15 x 15
Fixed Wedge Field x 6 MV x 15 Degrees x 100 cm SSD: Field sizes (cm <sup>2</sup> ): 4 x 4, 5 x 5, 8 x 8, 10 x 10, 12 x 12, 15 x 15, 20 x 20
Fixed Wedge Field x 6 MV x 30 Degrees x 100 cm SSD: Field sizes (cm <sup>2</sup> ): 4 x 4, 5 x 5, 8 x 8, 10 x 10, 12 x 12, 15 x 15, 20 x 20
Fixed Wedge Field x 6 MV x 45 Degrees x 100 cm SSD: Field sizes (cm <sup>2</sup> ): 4 x 4, 5 x 5, 8 x 8, 10 x 10, 12 x 12, 15 x 15, 20 x 20
Fixed Wedge Field x 6 MV x 60 Degrees x 100 cm SSD: Field sizes (cm <sup>2</sup> ): 4 x 4, 5 x 5, 8 x 8, 10 x 10, 12 x 12, 15 x 15
Fixed Wedge Field x 6 MV x 15 Degrees x 120 cm SSD: Field sizes (cm <sup>2</sup> ): 4 x 4, 5 x 5, 8 x 8, 10 x 10, 12 x 12, 15 x 15, 20 x 20
Fixed Wedge Field x 6 MV x 30 Degrees x 120 cm SSD: Field sizes (cm <sup>2</sup> ): 4 x 4, 5 x 5, 8 x 8, 10 x 10, 12 x 12, 15 x 15, 20 x 20
Fixed Wedge Field x 6 MV x 45 Degrees x 120 cm SSD: Field sizes (cm <sup>2</sup> ): 4 x 4, 5 x 5, 8 x 8, 10 x 10, 12 x 12, 15 x 15, 20 x 20
Fixed Wedge Field x 6 MV x 60 Degrees x 120 cm SSD: Field sizes (cm <sup>2</sup> ): 4 x 4, 5 x 5, 8 x 8, 10 x 10, 12 x 12, 15 x 15
Fixed Wedge Field x 15 MV x 15 Degrees x 85 cm SSD: Field sizes (cm <sup>2</sup> ): 4 x 4, 5 x 5, 8 x 8, 10 x 10, 12 x 12, 15 x 15, 20 x 20

Fixed Wedge Field x 15 MV x 30 Degrees x 85 cm SSD: Field sizes (cm <sup>2</sup> ): 4 x 4, 5 x 5, 8 x 8, 10 x 10, 12 x 12, 15 x 15, 20 x 20
Fixed Wedge Field x 15 MV x 45 Degrees x 85 cm SSD: Field sizes (cm <sup>2</sup> ): 4 x 4, 5 x 5, 8 x 8, 10 x 10, 12 x 12, 15 x 15, 20 x 20
Fixed Wedge Field x 15 MV x 60 Degrees x 85SSD: Field sizes (cm <sup>2</sup> ): 4 x 4, 5 x 5, 8 x 8, 10 x 10, 12 x 12, 15 x 15
Fixed Wedge Field x 15 MV x 15 Degrees x 100 cm SSD: Field sizes (cm <sup>2</sup> ): 4 x 4, 5 x 5, 8 x 8, 10 x 10, 12 x 12, 15 x 15, 20 x 20
Fixed Wedge Field x 15 MV x 30 Degrees x 100 cm SSD: Field sizes (cm <sup>2</sup> ): 4 x 4, 5 x 5, 8 x 8, 10 x 10, 12 x 12, 15 x 15, 20 x 20
Fixed Wedge Field x 15 MV x 45 Degrees x 100 cm SSD: Field sizes (cm <sup>2</sup> ): 4 x 4, 5 x 5, 8 x 8, 10 x 10, 12 x 12, 15 x 15, 20 x 20
Fixed Wedge Field x 15 MV x 60 Degrees x 100 cm SSD: Field sizes (cm <sup>2</sup> ): 4 x 4, 5 x 5, 8 x 8, 10 x 10, 12 x 12, 15 x 15
Fixed Wedge Field x 15 MV x 15 Degrees x 120 cm SSD: Field sizes (cm <sup>2</sup> ): 4 x 4, 5 x 5, 8 x 8, 10 x 10, 12 x 12, 15 x 15, 20 x 20
Fixed Wedge Field x 15 MV x 30 Degrees x 120 cm SSD: Field sizes (cm <sup>2</sup> ): 4 x 4, 5 x 5, 8 x 8, 10 x 10, 12 x 12, 15 x 15, 20 x 20
Fixed Wedge Field x 15 MV x 45 Degrees x 120 cm SSD: Field sizes (cm <sup>2</sup> ): 4 x 4, 5 x 5, 8 x 8, 10 x 10, 12 x 12, 15 x 15, 20 x 20
Fixed Wedge Field x 15 MV x 60 Degrees x 120 cm SSD: Field sizes (cm <sup>2</sup> ): 4 x 4, 5 x 5, 8 x 8, 10 x 10, 12 x 12, 15 x 15

Table 2.5: Block Tray Fields Clinical Setups.

Block Tray Field x 6 MV x 85 cm SSD: Field sizes (cm <sup>2</sup> ): 3x3, 5 x 5, 8 x 8, 10 x 10, 12 x 12, 15 x 15, 20 x 20, 30 x 30
Block Tray Field x 6 MV x 100 cm SSD: Field sizes (cm <sup>2</sup> ): 3x3, 5 x 5, 8 x 8, 10 x 10, 12 x 12, 15 x 15, 20 x 20, 30 x 30
Block Tray Field x 6 MV x 120 cm SSD: Field sizes (cm <sup>2</sup> ): 3x3, 5 x 5, 8 x 8, 10 x 10, 12 x 12, 15 x 15, 20 x 20, 30 x 30
Block Tray Field x 15 MV x 85 cm SSD: Field sizes (cm <sup>2</sup> ): 3x3, 5 x 5, 8 x 8, 10 x 10, 12 x 12, 15 x 15, 20 x 20, 30 x 30
Block Tray Field x 15 MV x 100 cm SSD: Field sizes (cm <sup>2</sup> ): 3x3, 5 x 5, 8 x 8, 10 x 10, 12 x 12, 15 x 15, 20 x 20, 30 x 30
Block Tray Field x 15 MV x 120 cm SSD: Field sizes (cm <sup>2</sup> ): 3x3, 5 x 5, 8 x 8, 10 x 10, 12 x 12, 15 x 15, 20 x 20, 30 x 30

## 2.6 Measurements with Attix Plane-Parallel Plate Ionization Chamber

The 6 MV and 15 MV photons beams were incident normally on the solid water phantom for all the Attix ion chamber measurements, that is, the solid water phantom and Attix ion chamber were positioned perpendicular to the central axis of the beams. When a patient is irradiated with a photon beam, backscattered photons also contribute to the dose absorbed by the patient. To account for this backscatter, the Attix ion chamber was fitted into the solid water that accompanied it and placed on a 10.0 cm thick (length x width: 30 x 30 cm) acrylic phantom material. For variation of depth of measurement, various thicknesses (slabs) of the solid water phantom were placed on the Attix ion chamber. Figure 2.8 shows the experimental setup for Attix ion chamber measurements. Measurements for all the clinical setups involving 6 MV photon beam were taken at depths from 0 cm up to 1.8 cm at 0.2 cm increments. For 15 MV open field clinical setups, measurements were taken at depths from 0 cm up to 3.8 cm at 0.2 cm increments while for other 15 MV clinical setups, measurements were taken at 0.2 cm increments up to 1.0 cm depth and at 0.4 cm increments thereafter. In the head of a linear accelerator is an assembly of ionization chambers used for monitoring the photon beam output, and the quantity of ionizing radiation that passes through this assembly is expressed in terms of monitor units (MU). The output of linear accelerators that deliver megavoltage photon beams is most commonly expressed in centigray per monitor unit - cGy/MU (Podgorsak, 2005). For the 6 MV and 15 MV photon beams, the number of monitor units used was 50 (50 MU) on the linac.

The Attix ion chamber, which was used in conjunction with a PTW electrometer, was operated at a bias voltage of  $\pm 300$  volts. The electrometer was set to measure charge in nano-coulombs (nC). The quantities of charge measured by the electrometer represented the buildup dose measurements made with the Attix chamber, that is, Attix chamber measurements were relative

dose but not absolute dose measurements. To make absolute dose measurements using Attix chamber the calibration of Attix chamber is required. Unfortunately the National Research Council of Canada (NRCC) at present does not provide calibrations for parallel plate ion chambers. At each depth for all open field clinical setups, two readings (accumulated charge in nC) each were taken for both the positive and negative polarities of the Attix ion chamber and the average of these readings taken as the final reading. It is recommended that after polarity reversal, adequate time must be allowed before taking the next reading so that the ion chamber reading can reach equilibrium, that is, to ensure that the electrometer comes to stable state; some chambers may take up to 20 minutes before a stable operating condition is reached (Malhotra et al., 1997; Shimono et al., 2009). In this research, polarity reversal was done on completion of all measurements for a given clinical setup and more than 1 hour was allowed after polarity reversal before readings were taken. For all clinical setups other than open field clinical setups, the average of two readings at each depth for only the positive polarity of the Attix ion chamber was taken. Temperature and pressure readings were also recorded during all measurements. All measurements at various depths with the 6 MV and 15 MV photon beams were divided by measurements made at the depths of 1.6 cm and 3.2 cm, respectively. That is, all 6 MV measurements were normalized to measurements at 1.6 cm depth while all 15 MV measurements were normalized to measurements at 3.2 cm depth. Thus buildup dose values measured at various depths were expressed in terms of relative dose; relative to dose at 1.6 cm depth (for 6 MV photon beam) and relative to dose at 3.2 cm depth (for the 15 MV photon beam). The normalization of measured buildup dose values was done so that measured dose values can be easily compared.

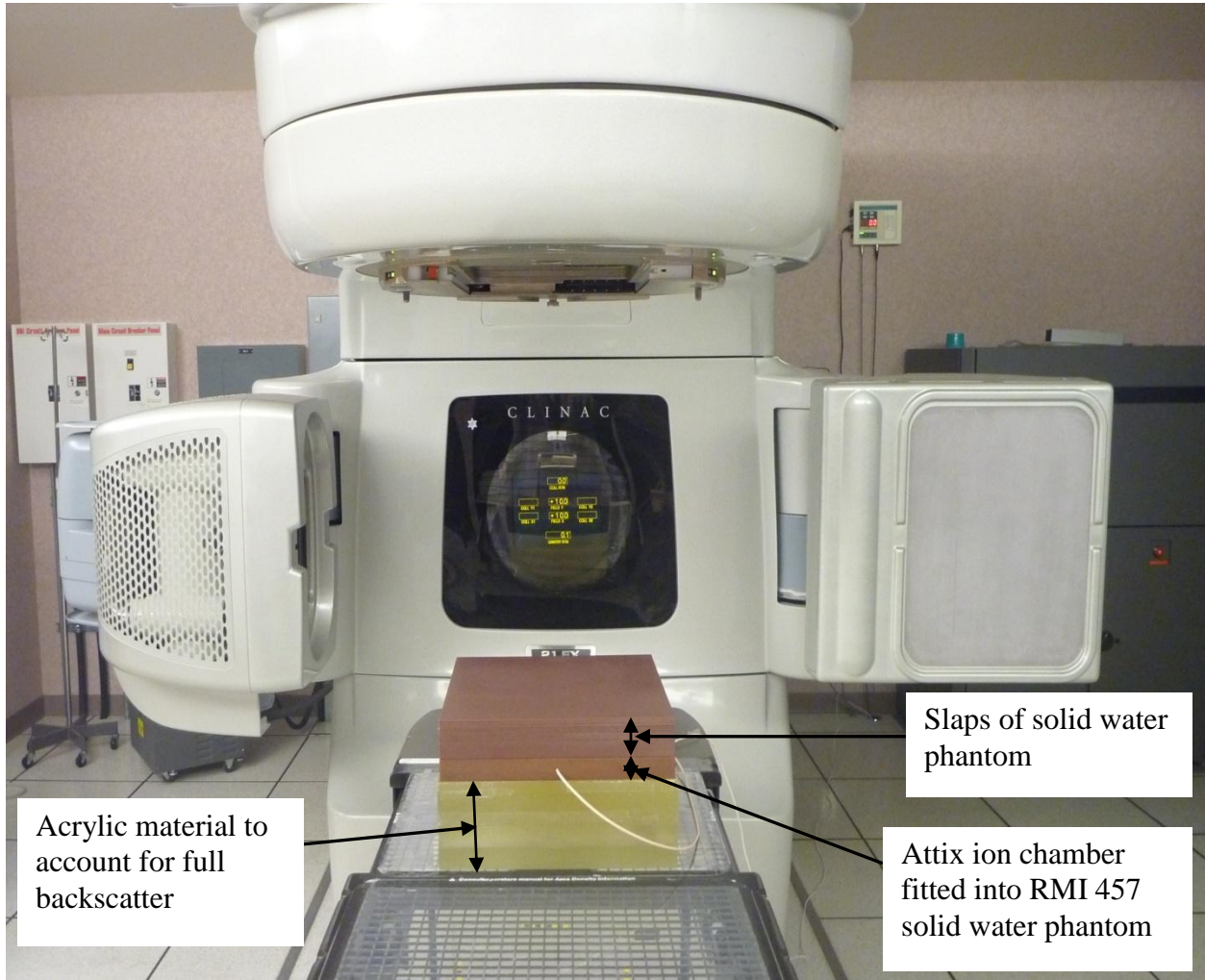


Figure 2.8: Experimental setup for measurements using Attix plane-parallel plate ion chamber.

## **2.6.1 Corrections Applied to Readings**

Polarity effect, temperature and pressure corrections were applied to the readings.

### **2.6.1.1 Polarity Effect Correction**

Under identical irradiation conditions, the use of potentials of opposite polarity in an ion chamber may give different readings; this phenomenon is referred to as the polarity effect (Shimono et al., 2009). The polarity effect for plane-parallel plate ion chamber is due to the lack of charge particle equilibrium at the collecting electrode. Factors that affect the magnitude of polarity effect are the thickness of the collecting electrode, the frontal surface area of the collecting electrode, the depth of the collecting electrode beneath the surface of the phantom, and the energy of the beam (Gerbi & Khan, 1987). It is the recommendation of American Association of Physicists in Medicine Task Group 25 (AAPM TG-25) that the readings of all ionization chambers be corrected if polarity effects greater than 1% are observed (Shimono et al., 2009). For all open field clinical setups, four readings were taken (two each for positive and negative polarities of the Attix ion chamber) at all depths and the average of the four readings computed. By averaging the four readings, polarity effect was corrected for (Wickman & Holmström, 1992). For non open field clinical setups, polarity effect was not corrected because the polarity effect for open field clinical setups was not greater than 1%.

### **2.6.1.2 Temperature and Pressure Corrections**

The mass of air in the sensitive volume of an ion chamber is affected by changes in ambient temperature and pressure. From equation (2.1), the mass of air in the sensitive volume of the ion chamber is one of the factors upon which the total charge,  $Q$ , produced depends. Temperature and pressure corrections are applied to account for these changes (Podgorsak, 2005).

Temperature and pressure corrections,  $P_{TP}$ , were done by normalizing all Attix ion chamber readings to standard conditions of temperature (22°C) and pressure (101.33 kPa, 1 atmosphere) using:

$$M = M_o \times \frac{273.2 + T(^{\circ}\text{C})}{273.2 + 22.0} \times \frac{101.33}{P \text{ (kPa)}} \quad (2.6)$$

where  $M$  is the corrected reading,  $M_o$  is the uncorrected reading,  $T$  and  $P$  are the temperature and pressure recorded during measurements with Attix ion chamber.

## 2.7 Measurements with Gafchromic EBT 2 Film

Gafchromic EBT 2 films from lot #: F03181001B (Expiration date: March, 2012) and lot #: A11031002 (Expiration date: November 2012) were used in this research. Measurements for clinical setups involving 6 MV photon beam were performed using EBT 2 films from lot #: F03181001B while for clinical setups involving 15 MV photon beam, EBT 2 films from lot #: A11031002 were used. Measurements with EBT 2 film were aimed at validating Attix ion chamber measurements and were performed only for clinical setups involving a source-to-surface distance (SSD) of 100 cm [ open field, EDW (15° and 60°) fields, PW (15° and 60°) fields, block tray field, field sizes: 5 x 5 cm<sup>2</sup>, 10 x 10 cm<sup>2</sup>, 15 x 15 cm<sup>2</sup> and 20 x 20 cm<sup>2</sup>].

There are various sources of uncertainties of analysis using Gafchromic film; the major ones include scanner uniformity, film uniformity, film orientation effect as well as scratches and surface defects. All films were irradiated and scanned according to the procedures suggested by the manufacturer. It has been reported that the uncertainties associated with measurements using EBT 2 film can be decreased to 3% if the procedures suggested by the manufacturers are followed (Fontanarosa et al., 2009).

Despite the low energy dependence of EBT 2, two calibration curves (dose response curves) were obtained for the EBT 2 film using the 6 MV and 15 MV photon beams. A total of 30 pieces ( $4 \times 4 \text{ cm}^2$ ) of films was used for the calibration curves (15 pieces cut from the same sheet of film from lot # F03181001B for the 6 MV photon beam and another 15 pieces cut from the same sheet of film but from lot # A11031002 for the 15 MV photon beam). The cut pieces of films were marked with marker to keep track of the orientation with respect to the sheet from which they were cut. To allow for mechanical stability, the film pieces were irradiated 24 hours after cutting (Andrés et al, 2010). Out of the 30 pieces of films, 15 pieces (from the same sheet and lot #) were irradiated by 6 MV photon beam and the remaining 15 pieces (also from the same sheet and lot #) were irradiated by 15 MV photon beam, to doses of 0, 10, 25, 30, 40, 50, 100, 150, 200, 250, 300, 350, 400, 450, and 500cGy, respectively. All irradiations were performed perpendicularly to the film plane at a source-to-surface distance (SSD) of 100 cm using a  $10 \times 10 \text{ cm}^2$  field size. Films irradiated by 6 MV photon beam were placed at depth of 1.5 cm ( $D_{\text{max}}$ ) while dose irradiated by 15 MV photon beam were placed at a depth of 3.0 cm ( $D_{\text{max}}$ ) using the solid water phantom slabs for this research. Enough acrylic materials were used to account for full backscatter. The output of the linear accelerator was measured before irradiation using a Farmer type (cylindrical) ion chamber with a PTW Unidos electrometer, and a variation of -0.51% (for the 6 MV photon beam) and -0.26% (for the 15 MV photon beam) were observed.

To minimize the uncertainty associated with incomplete post irradiation coloration, all films pieces were scanned 24 hours after irradiation (Buston et al., 2009), using the Epson Expression 10000XL colour scanner. To reduce the scan-to-scan uncertainty, every film piece was scanned five consecutive times and stored in TIFF format (tagged image file format). The final image was

calculated as the average of those five images (Andrés et al., 2010). The Epson Expression scanner settings were:

1. Scanning Mode: Professional Mode
2. Film: 'Positive Film,' which means that the dark areas of the film appear white in the scanned image and exhibit high pixel values (Martišíková et al., 2008).
3. Scan Resolution: 72 dots per inch (dpi)
4. Colour Depth: 48 bit rgb (16 bit channel)

Each piece of film was placed in the middle of the scanner bed and scanned in the landscape orientation, i.e., short dimension of the film parallel to the long dimension of the scanner bed. All film pieces were scanned before and after exposure. The red channel of scanned images was extracted and analyzed over a 1cm x 1cm central region of interest (ROI) using FILM QA<sup>TM</sup> Verification Software-the mean pixel value of ROI measured and the mean and standard deviation determined. To avoid possible differences in film response depending on the side of the film facing the scanner lamp, all film pieces were scanned with the 175  $\mu\text{m}$  side facing the glass window on the bed of the scanner (Desroches et al., 2010).

The net optical density (net OD) of each piece of film was computed using equation (2.5) and the dose versus net OD was plotted. The calibration curve obtained using the 6 MV photon beam was fitted by a polynomial function of the 4<sup>th</sup> order while that obtained using the 15 MV photon beam was fitted by a 2<sup>nd</sup> order polynomial function. Usually, a calibration curve or Sensitometric curve (dose response curve) is a plot of net OD versus Dose; the reverse is plotted for easier determination of dose from a given optical density. The calibration curves obtained are as shown in Figures 2.9 and 2.10.

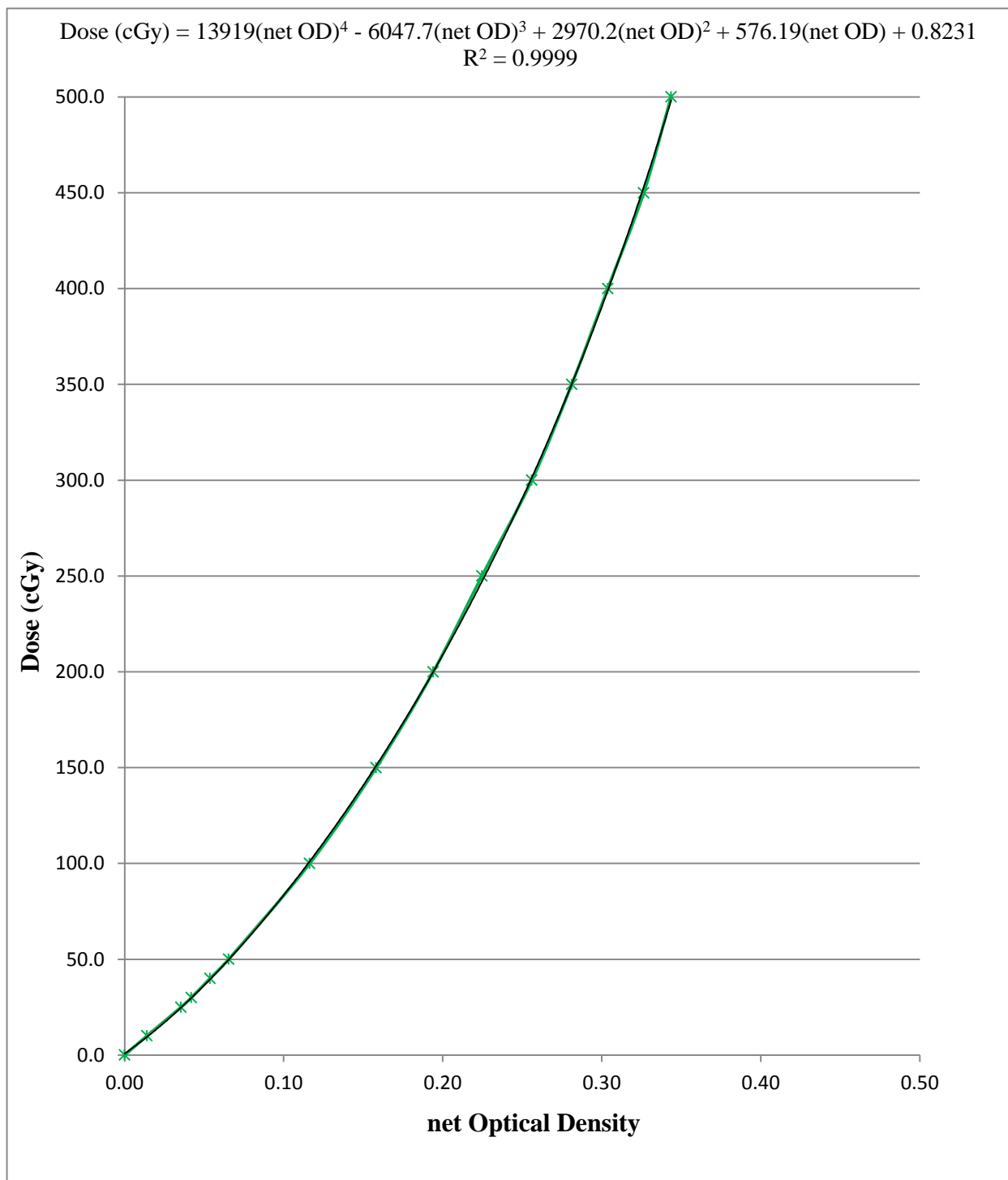


Figure 2.9: EBT 2 film calibration curve obtained using 6 MV photon beam. The black line represents the fitted polynomial function.

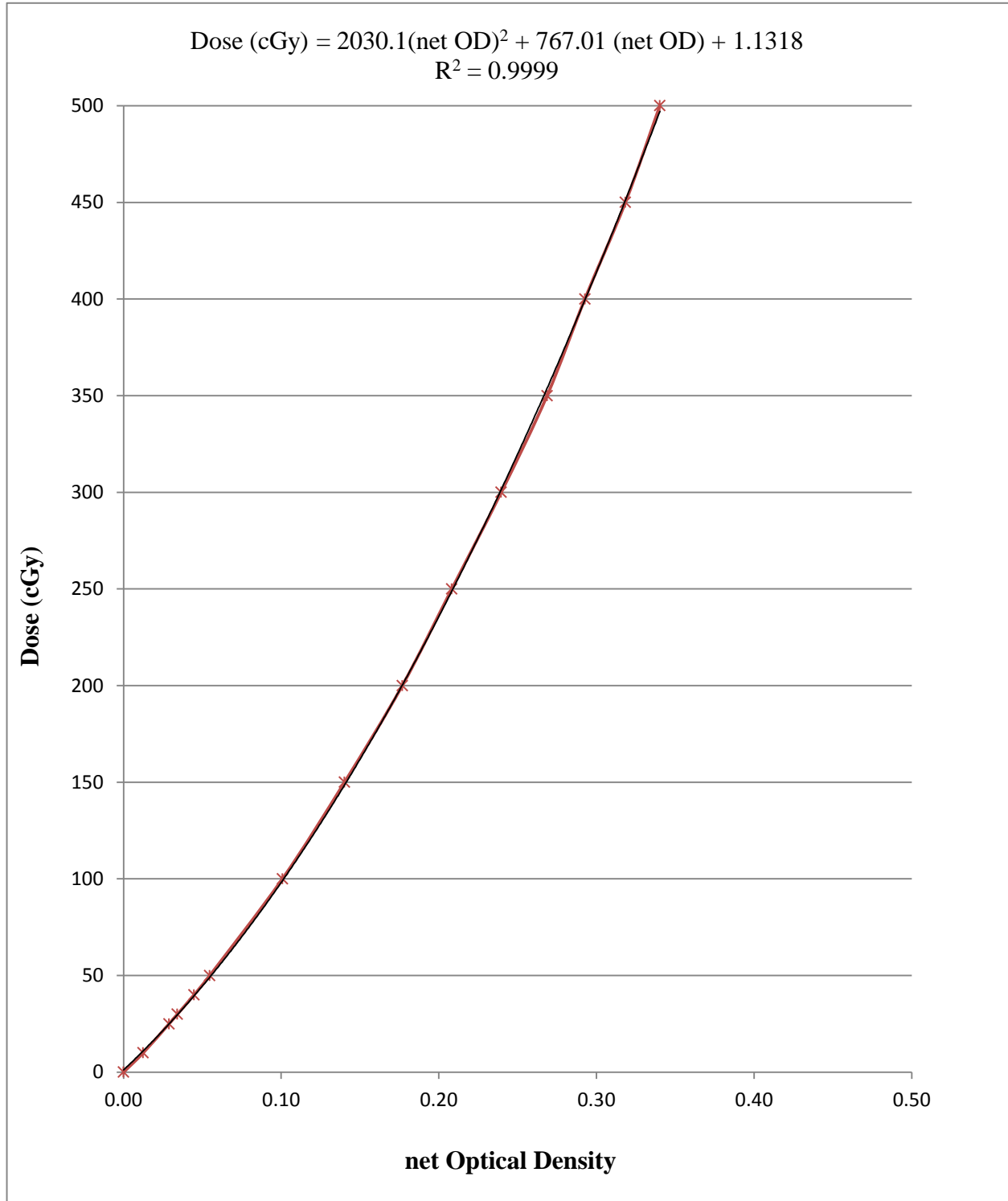


Figure 2.10: EBT 2 film calibration curve obtained using 15 MV photon beam. The black line represents the fitted polynomial function.

For the depth dose measurements, a total of 529 film pieces ( $4 \times 4 \text{ cm}^2$  each) cut from sheets of EBT 2 films were used. Out of the 529 film pieces, 253 pieces were irradiated by 6 MV photon beam and 276 pieces by 15 MV photon beam. The film pieces were irradiated one at a time at each required depth and all irradiations were performed perpendicularly to the film plane. Scanning and analysis of exposed film pieces were done in the same manner as film pieces used for calibration curves. The net OD of each piece of film was computed and the corresponding dose (cGy) determined using the fitted polynomial functions of the calibration curves that were obtained. The determined doses were normalized at a depth of 1.6 cm for 6 MV photon beam and at a depth of 3.2 cm for 6 MV photon beam.

## **2.8 Remodeling of the Electron Contamination Models in Pinnacle<sup>3</sup>**

Buildup dose measurements made using the Attix parallel-plate ionization chamber for all the clinical setups, with the exception of clinical setups involving block tray, were entered into Pinnacle<sup>3</sup>. The electron contamination models in Pinnacle<sup>3</sup> were then remodeled using the automodel feature of Pinnacle<sup>3</sup>. Buildup dose measurements of clinical setups involving block tray were not entered into Pinnacle<sup>3</sup> because the automodel feature of Pinnacle<sup>3</sup> does not model electron contamination for block tray fields. After the remodeling of the electron contamination models, buildup dose calculations were performed using Pinnacle<sup>3</sup>.

## **2.9 Pinnacle<sup>3</sup> Treatment Planning System Calculations**

Buildup dose calculations on Pinnacle<sup>3</sup> TPS (version 9.0), for all the clinical setups in this study, were performed using a water phantom (with a homogenous density of  $1\text{g/cm}^3$ ) created by the TPS. The calculation grid resolution size used in the TPS was 0.1 cm. All doses calculated using

the 6 MV photon beam were normalized at a depth of 1.6 cm and those using the 15 MV photon beam, normalized at a depth of 3.2 cm. For both photon beams, 50 MU was used.

## Chapter 3

### Results and Discussions

#### 3.1 Results

##### 3.1.1 Validation Measurements using GafChromic EBT 2 Film

Validation measurements using EBT 2 film, that is, comparison of buildup dose measurements made using EBT 2 film with that using Attix pp ion chamber, were performed for clinical setups involving 6 MV and 15 MV photon beams, 100 cm SSD, open fields, enhanced dynamic wedge fields (angles 15 and 60 degrees), physical wedge fields (angles 15 and 60 degrees), block tray fields and field sizes of 5 x 5, 10 x 10, 15 x 15, and 20 x 20 cm<sup>2</sup>. The total number of clinical setups for which EBT 2 film and Attix pp ion chamber buildup dose measurements were compared was 46 (23 each for the 6 MV and 15 MV photon beams). For each clinical setup, the graph of relative dose versus depth (RD graph) of EBT 2 film buildup dose measurements and the RD graph of Attix pp ion chamber buildup dose measurements were plotted and compared. The comparison of these RD graphs, plotted for the 46 clinical setups, was done in order to have a pictorial view of the differences between buildup dose measurements performed using EBT 2 film and Attix pp ion chamber. A total of 92 RD graphs (i.e., 46 pairs of RD graphs) were plotted and since all these graphs cannot be shown in this thesis because of space limitation, only some of these graphs, which are a general representation of the 92 RD graphs plotted, are as shown in Figures 3.1 to 3.12. There was a good agreement between the measurements made using EBT 2 film and the Attix pp ion chamber for the open fields as well as for the wedged and block tray fields. The mean errors for all the buildup dose values measured using EBT 2 film were  $\pm 0.21\%$  (1SD) and  $\pm 0.04\%$  (1SD) for the 6 MV and 15 MV photon beams, respectively while the mean

error in the buildup dose values measured using Attix chamber was  $\pm 0.18\%$  (1SD) for both the 6 MV and 15 MV photon beams. The mean absolute dose difference between all EBT 2 and Attix chamber measured buildup dose values was  $1.4\% \pm 1.5\%$  (1SD) for the 6 MV photon beam and  $1.1 \pm 1.0\%$  (1SD) for the 15 MV photon beam. These provide a good confidence in the measurements made using Attix pp ion chamber in the buildup region.

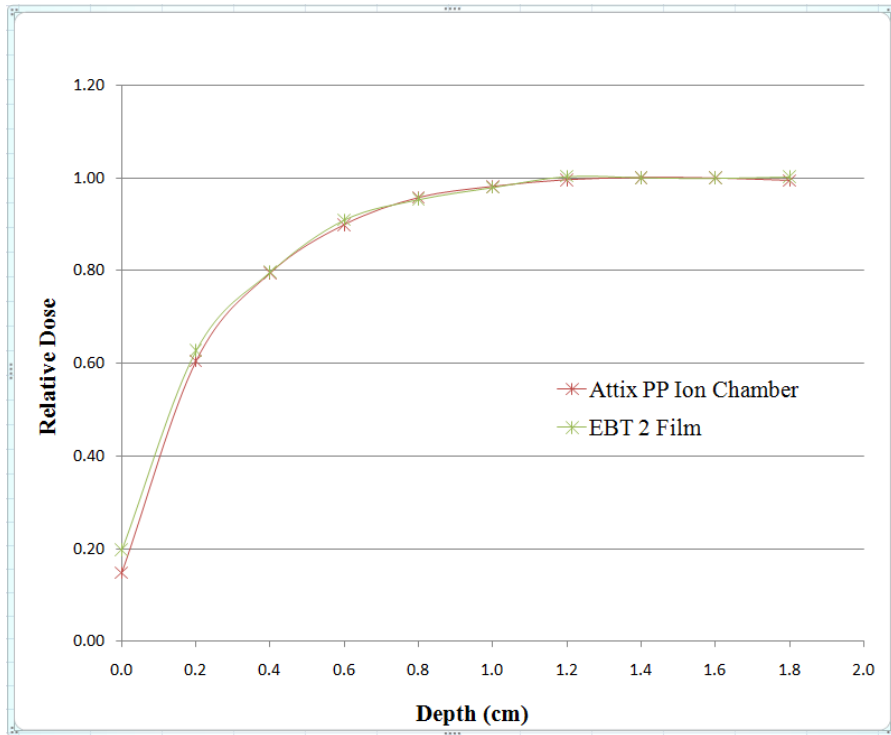


Figure 3.1: A comparison of EBT 2 film and Attix pp ion chamber RD graphs for 6 MV x 100 cm SSD x Open Field (10 x 10 cm<sup>2</sup> FS).

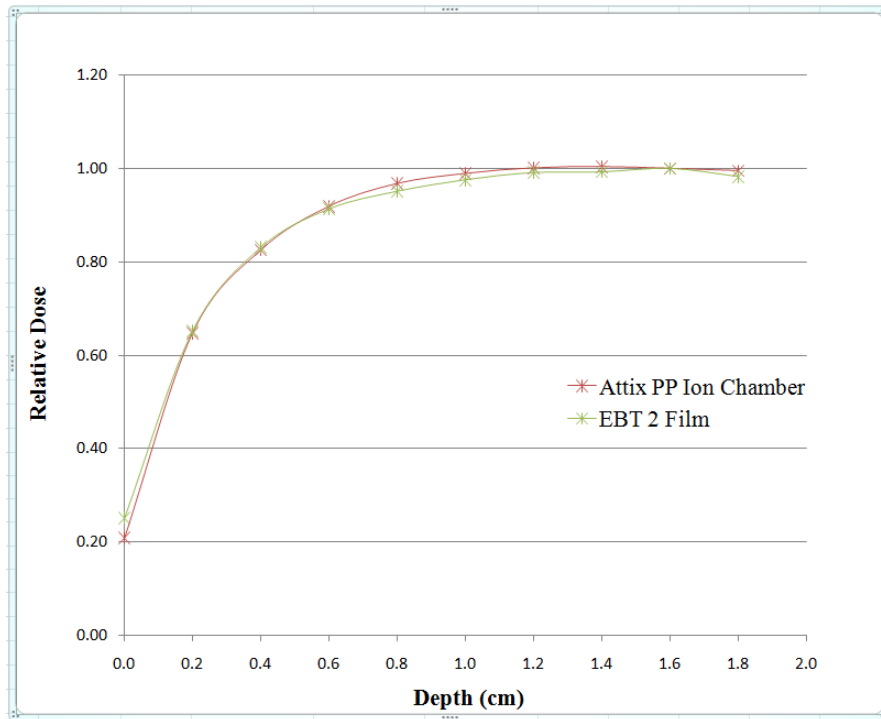


Figure 3.2: A comparison of EBT 2 film and Attix pp ion chamber RD graphs for 6 MV x 100 cm SSD x EDW (15°) Field (15 x 15 cm<sup>2</sup> FS).

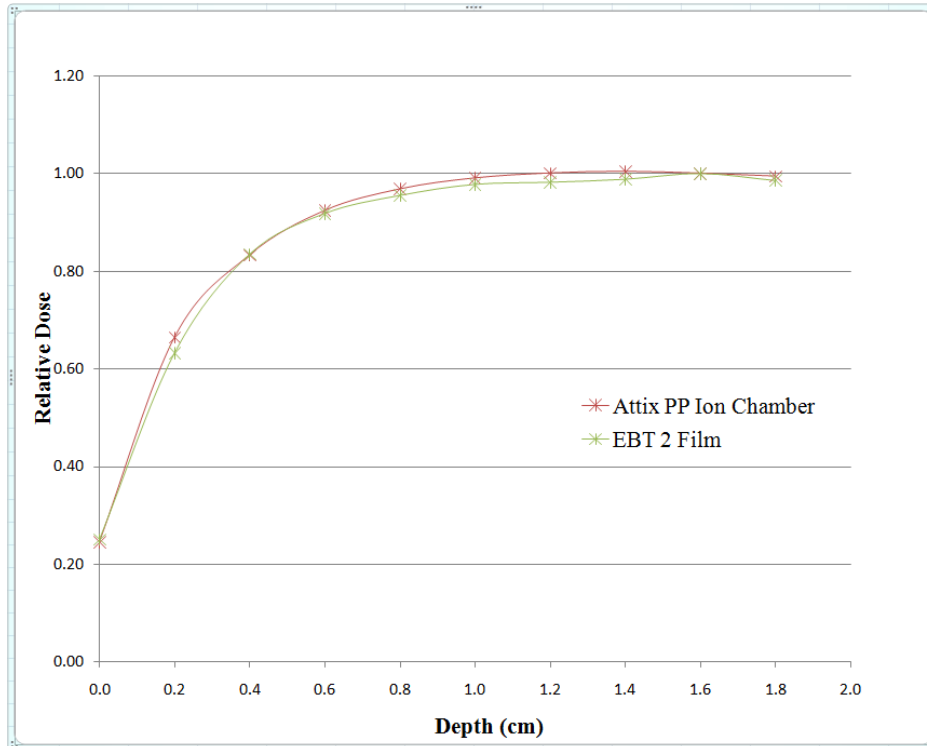


Figure 3.3: A comparison of EBT 2 film and Attix pp ion chamber RD graphs for 6 MV x 100 cm SSD x EDW (60°) Field (15 x 15 cm<sup>2</sup> FS).

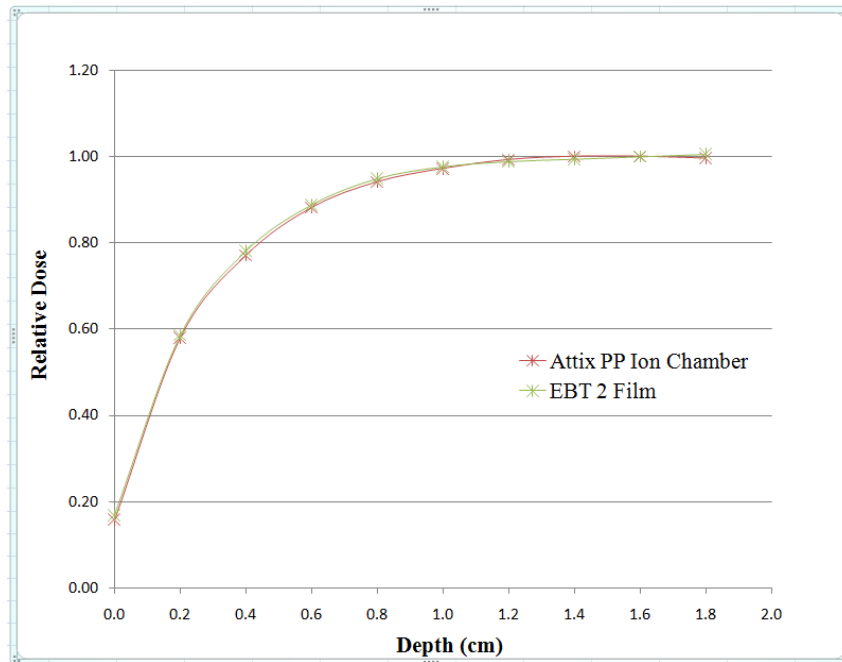


Figure 3.4: A comparison of EBT 2 film and Attix pp ion chamber RD graphs for 6 MV x 100 cm SSD x PW (15°) Field (10 x 10 cm<sup>2</sup> FS).

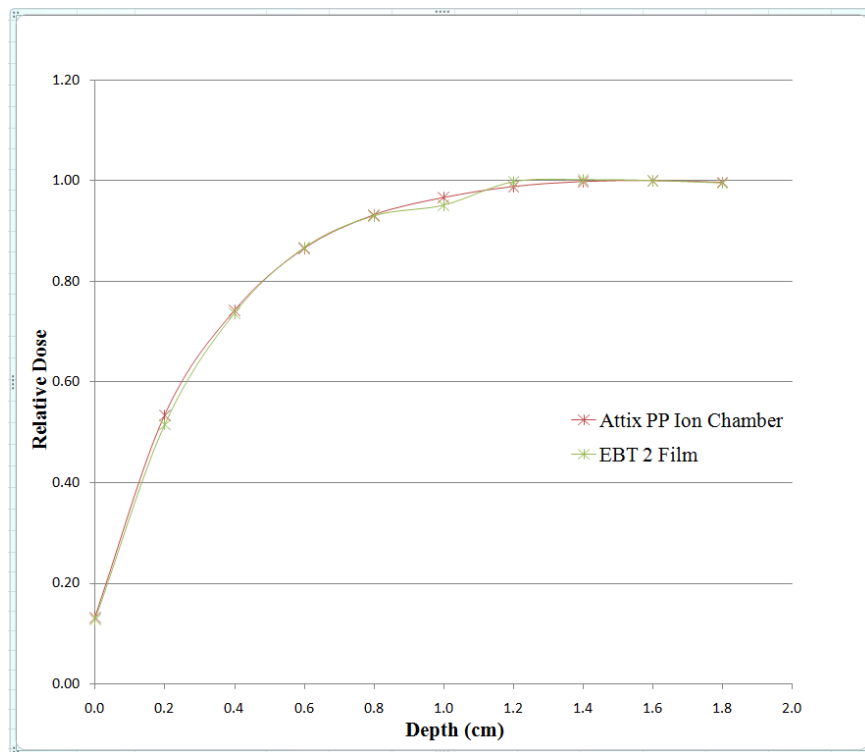


Figure 3.5: A comparison of EBT 2 film and Attix pp ion chamber RD graphs for 6 MV x 100 cm SSD x PW (60°) Field (10 x 10 cm<sup>2</sup> FS).

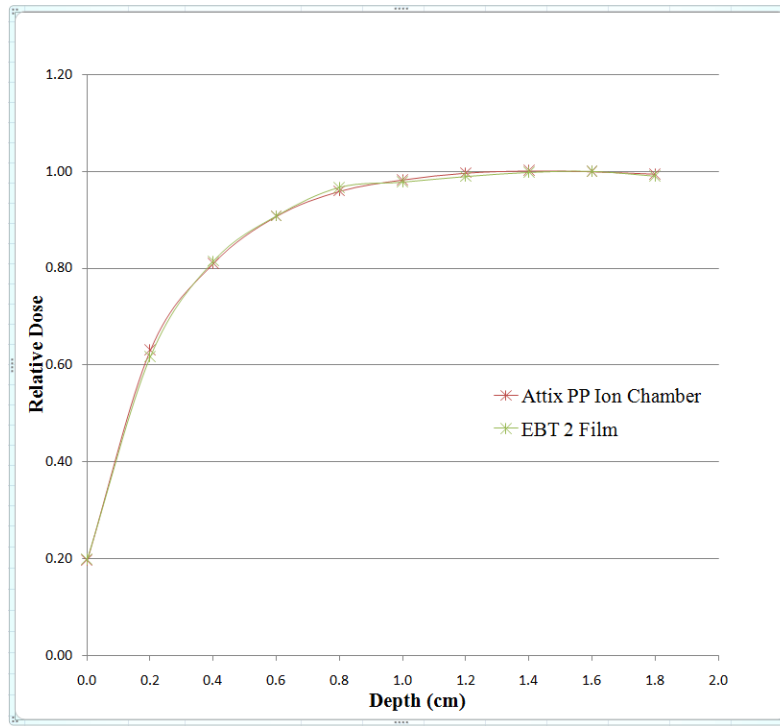


Figure 3.6: A comparison of EBT 2 film and Attix pp ion chamber RD graphs for 6 MV x 100 cm SSD x Block Tray Field (10 x 10 cm<sup>2</sup> FS).

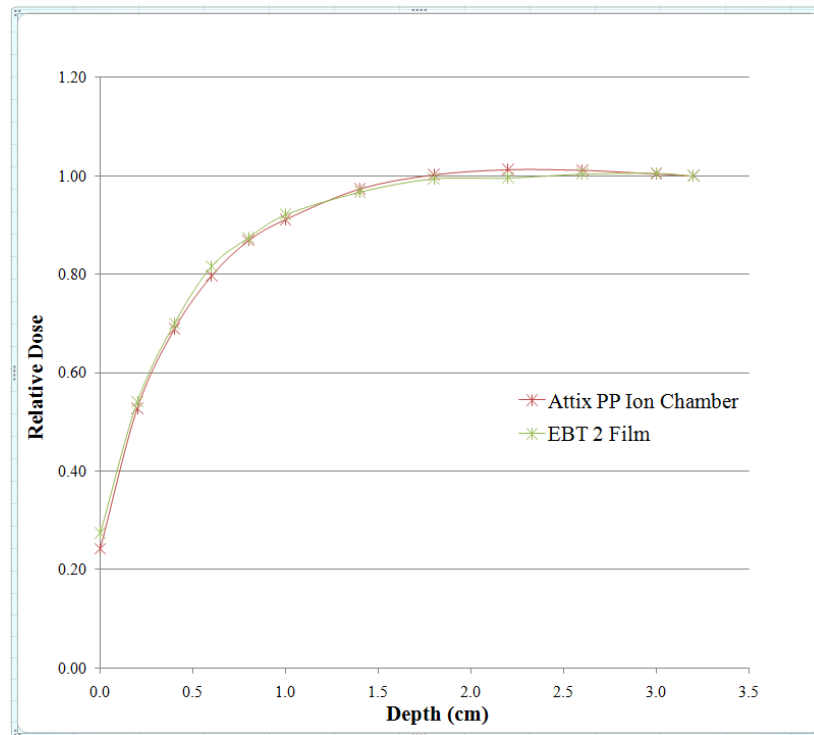


Figure 3.7: A comparison of EBT 2 film and Attix pp ion chamber RD graphs for 15 MV x 100 cm SSD x Open Field (20 x 20 cm<sup>2</sup> FS).

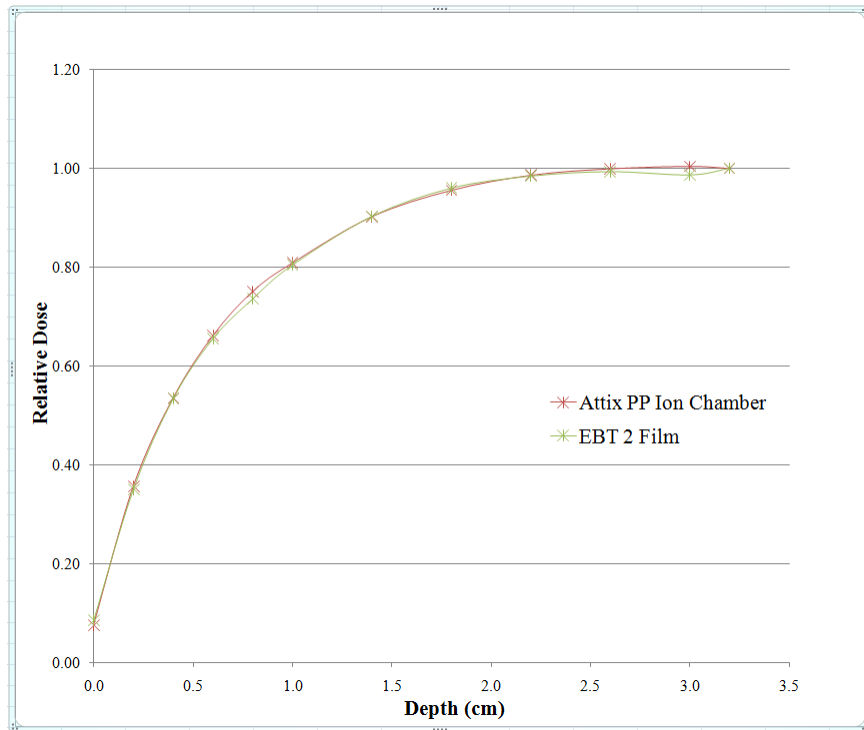


Figure 3.8: A comparison of EBT 2 film and Attix pp ion chamber RD graphs for 15 MV x 100 cm SSD x EDW (15°) Field (5 x 5 cm<sup>2</sup> FS).

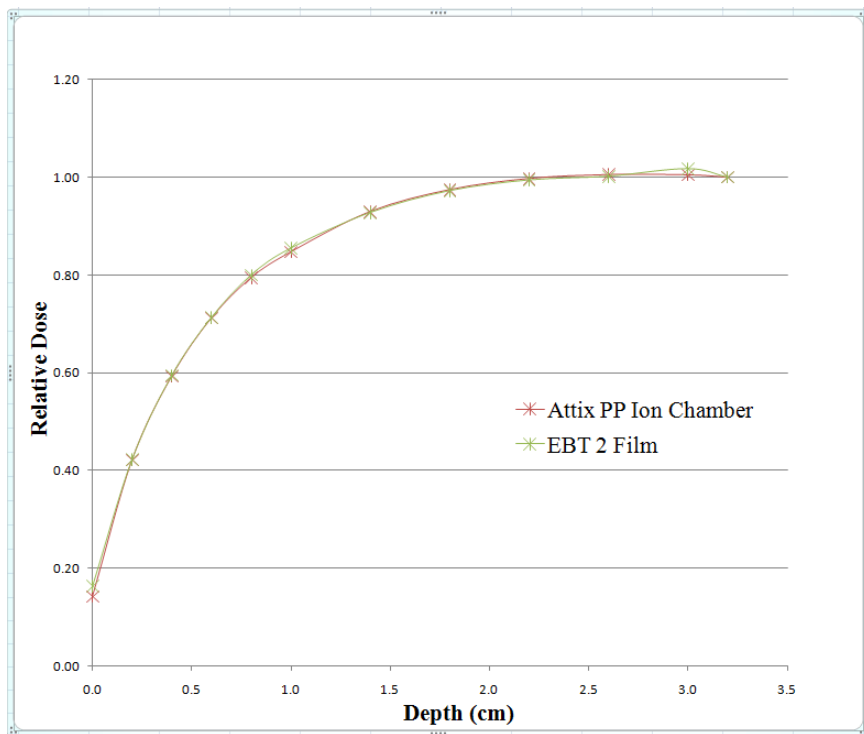


Figure 3.9: A comparison of EBT 2 film and Attix pp ion chamber RD graphs for 15 MV x 100 cm SSD x EDW (60°) Field (10 x 10 cm<sup>2</sup> FS).

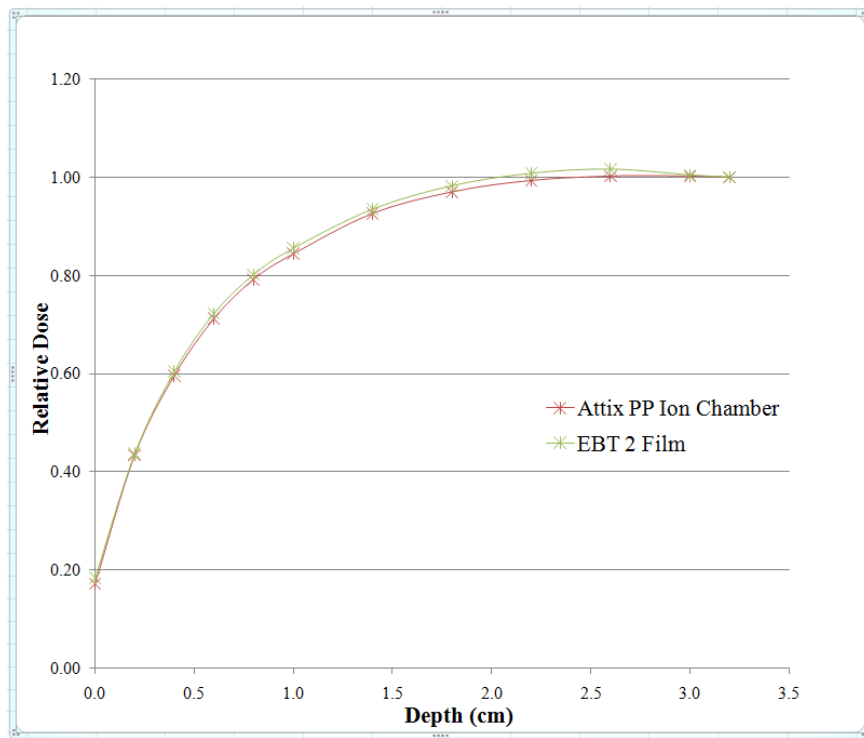


Figure 3.10: A comparison of EBT 2 film and Attix pp ion chamber RD graphs for 15 MV x 100 cm SSD x PW (15°) Field (15 x 15 cm<sup>2</sup> FS).

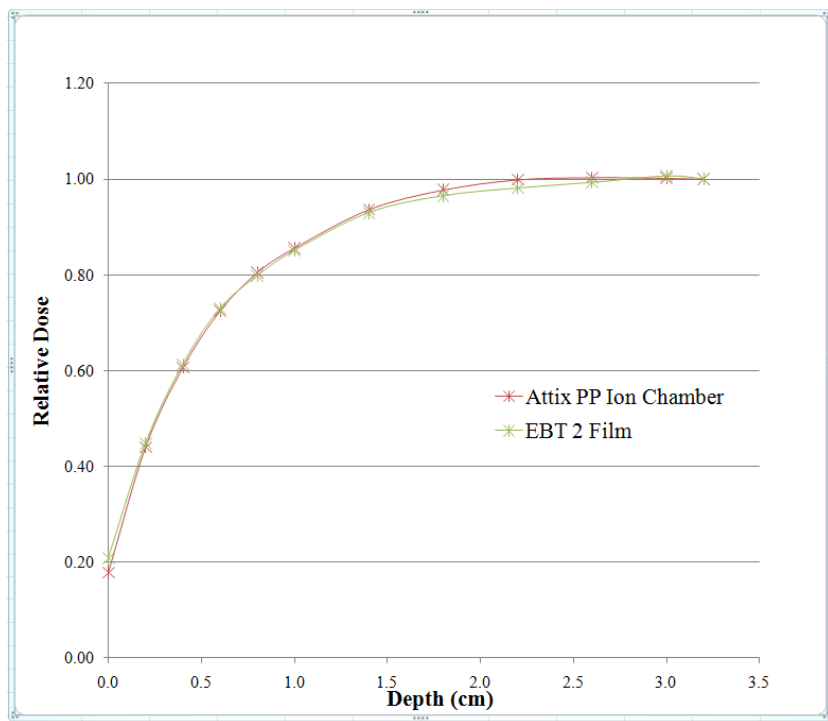


Figure 3.11: A comparison of EBT 2 film and Attix pp ion chamber RD graphs for 15 MV x 100 cm SSD x PW (60°) Field (15 x 15 cm<sup>2</sup> FS).

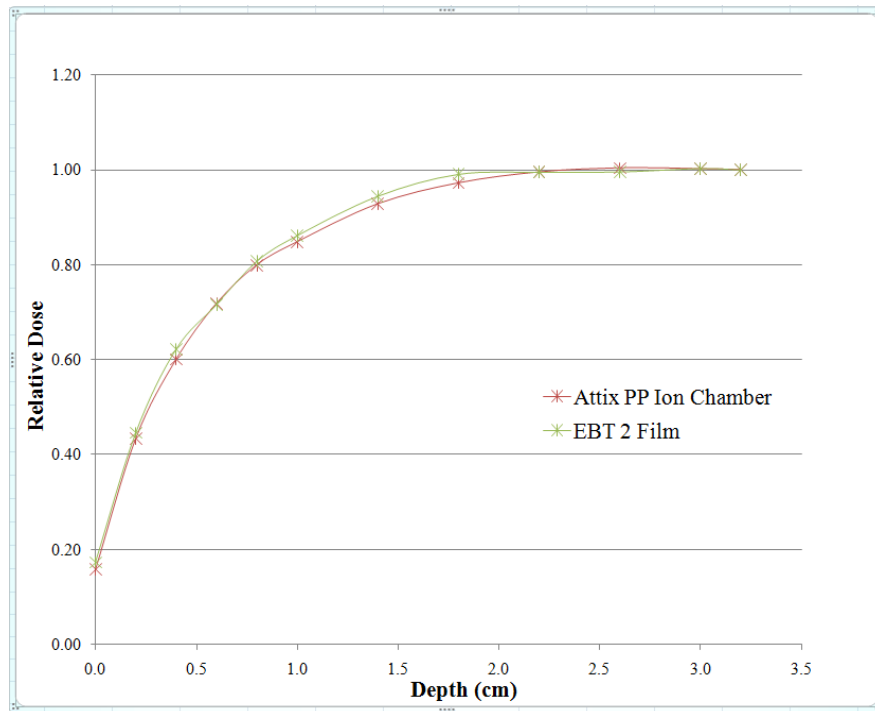


Figure 3.12: A comparison of EBT 2 film and Attix pp ion chamber RD graphs for 15 MV x 100 cm SSD x Block Tray Field (10 x 10 cm<sup>2</sup> FS).

### 3.1.2 Measured and Calculated Buildup Doses

Pinnacle<sup>3</sup> was originally commissioned with measured data obtained using a cylindrical ionization chamber in a water phantom. Measured and calculated buildup doses using Attix pp ion chamber and Pinnacle<sup>3</sup> respectively, were performed for a variety of clinical setups involving 6 MV and 15 MV photon beams, 85 cm SSD, 100 cm SSD, 120 cm SSD, open fields, enhanced dynamic wedge fields (angles 30 and 60 degrees), physical wedge fields (angles 15, 30, 45 and 60 degrees), block tray fields and field sizes of 3 x 3, 4 x 4, 5 x 5, 8 x 8, 10 x 10, 12 x 12, 15 x 15, 20 x 20 and 30 x 30 cm<sup>2</sup>. The total number of clinical setups for which measurements and calculations of buildup doses were performed was 342 (171 each for the 6 MV and 15 MV photon beams). For each clinical setup, the relative dose versus depth graph (RD graph) of Attix

pp ion chamber buildup dose measurements and the RD graph of Pinnacle<sup>3</sup> buildup dose calculations were plotted and compared. The comparison of these RD graphs, plotted for the 342 clinical setups, was done in order to also have a pictorial view of the differences between experimentally measured (Exp.) buildup dose using Attix pp ion chamber and the buildup dose calculated by Pinnacle<sup>3</sup> (P3). A total of 684 RD graphs (i.e. 342 pairs of RD graphs) were plotted and analyzed. As was previously stated, the limitation of space does not allow the presentation of all the RD graphs plotted but some these graphs, which are a general representation of all the RD graphs plotted, are as shown in Figures 3.13 to 3.32. The mean absolute dose difference between all Attix chamber measured and Pinnacle<sup>3</sup> calculated buildup dose values was  $6.3\% \pm 11.9\%$  (1SD) for the 6 MV photon beam and  $2.6 \pm 4.1\%$  (1SD) for the 15 MV photon beam.

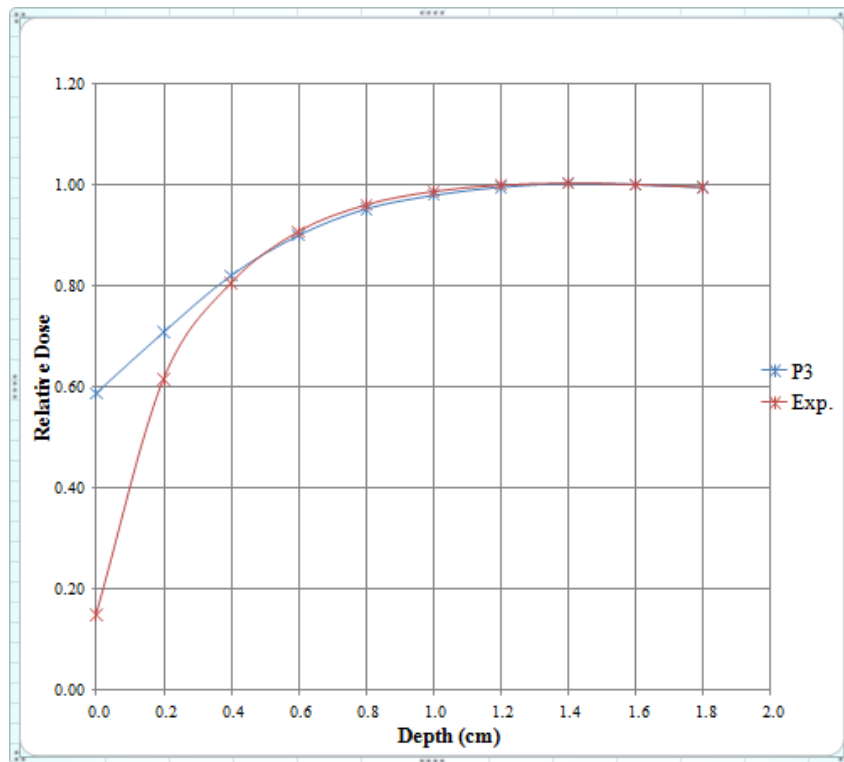


Figure 3.13: RD graphs for 6 MV x 85 cm SSD x Open Field (10 x 10 cm<sup>2</sup> FS).

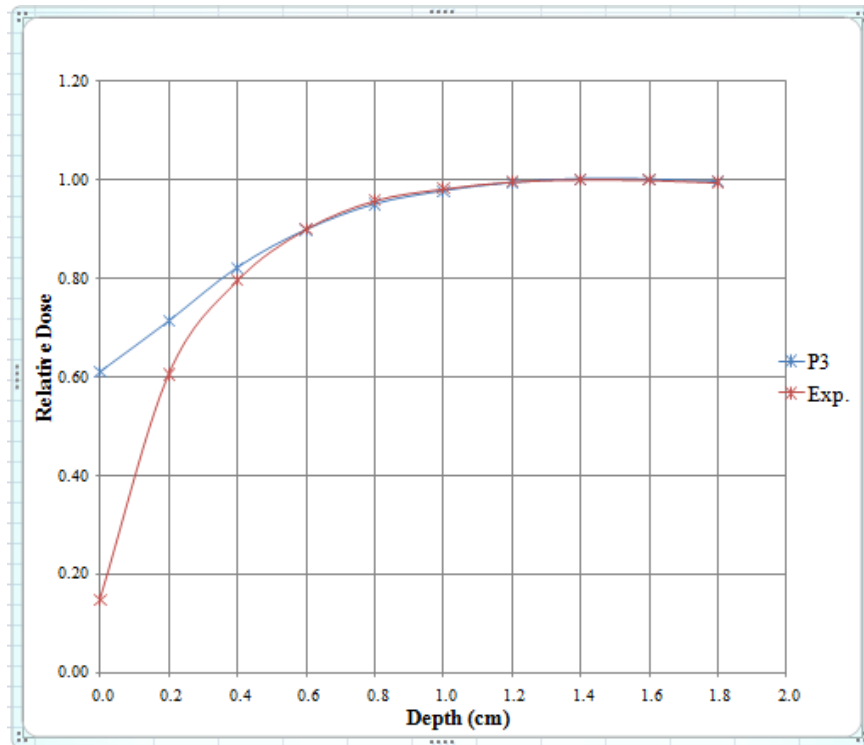


Figure 3.14: RD graphs for 6 MV x 100 cm SSD x Open Field (10 x 10 cm<sup>2</sup> FS).

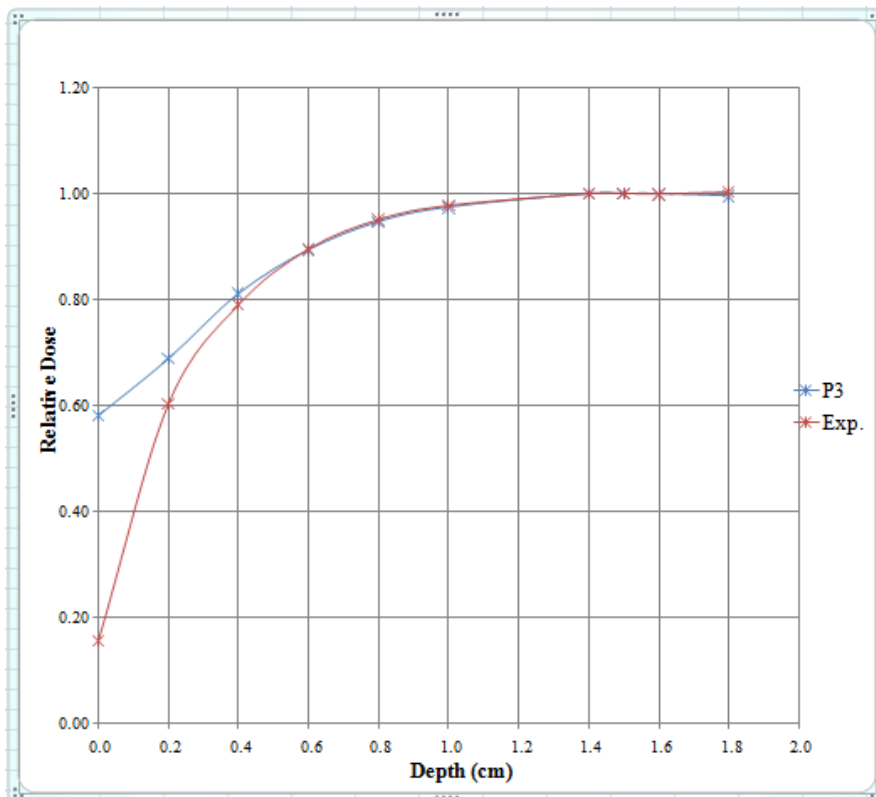


Figure 3.15: RD graphs for 6 MV x 120 cm SSD x Open Field (10 x 10 cm<sup>2</sup> FS).

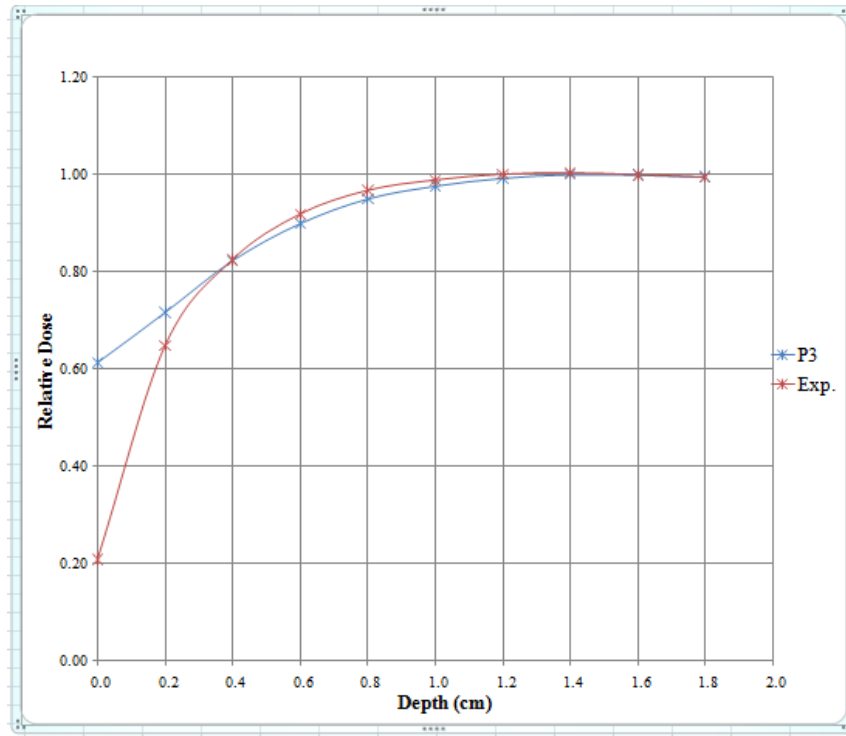


Figure 3.16: RD graphs for 6 MV x 100 cm SSD x EDW (15°) Field (15 x 15 cm<sup>2</sup> FS).

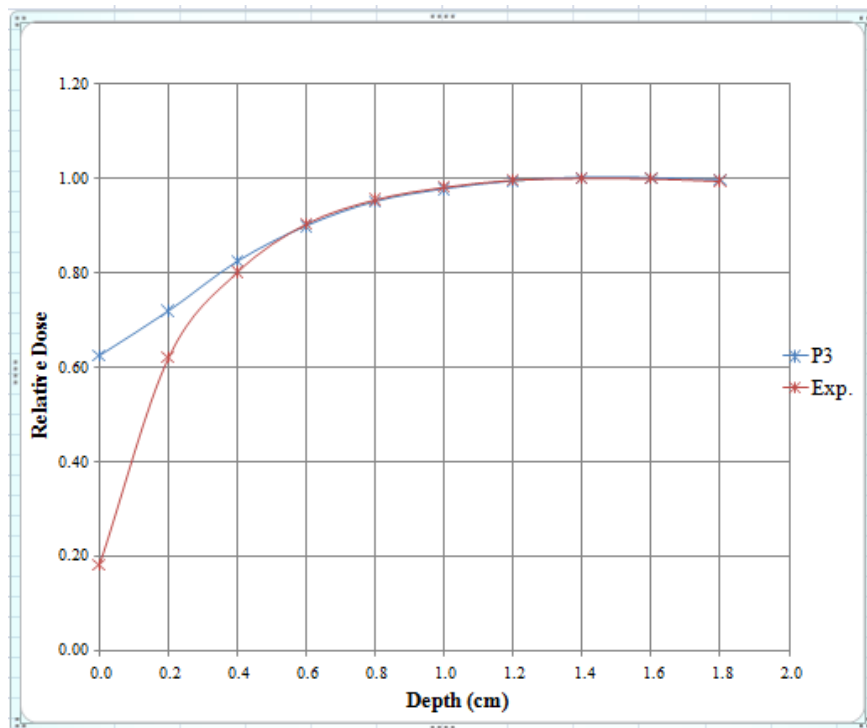


Figure 3.17: RD graphs for 6 MV x 100 cm SSD x EDW (60°) Field (10 x 10 cm<sup>2</sup> FS).

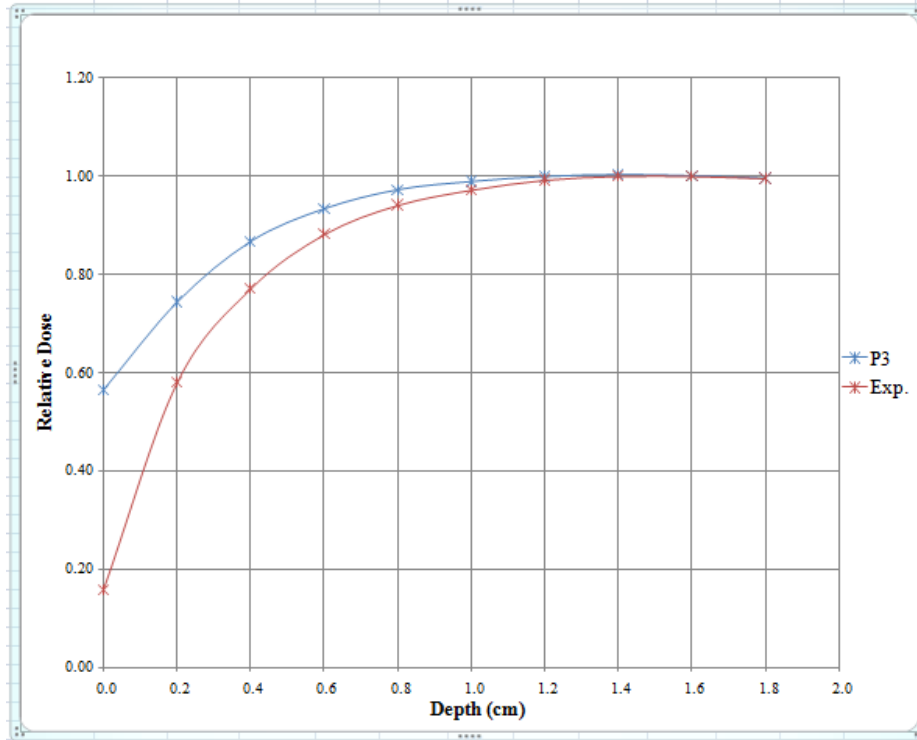


Figure 3.18: RD graphs for 6 MV x 100 cm SSD x PW (15°) Field (10 x 10 cm<sup>2</sup> FS).

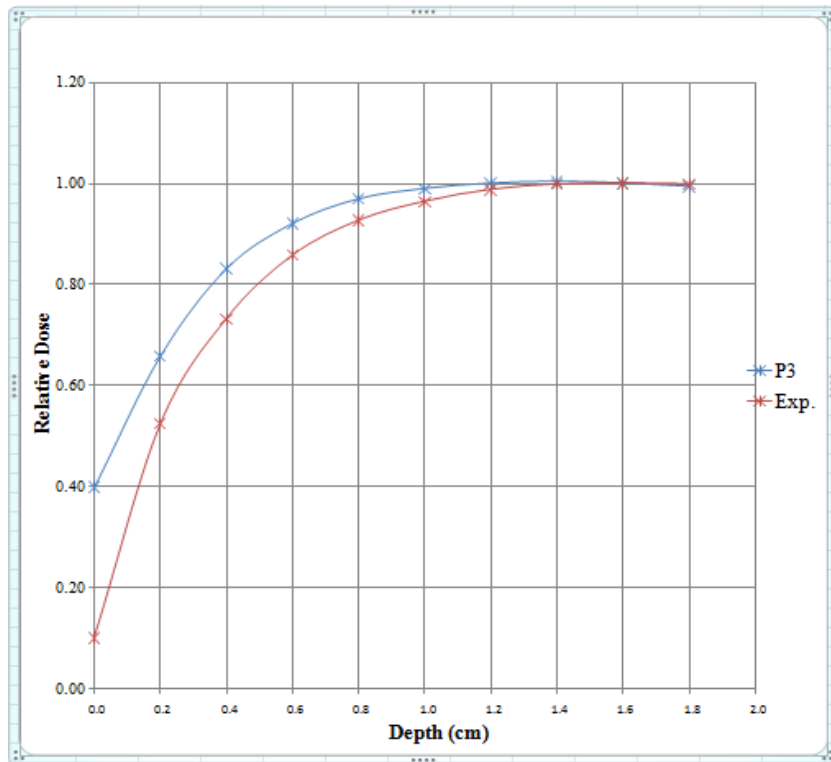


Figure 3.19: RD graphs for 6 MV x 100 cm SSD x PW (30°) Field (5 x 5 cm<sup>2</sup> FS).

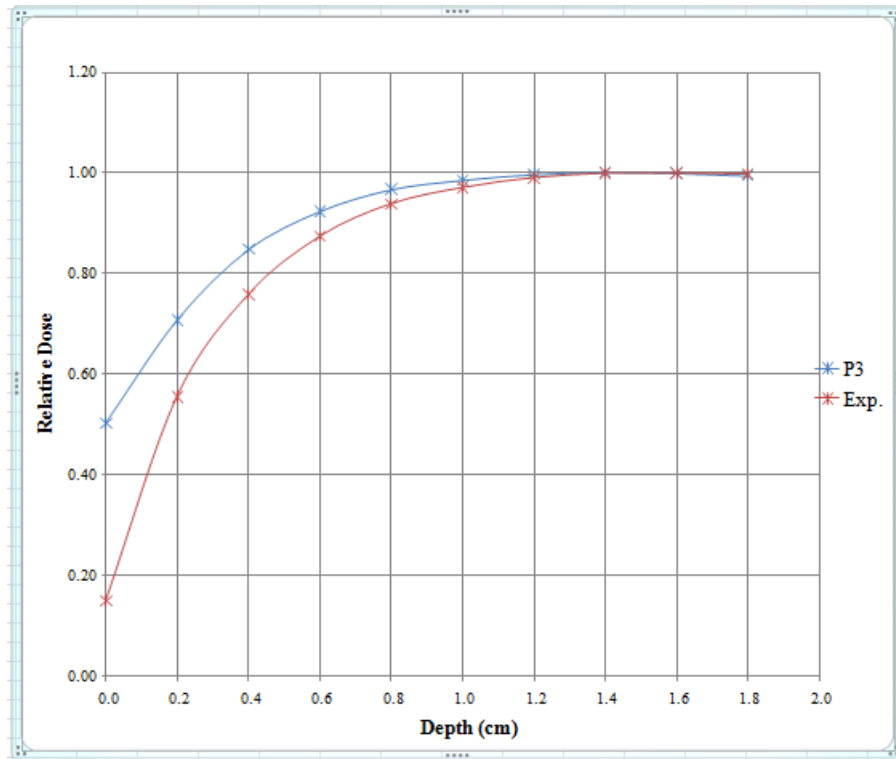


Figure 3.20: RD graphs for 6 MV x 100 cm SSD x PW (45°) Field (12 x 12 cm<sup>2</sup> FS).

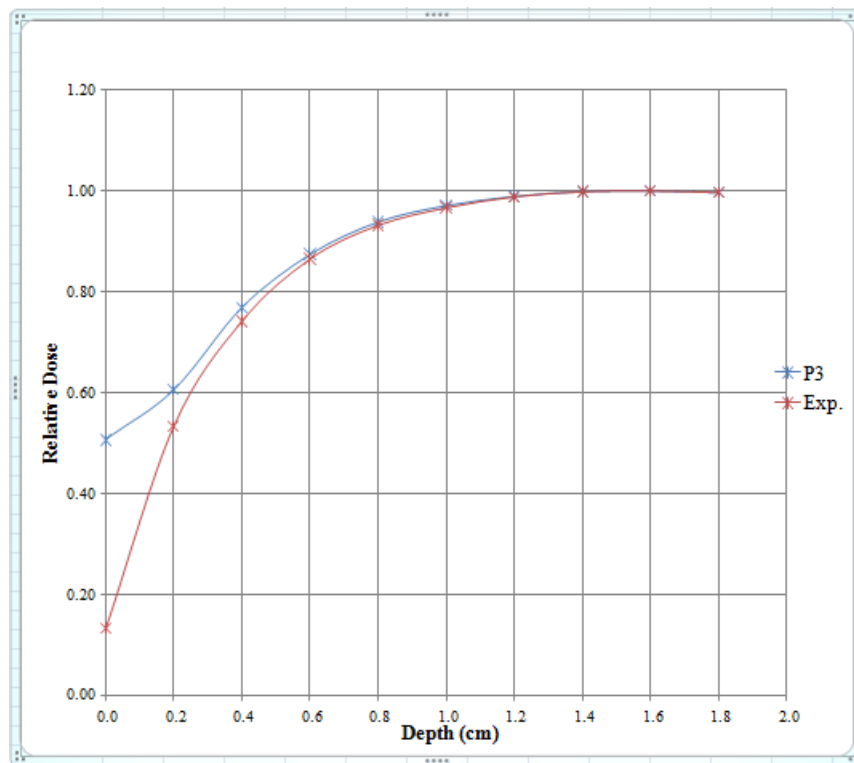


Figure 3.21: RD graphs for 6 MV x 100 cm SSD x PW (60°) Field (10 x 10 cm<sup>2</sup> FS).

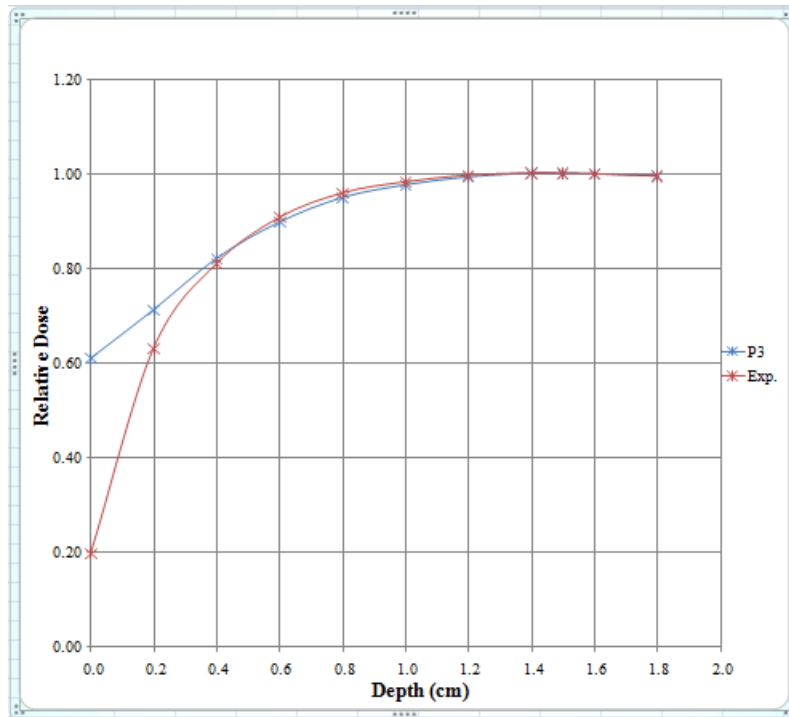


Figure 3.22: RD graphs for 6 MV x 100 cm SSD x Block Tray Field (10 x 10 cm<sup>2</sup> FS).

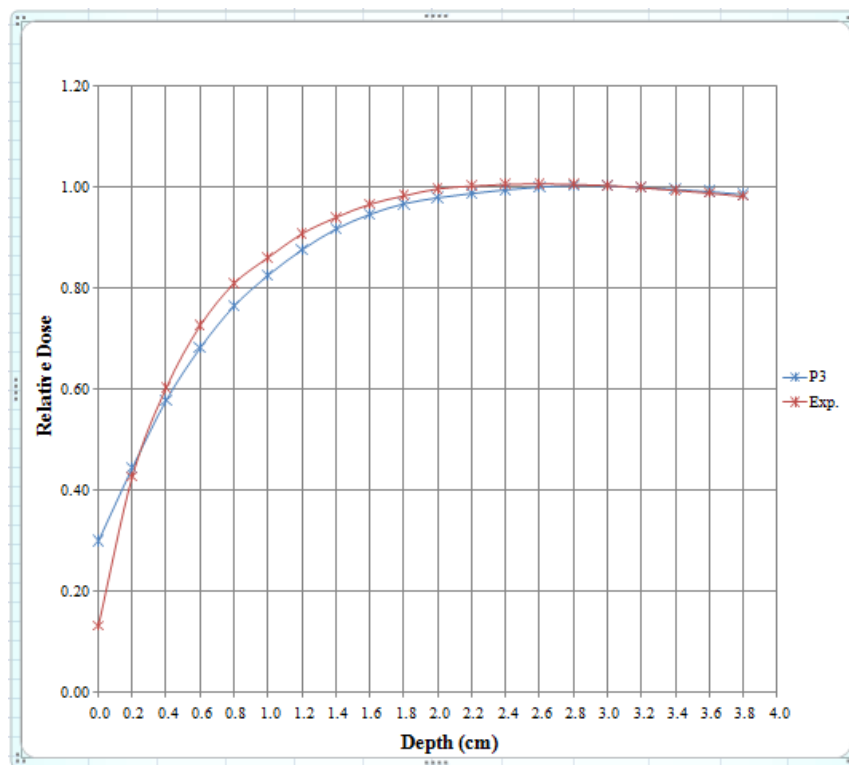


Figure 3.23: RD graphs for 15 MV x 85 cm SSD x Open Field (10 x 10 cm<sup>2</sup> FS).

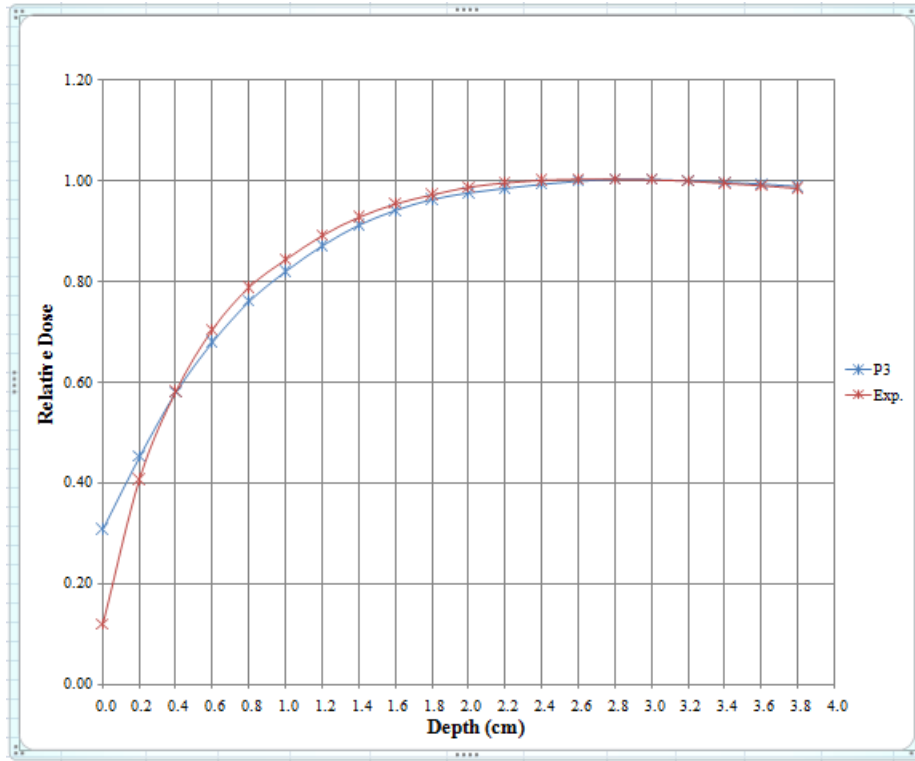


Figure 3.24: RD graphs for 15 MV x 100 cm SSD x Open Field (10 x 10 cm<sup>2</sup> FS).

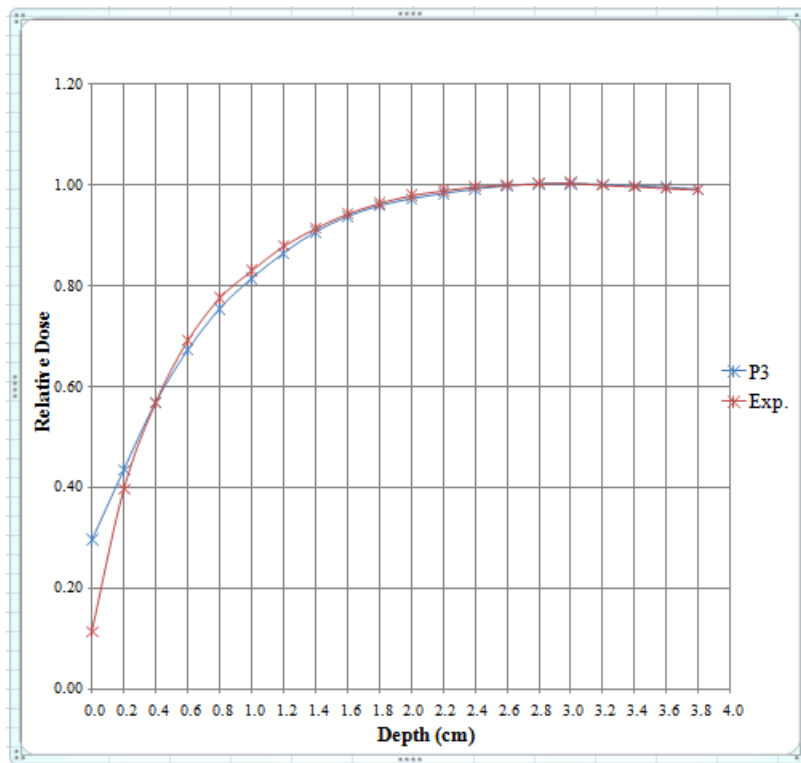


Figure 3.25: RD graphs for 15 MV x 120 cm SSD x Open Field (10 x 10 cm<sup>2</sup> FS).

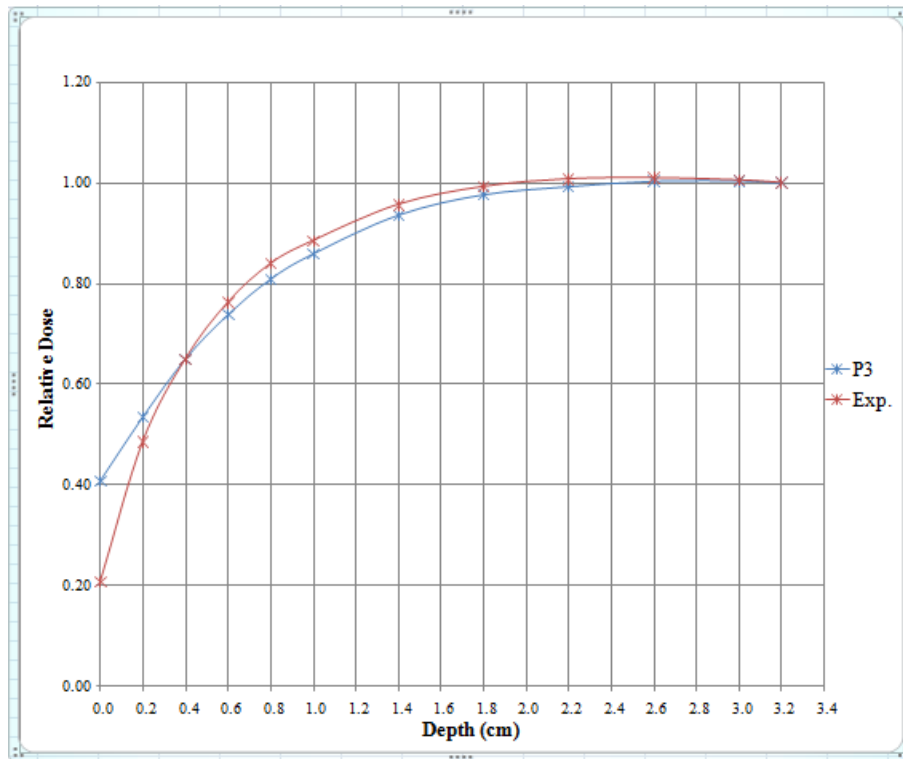


Figure 3.26: RD graphs for 15 MV x 100 cm SSD x EDW (15°) Field (15 x 15 cm<sup>2</sup> FS).

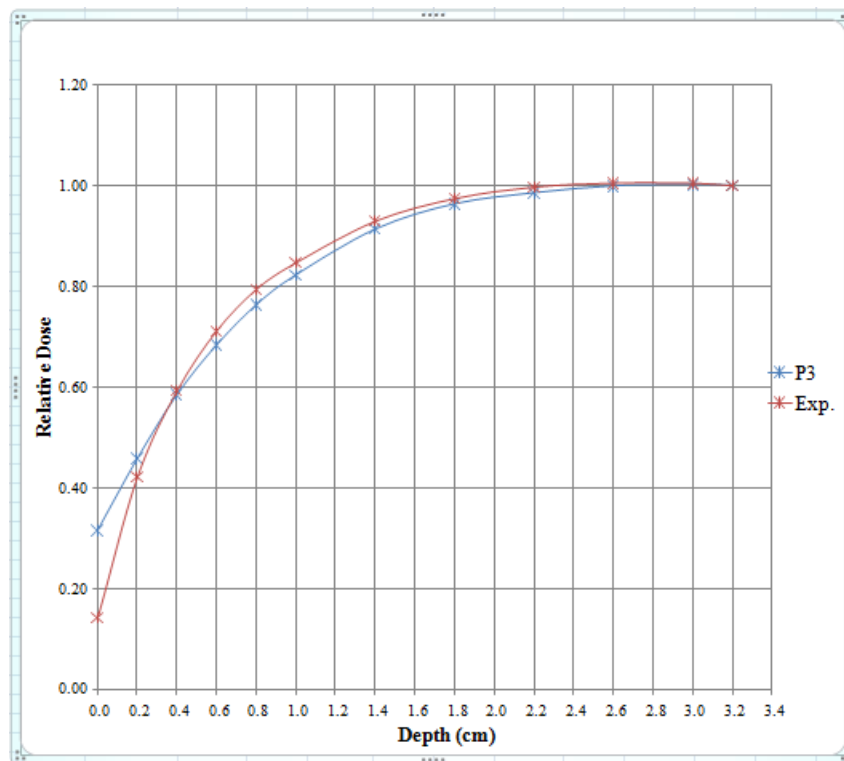


Figure 3.27: RD graphs for 15 MV x 100 cm SSD x EDW (60°) Field (10 x 10 cm<sup>2</sup> FS).

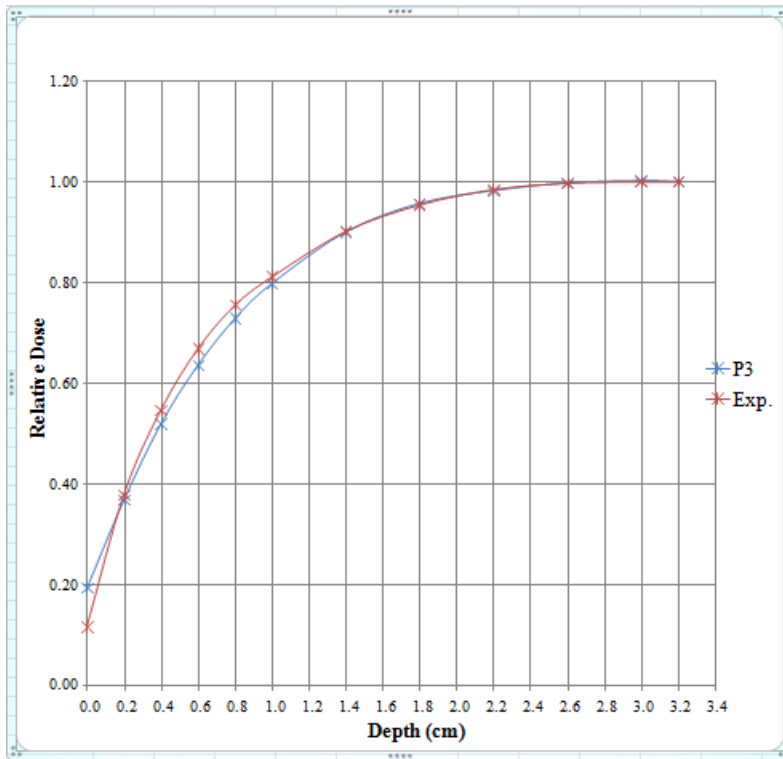


Figure 3.28: RD graphs for 15 MV x 100 cm SSD x PW (15°) Field (10 x 10 cm<sup>2</sup> FS).

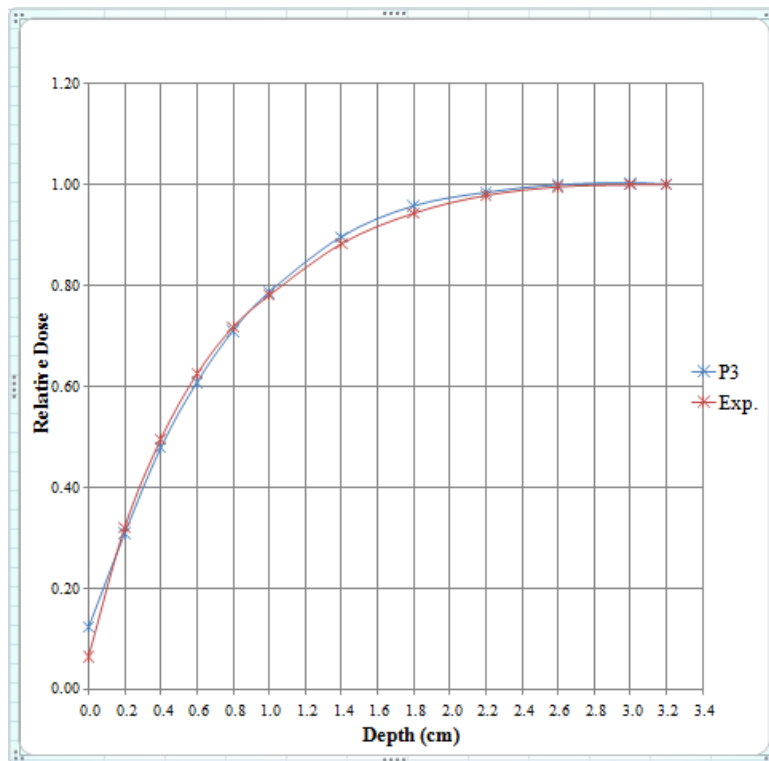


Figure 3.29: RD graphs for 15 MV x 100 cm SSD x PW (30°) Field (5 x 5 cm<sup>2</sup> FS).

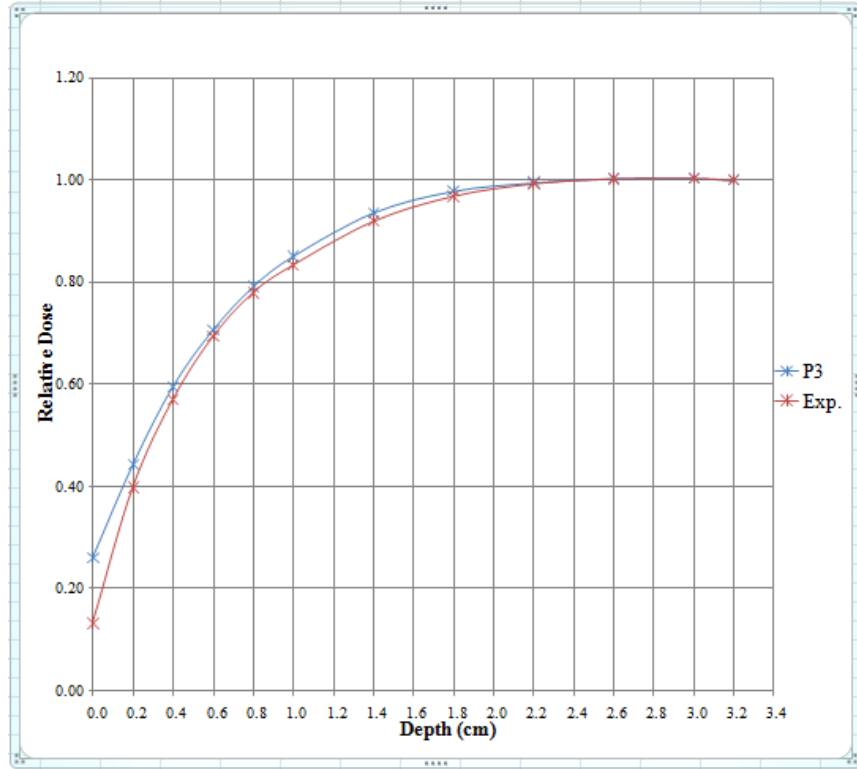


Figure 3.30: RD graphs for 15 MV x 100 cm SSD x PW (45°) Field (12 x 12 cm<sup>2</sup> FS).

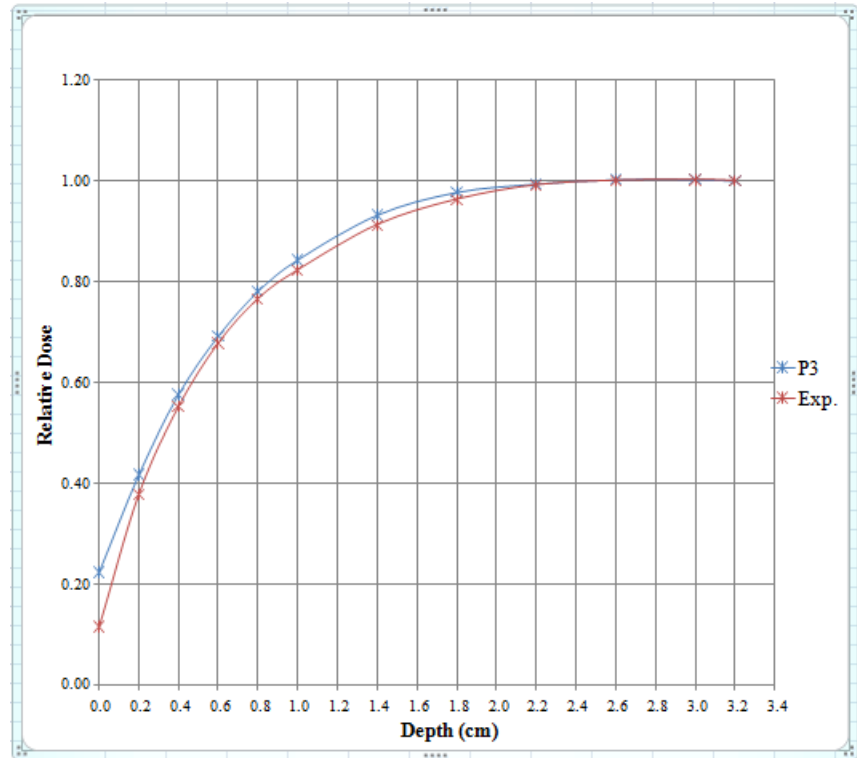


Figure 3.31: RD graphs for 15 MV x 100 cm SSD x PW (60°) Field (10 x 10 cm<sup>2</sup> FS).

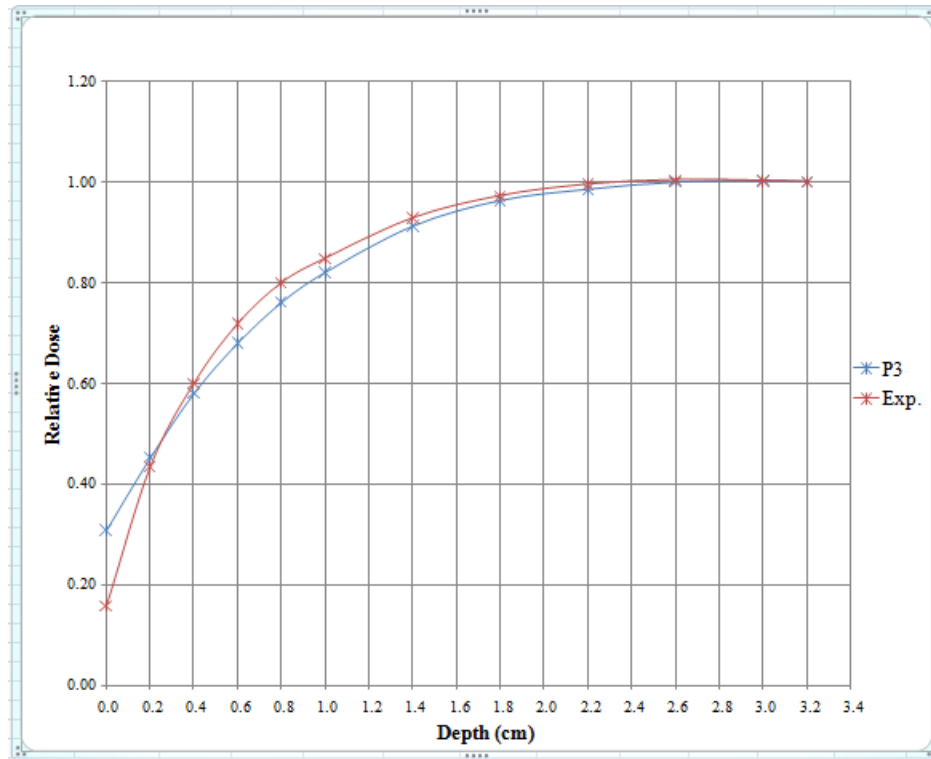


Figure 3.32: RD graphs for 15 MV x 100 cm SSD x Block Tray Field (10 x 10 cm<sup>2</sup> FS).

### 3.1.3 Analysis of Measured and Calculated Buildup Doses

Experimentally measured (using Attix pp ion chamber) and calculated (using P3) buildup doses were analyzed for all the clinical setups for which measurements were performed. The dose-difference (DD) and distance-to-agreement (DTA) technique was used for the analysis of these dose points. Equation (1.4) was used to calculate the dose differences for various points while the distance to agreement (DTA) was determined from the relative dose graphs. It is important to use the DTA technique which complements the simple DD technique as it has been reported that the DD is overly sensitive in regions of high dose gradients (Harms et al., 1998) which happens in the dose buildup regions of the photon beams. The results were analyzed using Venselaar et al. (2001) criteria as well as much tighter criteria of less than 2% or 2 mm, i.e., dose difference less than 2% or distance to agreement less than 2 mm. Summaries of the analysis of

the results based on Venselaar et al. (2001) criteria are as shown in Tables 3.1 to 3.16 while Tables 3.17 to 3.32 show summaries of the results meeting the criteria of less than 2% or 2 mm.

Table 3.1: Summary of the analysis of the results based on Venselaar et al. (2001) criteria for 6 MV x Open Fields.

<b>6 MV x Open Fields</b>	<b>85 cm SSD</b>	<b>100 cm SSD</b>	<b>120 cm SSD</b>	<b>Total</b>
Number of dose points	80	80	80	240
Number of points meeting Venselaar et al. (2001) criteria of DD < 10% or DTA < 2 mm	78	77	76	231
Percent of points meeting the criteria	97.5%	96.3%	95.0%	96.3%

Table 3.2: Summary of the analysis of the results based on Venselaar et al. (2001) criteria for 6 MV x EDW (15°) Fields.

<b>6 MV x EDW (15 degrees) Fields</b>	<b>85 cm SSD</b>	<b>100 cm SSD</b>	<b>120 cm SSD</b>	<b>Total</b>
Number of dose points	70	70	70	210
Number of points meeting Venselaar et al. (2001) criteria of DD < 15% or DTA < 3 mm	70	70	70	210
Percent of points meeting the criteria	100.0%	100.0%	100.0%	100.0%

Table 3.3: Summary of the analysis of the results based on Venselaar et al. (2001) criteria for 6 MV x EDW (60°) Fields.

<b>6 MV x EDW (60 degrees) Fields</b>	<b>85 cm SSD</b>	<b>100 cm SSD</b>	<b>120 cm SSD</b>	<b>Total</b>
Number of dose points	70	70	70	210
Number of points meeting Venselaar et al. (2001) criteria of DD < 15% or DTA < 3 mm	70	70	70	210
Percent of points meeting the criteria	100.0%	100.0%	100.0%	100.0%

Table 3.4: Summary of the analysis of the results based on Venselaar et al. (2001) criteria for 6 MV x PW (15°) Fields.

<b>6 MV x PW (15 degrees) Fields</b>	<b>85 cm SSD</b>	<b>100 cm SSD</b>	<b>120 cm SSD</b>	<b>Total</b>
Number of dose points	70	70	70	210
Number of points meeting Venselaar et al. (2001) criteria of DD < 15% or DTA < 3 mm	70	70	69	209
Percent of points meeting the criteria	100.0%	100.0%	98.6%	99.5%

Table 3.5: Summary of the analysis of the results based on Venselaar et al. (2001) criteria for 6 MV x PW (30°) Fields.

<b>6 MV x PW (30 degrees) Fields</b>	<b>85 cm SSD</b>	<b>100 cm SSD</b>	<b>120 cm SSD</b>	<b>Total</b>
Number of dose points	70	70	70	210
Number of points meeting Venselaar et al. (2001) criteria of DD < 15% or DTA < 3 mm	70	69	68	207
Percent of points meeting the criteria	100.0%	98.6%	97.1%	98.6%

Table 3.6: Summary of the analysis of the results based on Venselaar et al. (2001) criteria for 6 MV x PW (45°) Fields.

<b>6 MV x PW (45 degrees) Fields</b>	<b>85 cm SSD</b>	<b>100 cm SSD</b>	<b>120 cm SSD</b>	<b>Total</b>
Number of dose points	70	70	70	210
Number of points meeting Venselaar et al. (2001) criteria of DD < 15% or DTA < 3 mm	70	70	70	210
Percent of points meeting the criteria	100.0%	100.0%	100.0%	100.0%

Table 3.7: Summary of the analysis of the results based on Venselaar et al. (2001) criteria for 6 MV x PW (60°) Fields.

<b>6 MV x PW (60 degrees) Fields</b>	<b>85 cm SSD</b>	<b>100 cm SSD</b>	<b>120 cm SSD</b>	<b>Total</b>
Number of dose points	60	60	60	180
Number of points meeting Venselaar et al. (2001) criteria of DD < 15% or DTA < 3 mm	60	60	60	180
Percent of points meeting the criteria	100.0%	100.0%	100.0%	100.0%

Table 3.8: Summary of the analysis of the results based on Venselaar et al. (2001) criteria for 6 MV x Block Tray Fields.

<b>6 MV x Block Tray Fields</b>	<b>85 cm SSD</b>	<b>100 cm SSD</b>	<b>120 cm SSD</b>	<b>Total</b>
Number of dose points	80	80	80	240
Number of points meeting Venselaar et al. (2001) criteria of DD < 15% or DTA < 3 mm	79	80	80	239
Percent of points meeting the criteria	98.8%	100.0%	100.0%	99.6%

Table 3.9: Summary of the analysis of the results based on Venselaar et al. (2001) criteria for 15 MV x Open Fields.

<b>15 MV x Open Fields</b>	<b>85 cm SSD</b>	<b>100 cm SSD</b>	<b>120 cm SSD</b>	<b>Total</b>
Number of dose points	160	160	160	480
Number of points meeting Venselaar et al. (2001) criteria of DD < 10% or DTA < 2 mm	160	160	160	480
Percent of points meeting the criteria	100.0%	100.0%	100.0%	100.0%

Table 3.10: Summary of the analysis of the results based on Venselaar et al. (2001) criteria for 15 MV x EDW (15°) Fields.

<b>15 MV x EDW (15 degrees) Fields</b>	<b>85 cm SSD</b>	<b>100 cm SSD</b>	<b>120 cm SSD</b>	<b>Total</b>
Number of dose points	84	84	84	252
Number of points meeting Venselaar et al. (2001) criteria of DD < 15% or DTA < 3 mm	84	84	84	252
Percent of points meeting the criteria	100.0%	100.0%	100.0%	100.0%

Table 3.11: Summary of the analysis of the results based on Venselaar et al. (2001) criteria for 15 MV x EDW (60°) Fields.

<b>15 MV x EDW (60 degrees) Fields</b>	<b>85 cm SSD</b>	<b>100 cm SSD</b>	<b>120 cm SSD</b>	<b>Total</b>
Number of dose points	84	84	84	252
Number of points meeting Venselaar et al. (2001) criteria of DD < 15% or DTA < 3 mm	84	84	84	252
Percent of points meeting the criteria	100.0%	100.0%	100.0.0%	100.0%

Table 3.12: Summary of the analysis of the results based on Venselaar et al. (2001) criteria for 15 MV x PW (15°) Fields.

<b>15 MV x PW (15 degrees) Fields</b>	<b>85 cm SSD</b>	<b>100 cm SSD</b>	<b>120 cm SSD</b>	<b>Total</b>
Number of dose points	84	84	84	252
Number of points meeting Venselaar et al. (2001) criteria of DD < 15% or DTA < 3 mm	84	84	84	252
Percent of points meeting the criteria	100.0%	100.0%	100.0%	100.0%

Table 3.13: Summary of the analysis of the results based on Venselaar et al. (2001) criteria for 15 MV x for PW (30°) Fields.

<b>15 MV x PW (30 degrees) Fields</b>	<b>85 cm SSD</b>	<b>100 cm SSD</b>	<b>120 cm SSD</b>	<b>Total</b>
Number of dose points	84	84	84	252
Number of points meeting Venselaar et al. (2001) criteria of DD < 15% or DTA < 3 mm	84	84	84	252
Percent of points meeting the criteria	100.0%	100.0%	100.0%	100.0%

Table 3.14: Summary of the analysis of the results based on Venselaar et al. (2001) criteria for 15 MV x PW (45°) Fields.

<b>15 MV x PW (45 degrees) Fields</b>	<b>85 cm SSD</b>	<b>100 cm SSD</b>	<b>120 cm SSD</b>	<b>Total</b>
Number of dose points	84	84	84	252
Number of points meeting Venselaar et al. (2001) criteria of DD < 15% or DTA < 3 mm	84	84	84	252
Percent of points meeting the criteria	100.0%	100.0%	100.0%	100.0%

Table 3.15: Summary of the analysis of the results based on Venselaar et al. (2001) criteria for 15 MV x PW (60°) Fields.

<b>15 MV x PW (60 degrees) Fields</b>	<b>85 cm SSD</b>	<b>100 cm SSD</b>	<b>120 cm SSD</b>	<b>Total</b>
Number of dose points	72	72	72	216
Number of points meeting Venselaar et al. (2001) criteria of DD < 15% or DTA < 3 mm	72	72	72	216
Percent of points meeting the criteria	100.0%	100.0%	100.0%	100.0%

Table 3.16: Summary of the analysis of the results based on Venselaar et al. (2001) criteria for 15 MV x Block Tray Fields.

<b>15 MV x Block Tray Fields</b>	<b>85 cm SSD</b>	<b>100 cm SSD</b>	<b>120 cm SSD</b>	<b>Total</b>
Number of dose points	96	96	96	228
Number of points meeting Venselaar et al. (2001) criteria of DD < 15% or DTA < 3 mm	93	96	96	285
Percent of points meeting the criteria	96.9%	100.0%	100.0%	99.0%

With reference to Tables 3.1 to 3.16,

1. for the 6 MV photon beam:

- (a) out of a total of 240 buildup dose values involving open field (simple geometry) measured (using Attix pp ion chamber) and calculated (using P3), 231 (96.3%) met the Venselaar et al. (2001) criteria of DD < 10% or DTA < 2 mm;
- (b) out of a total of 1,470 buildup dose values involving physical wedges, enhanced dynamic wedges and block tray (complex geometries) measured (using Attix pp ion chamber) and calculated (using P3), 1,465 (99.7%) met the Venselaar et al. (2001) criteria of DD < 15% or DTA < 3 mm;

2. for the 15 MV photon beam:

- (a) all the 480 buildup dose values involving open field (simple geometry) measured (using Attix pp ion chamber) and calculated (using P3) met the Venselaar et al. (2001) criteria of DD < 10% or DTA < 2 mm;
- (b) out of a total of 1,764 buildup dose values involving physical wedges, enhanced dynamic wedges and block tray (complex geometries) measured (using Attix pp ion chamber) and calculated (using P3), 1,761 (99.8%) met the Venselaar et al. (2001) criteria of DD < 15% or DTA < 3 mm.

As shown in these tables (i.e., Tables 3.1 to 3.16) most of the points were able to meet the criteria suggested by Venselaar et al. (2001). However the guidelines provided by these authors are quite liberal in order to accommodate a wide variety of treatment planning systems and the equipment available in many clinics in different countries. However a well equipped clinic and with access to treatment planning systems with superior dose calculation algorithms should meet much tighter criteria. The following tables (Tables 3.17 to 3.32) show analysis based on the criteria of 2% or 2 mm, which is most commonly used in radiation treatment field.

Table 3.17: Summary of the analysis of the results based on the criteria of less than 2% or 2 mm for 6 MV x Open Fields.

<b>6 MV x Open Fields</b>	<b>85 cm SSD</b>	<b>100 cm SSD</b>	<b>120 cm SSD</b>	<b>Total</b>
Number of dose points	80	80	80	240
Number of points meeting the criteria of DD < 2% or DTA < 2 mm	75	75	74	224
Percent of points meeting the criteria	93.8%	93.8%	92.5%	93.3%

Table 3.18: Summary of the analysis of the results based on the criteria of less than 2% or 2 mm for 6 MV x EDW (15°) Fields.

<b>6 MV x EDW (15 degrees) Fields</b>	<b>85 cm SSD</b>	<b>100 cm SSD</b>	<b>120 cm SSD</b>	<b>Total</b>
Number of dose points	70	70	70	210
Number of points meeting the criteria of DD < 2% or DTA < 2 mm	68	70	70	208
Percent of points meeting the criteria	97.1%	100.0%	100.0%	99.0%

Table 3.19: Summary of the analysis of the results based on the criteria of less than 2% or 2 mm for 6 MV x EDW (60°) Fields.

<b>6 MV x EDW (60 degrees) Fields</b>	<b>85 cm SSD</b>	<b>100 cm SSD</b>	<b>120 cm SSD</b>	<b>Total</b>
Number of dose points	70	70	70	210
Number of points meeting the criteria of DD < 2% or DTA < 2 mm	67	70	70	207
Percent of points meeting the criteria	95.7%	100.0%	100.0%	98.6%

Table 3.20: Summary of the analysis of the results based on the criteria of less than 2% or 2 mm for 6 MV x PW (15°) Fields.

<b>6 MV x PW (15 degrees) Fields</b>	<b>85 cm SSD</b>	<b>100 cm SSD</b>	<b>120 cm SSD</b>	<b>Total</b>
Number of dose points	70	70	70	210
Number of points meeting the criteria of DD < 2% or DTA < 2 mm	67	69	64	200
Percent of points meeting the criteria	95.7%	98.6%	91.4%	95.2%

Table 3.21: Summary of the analysis of the results based on the criteria of less than 2% or 2 mm for 6 MV x for PW (30°) Fields.

<b>6 MV x PW (30 degrees) Fields</b>	<b>85 cm SSD</b>	<b>100 cm SSD</b>	<b>120 cm SSD</b>	<b>Total</b>
Number of dose points	70	70	70	210
Number of points meeting the criteria of DD < 2% or DTA < 2 mm	54	54	53	161
Percent of points meeting the criteria	77.1%	77.1%	75.7%	76.7%

Table 3.22: Summary of the analysis of the results based on the criteria of less than 2% or 2 mm for 6 MV x PW (45°) Fields.

<b>6 MV x PW (45 degrees) Fields</b>	<b>85 cm SSD</b>	<b>100 cm SSD</b>	<b>120 cm SSD</b>	<b>Total</b>
Number of dose points	70	70	70	210
Number of points meeting the criteria of DD < 2% or DTA < 2 mm	70	70	65	205
Percent of points meeting the criteria	100.0%	100.0%	92.9%	97.6%

Table 3.23: Summary of the analysis of the results based on the criteria of less than 2% or 2 mm for 6 MV x PW (60°) Fields.

<b>6 MV x PW (60 degrees) Fields</b>	<b>85 cm SSD</b>	<b>100 cm SSD</b>	<b>120 cm SSD</b>	<b>Total</b>
Number of dose points	60	60	60	180
Number of points meeting the criteria of DD < 2% or DTA < 2 mm	60	60	60	180
Percent of points meeting the criteria	100.0%	100.0%	100.0%	100.0%

Table 3.24: Summary of the analysis of the results based on the criteria of less than 2% or 2 mm for 6 MV x Block Tray Fields.

<b>6 MV x Block Tray Fields</b>	<b>85 cm SSD</b>	<b>100 cm SSD</b>	<b>120 cm SSD</b>	<b>Total</b>
Number of dose points	80	80	80	240
Number of points meeting the criteria of DD < 2% or DTA < 2 mm	68	74	76	218
Percent of points meeting the criteria	85.0%	92.5%	95.0%	90.8%

Table 3.25: Summary of the analysis of the results based on the criteria of less than 2% or 2 mm for 15 MV x Open Fields.

<b>15 MV x Open Fields</b>	<b>85 cm SSD</b>	<b>100 cm SSD</b>	<b>120 cm SSD</b>	<b>Total</b>
Number of dose points	160	160	160	480
Number of points meeting the criteria of DD < 2% or DTA < 2 mm	147	160	159	466
Percent of points meeting the criteria	91.9%	100.0%	99.4%	97.1%

Table 3.26: Summary of the analysis of the results based on the criteria of less than 2% or 2 mm for 15 MV x EDW (15°) Fields.

<b>15 MV x EDW (15 degrees) Fields</b>	<b>85 cm SSD</b>	<b>100 cm SSD</b>	<b>120 cm SSD</b>	<b>Total</b>
Number of dose points	84	84	84	252
Number of points meeting the criteria of DD < 2% or DTA < 2 mm	81	84	84	249
Percent of points meeting the criteria	96.4%	100.0%	100.0%	98.8%

Table 3.27: Summary of the analysis of the results based on the criteria of less than 2% or 2 mm for 15 MV x EDW (60°) Fields.

<b>15 MV x EDW (60 degrees) Fields</b>	<b>85 cm SSD</b>	<b>100 cm SSD</b>	<b>120 cm SSD</b>	<b>Total</b>
Number of dose points	84	84	84	252
Number of points meeting the criteria of DD < 2% or DTA < 2 mm	79	84	84	247
Percent of points meeting the criteria	94.0%	100.0%	100.0%	98.0%

Table 3.28: Summary of the analysis of the results based on the criteria of less than 2% or 2 mm for 15 MV x PW (15°) Fields.

<b>15 MV x PW (15 degrees) Fields</b>	<b>85 cm SSD</b>	<b>100 cm SSD</b>	<b>120 cm SSD</b>	<b>Total</b>
Number of dose points	84	84	84	252
Number of points meeting the criteria of DD < 2% or DTA < 2 mm	84	84	83	251
Percent of points meeting the criteria	100.0%	100.0%	98.8%	99.6%

Table 3.29: Summary of the analysis of the results based on the criteria of less than 2% or 2 mm for 15 MV x for PW (30°) Fields.

<b>15 MV x PW (30 degrees) Fields</b>	<b>85 cm SSD</b>	<b>100 cm SSD</b>	<b>120 cm SSD</b>	<b>Total</b>
Number of dose points	84	84	84	252
Number of points meeting the criteria of DD < 2% or DTA < 2 mm	84	82	74	240
Percent of points meeting the criteria	100.0%	97.6%	88.1%	95.2%

Table 3.30: Summary of the analysis of the results based on the criteria of less than 2% or 2 mm for 15 MV x PW (45°) Fields.

<b>15 MV x PW (45 degrees) Fields</b>	<b>85 cm SSD</b>	<b>100 cm SSD</b>	<b>120 cm SSD</b>	<b>Total</b>
Number of dose points	84	84	84	252
Number of points meeting the criteria of DD < 2% or DTA < 2 mm	84	83	79	246
Percent of points meeting the criteria	100.0%	98.8%	94.0%	97.6%

Table 3.31: Summary of the analysis of the results based on the criteria of less than 2% or 2 mm for 15 MV x PW (60°) Fields.

<b>15 MV x PW (60 degrees) Fields</b>	<b>85 cm SSD</b>	<b>100 cm SSD</b>	<b>120 cm SSD</b>	<b>Total</b>
Number of dose points	72	72	72	216
Number of points meeting the criteria of DD < 2% or DTA < 2 mm	72	72	70	214
Percent of points meeting the criteria	100.0%	100.0%	97.2%	99.1%

Table 3.32: Summary of the analysis of the results based on the criteria of less than 2% or 2 mm for 15 MV x Block Tray Fields.

<b>15 MV x Block Tray Fields</b>	<b>85 cm SSD</b>	<b>100 cm SSD</b>	<b>120 cm SSD</b>	<b>Total</b>
Number of dose points	96	96	96	288
Number of points meeting the criteria of DD < 2% or DTA < 2 mm	60	89	95	244
Percent of points meeting the criteria	62.5%	92.7%	99.0%	84.7%

As shown in Tables 3.17 to 3.32 most of the points not meeting the criteria are for open fields, fields with block tray, fields with physical wedges of 15 degree and 30 degree and for fields with shorter SSDs. It is also interesting to note the match for 15 MV beams is better than 6 MV beams for majority of these points. As pointed out earlier the modeling in Pinnacle<sup>3</sup> was based on the measurements done using a cylindrical chamber (Model IC 15: radius of 3 mm, outer diameter of 6.8 mm and active volume of 0.13 cm<sup>3</sup>), which is thought to be not a suitable chamber for these measurements in the buildup region. Remodeling of the electron contamination was required based on the measurements using the Attix pp ion chamber.

After the remodeling of the electron contamination models (EC models) in P3 using the new buildup dose measurements (i.e., buildup dose measurements performed using the Attix pp ion chamber), buildup dose calculations were again performed using P3. Buildup dose calculations

were performed for all clinical setups for which measurement were performed with the exception of clinical setups involving block tray. The auto modeling feature in P3 used to remodel the EC models. Relative dose graphs of calculated (after EC models remodeling) and experimentally measured buildup doses were again plotted (588 RD graphs, i.e., 294 pairs). The deviations between the calculated and measured buildup doses were also analyzed in the same manner as was done before the remodeling of EC models. After the EC remodeling, the mean absolute dose difference between Attix chamber measured and Pinnacle<sup>3</sup> calculated buildup dose values was  $2.0\% \pm 3.4\%$  (1SD) for the 6 MV photon beam and  $1.5 \pm 2.4\%$  (1SD) for the 15 MV photon beam as compared to absolute dose differences of  $6.3\% \pm 11.9\%$  (1SD) and  $2.6 \pm 4.1\%$  (1SD) for the 6 MV and 15 MV photon beams, respectively before the remodeling of the EC models. Some of the RD graphs plotted are as shown in Figures 3.33 to 3.50. Tables 3.33 to 3.46 show summaries of the analysis based on the criteria of less than 2% or 2 mm.

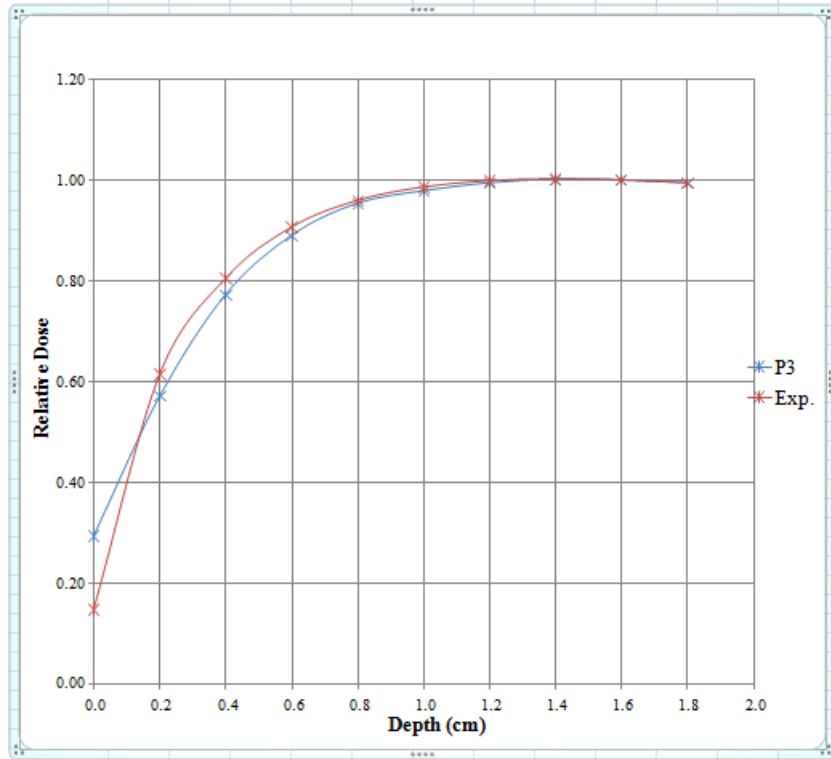


Figure 3.33: RD graphs for 6 MV x 85 cm SSD x Open Field (10 x 10 cm<sup>2</sup> FS) after EC remodeling.

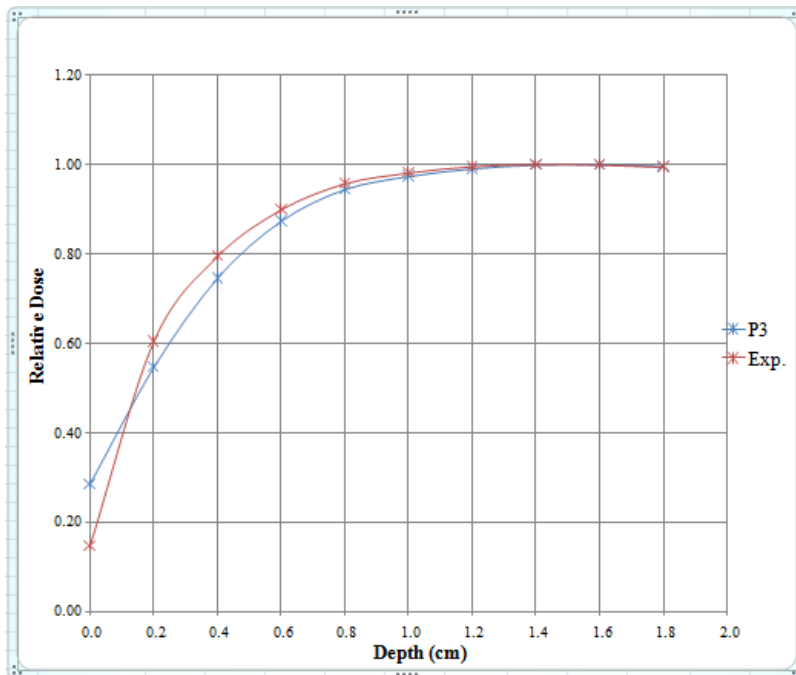


Figure 3.34: RD graphs for 6 MV x 100 cm SSD x Open Field (10 x 10 cm<sup>2</sup> FS) after EC remodeling.

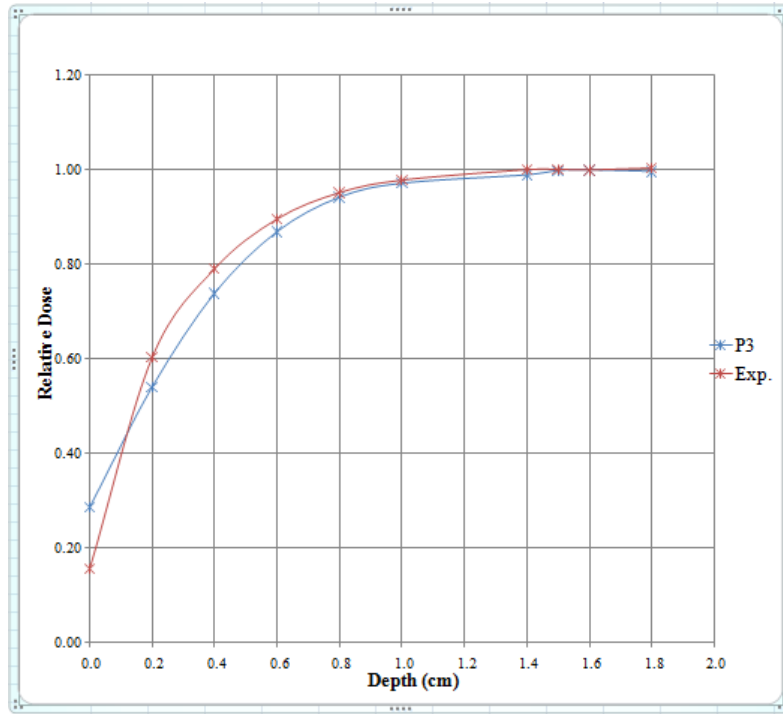


Figure 3.35: RD graphs for 6 MV x 120 cm SSD x Open Field (10 x 10 cm<sup>2</sup> FS) after EC remodeling.

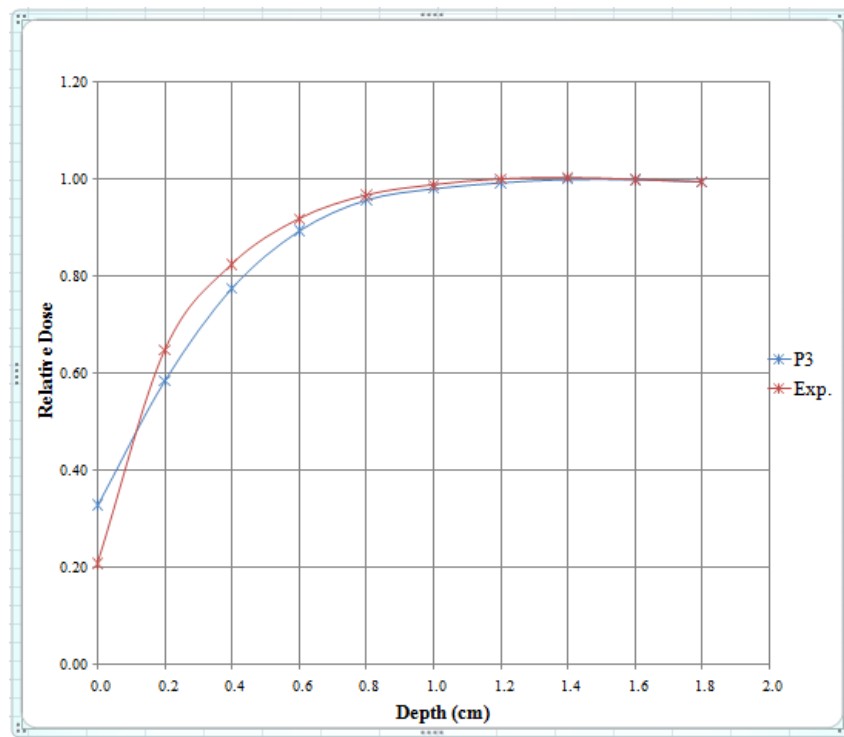


Figure 3.36: RD graphs for 6 MV x 100 cm SSD x EDW (15°) Field (15 x 15 cm<sup>2</sup> FS) after EC remodeling.

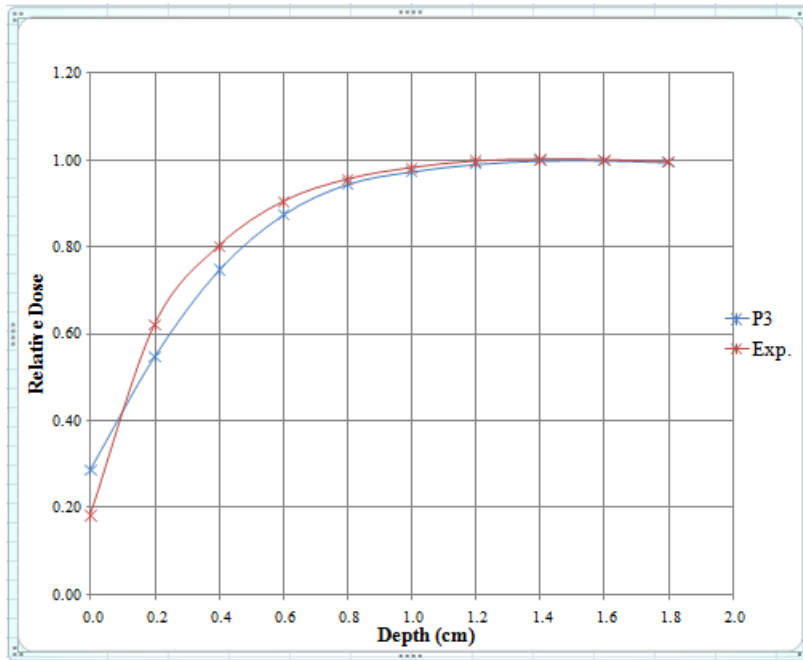


Figure 3.37: RD graphs for 6 MV x 100 cm SSD x EDW (60°) Field (10 x 10 cm<sup>2</sup> FS) after EC remodeling.

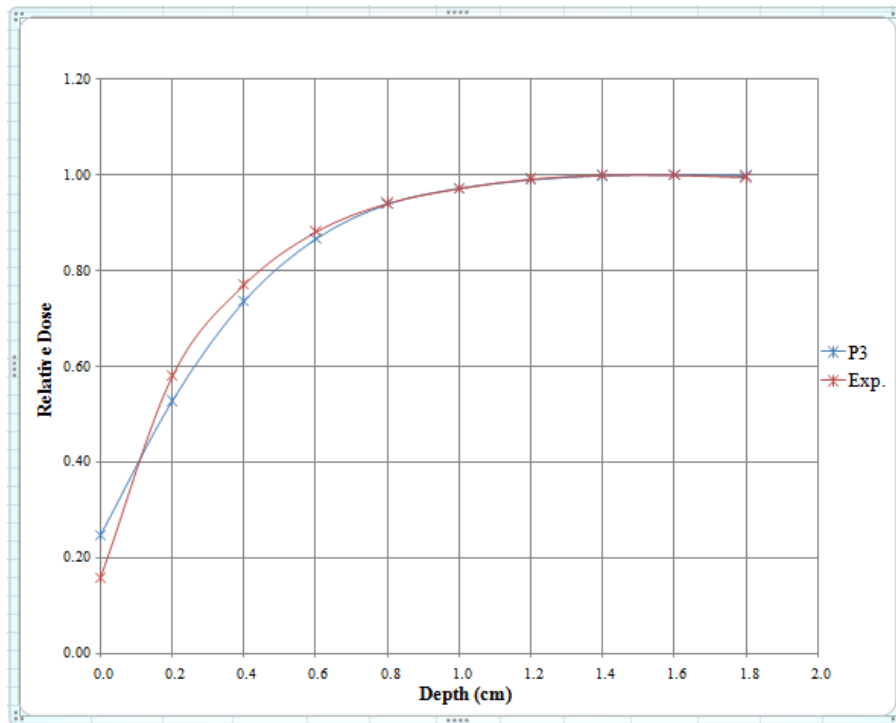


Figure 3.38: RD graphs for 6 MV x 100 cm SSD x PW (15°) Field (10 x 10 cm<sup>2</sup> FS) after EC remodeling.

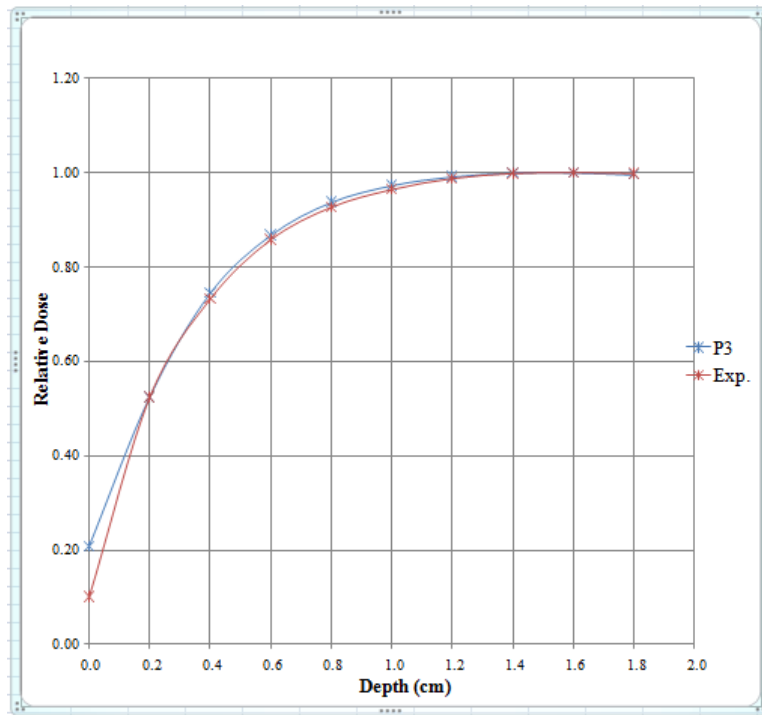


Figure 3.39: RD graphs for 6 MV x 100 cm SSD x PW (30°) Field (5 x 5 cm<sup>2</sup> FS) after EC remodeling.

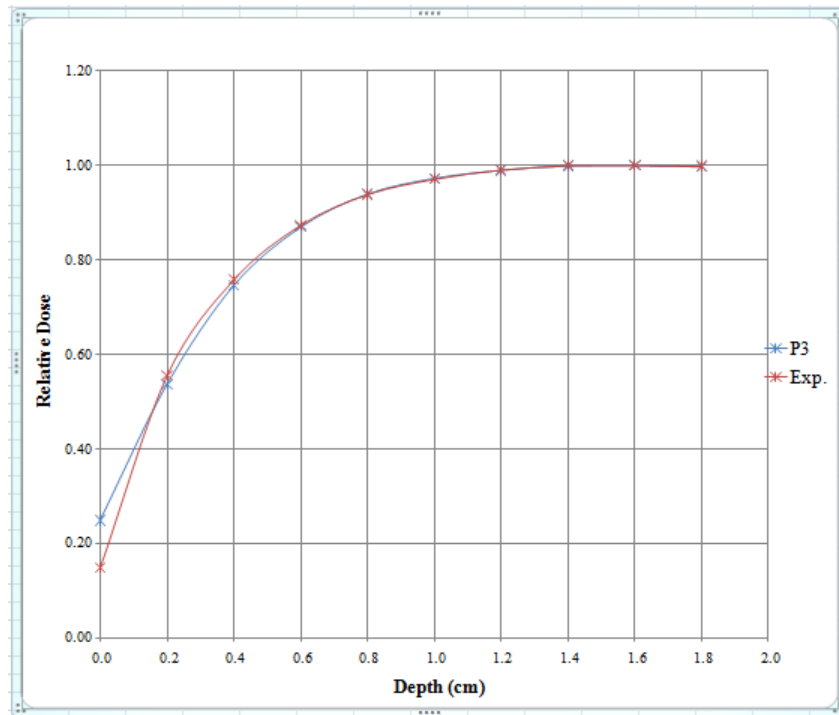


Figure 3.40: RD graphs for 6 MV x 100 cm SSD x PW (45°) Field (12 x 12 cm<sup>2</sup> FS) after EC remodeling.

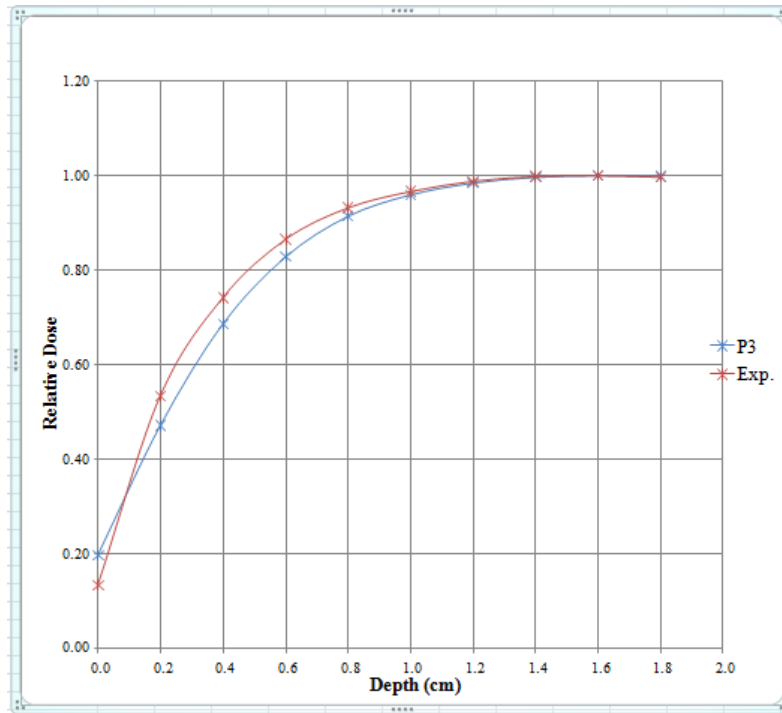


Figure 3.41: RD graphs for 6 MV x 100 cm SSD x PW (60°) Field (10 x 10 cm<sup>2</sup> FS) after EC remodeling.

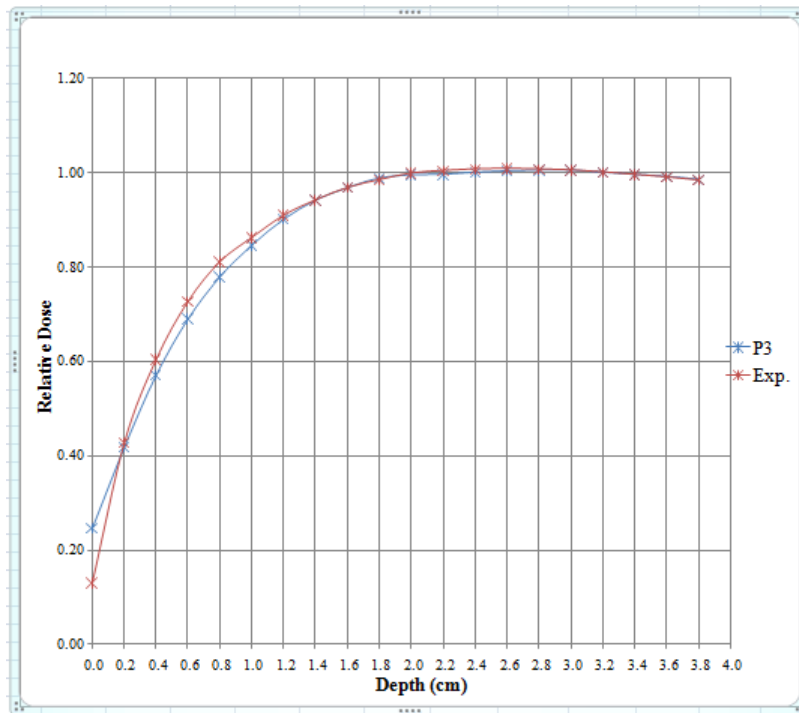


Figure 3.42: RD graphs for 15 MV x 85 cm SSD x Open Field (10 x 10 cm<sup>2</sup> FS) after EC remodeling.

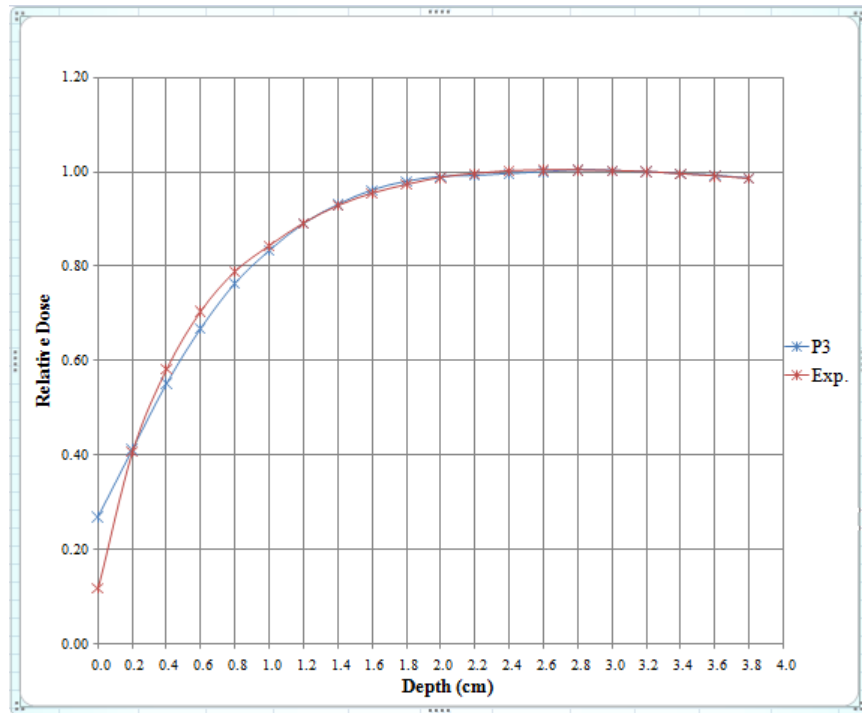


Figure 3.43: RD graphs for 15 MV x 100 cm SSD x Open Field (10 x 10 cm<sup>2</sup> FS) after EC remodeling.

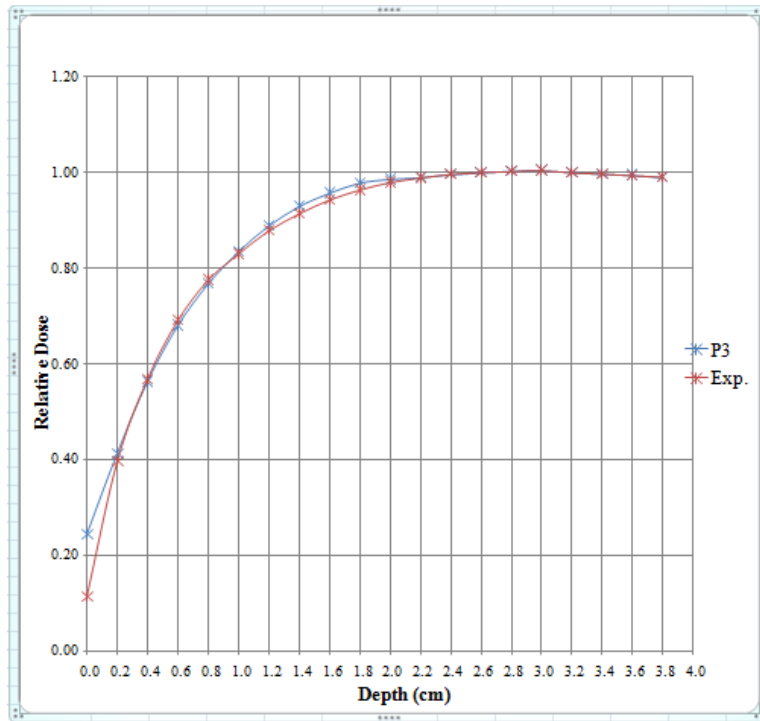


Figure 3.44: RD graphs for 15 MV x 120 cm SSD x Open Field (10 x 10 cm<sup>2</sup> FS) after EC remodeling.

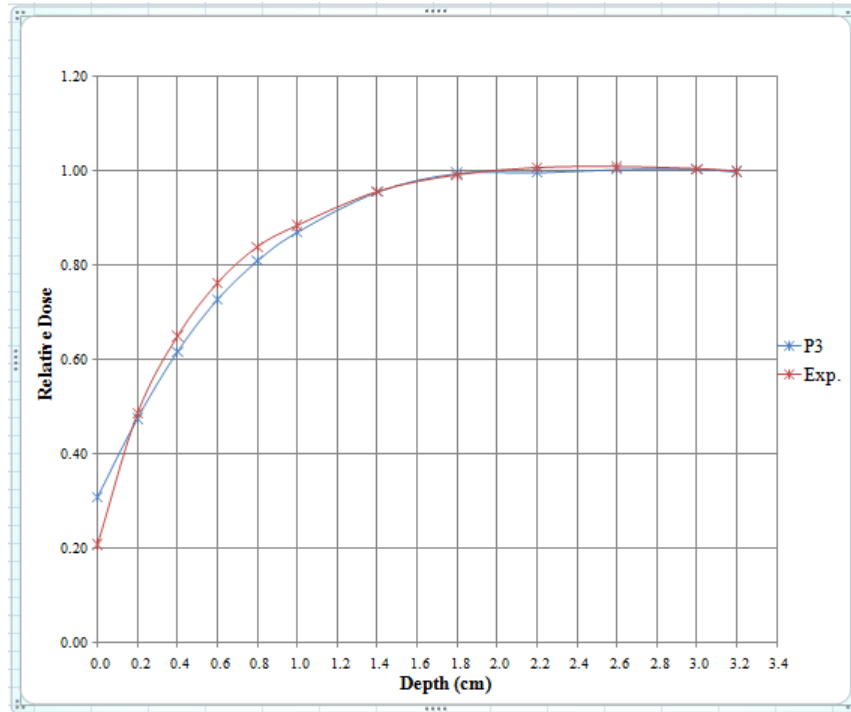


Figure 3.45: RD graphs for 15 MV x 100 cm SSD x EDW (15°) Field (15 x 15 cm<sup>2</sup> FS) after EC remodeling.

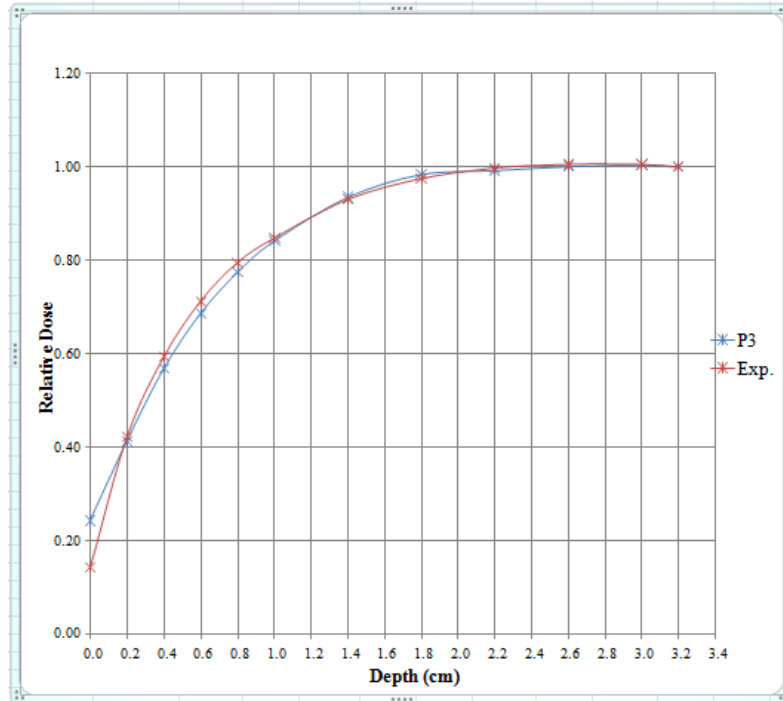


Figure 3.46: RD graphs for 15 MV x 100 cm SSD x EDW (60°) Field (10 x 10 cm<sup>2</sup> FS) after EC remodeling.

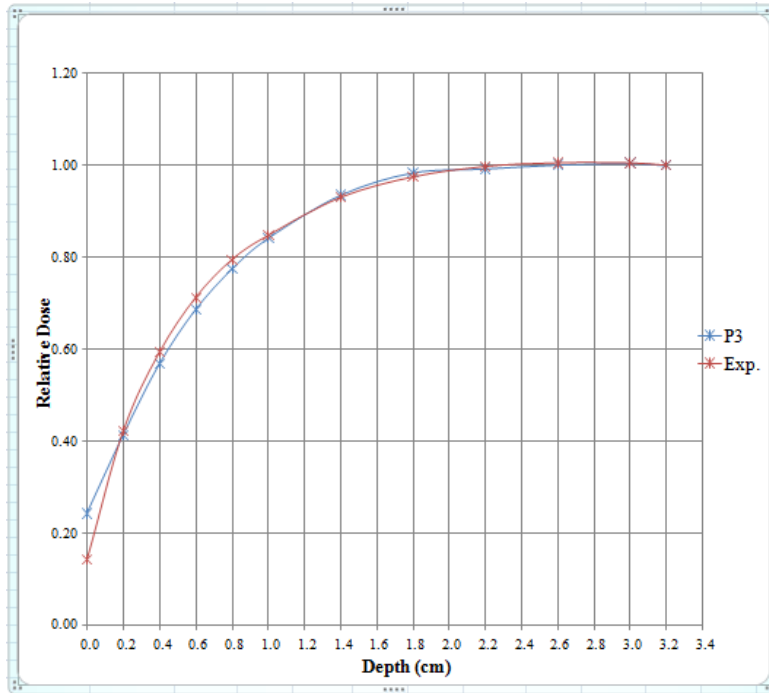


Figure 3.47: RD graphs for 15 MV x 100 cm SSD x PW (15°) Field (10 x 10 cm<sup>2</sup> FS) after EC remodeling.

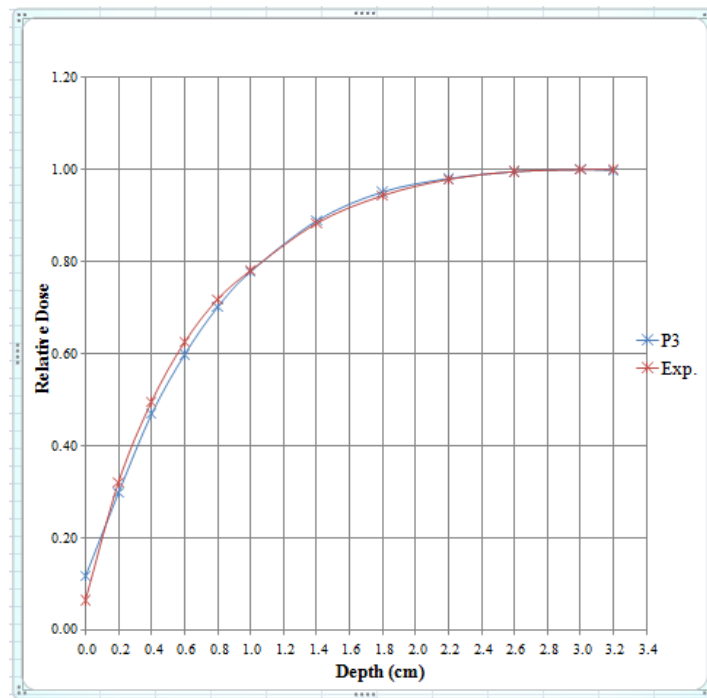


Figure 3.48: RD graphs for 15 MV x 100 cm SSD x PW (30°) Field (5 x 5 cm<sup>2</sup> FS) after EC remodeling.

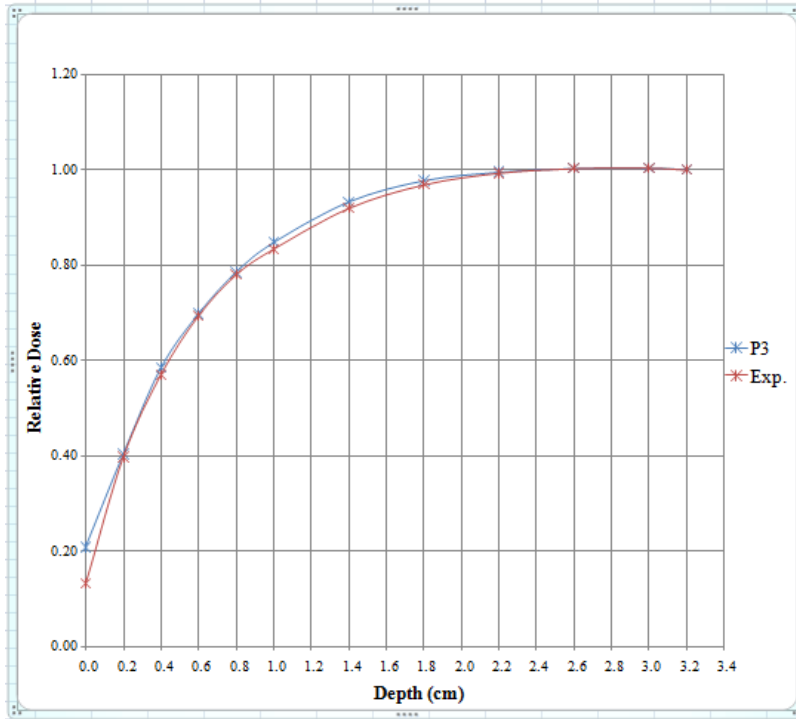


Figure 3.49: RD graphs for 15 MV x 100 cm SSD x PW (45°) Field (12 x 12 cm<sup>2</sup> FS) after EC remodeling.

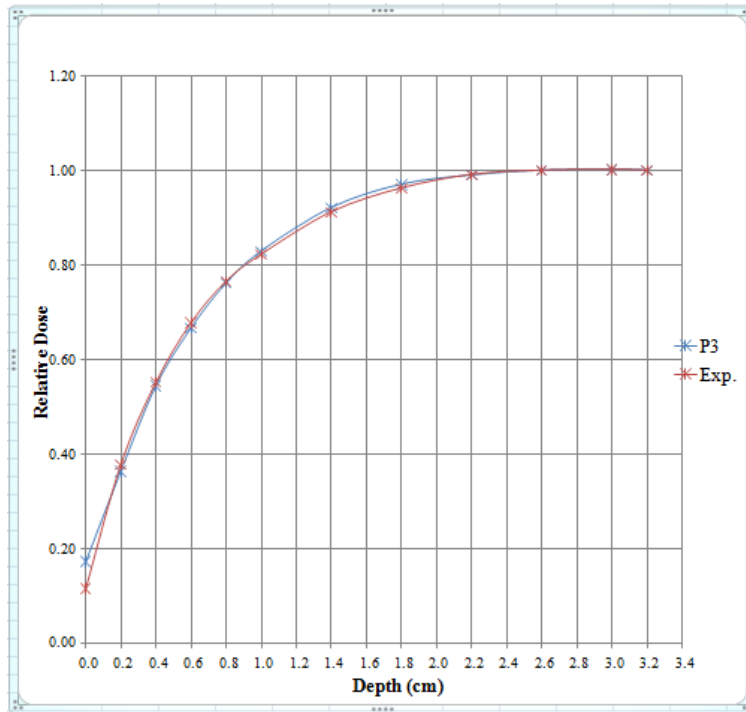


Figure 3.50: RD graphs for 15 MV x 100 cm SSD x PW (60°) Field (10 x 10 cm<sup>2</sup> FS) after EC remodeling.

Table 3.33: Summary of the analysis of the results based on the criteria of less than 2% or 2 mm for 6 MV x Open Fields after EC remodeling.

<b>6 MV x Open Fields</b>	<b>85 cm SSD</b>	<b>100 cm SSD</b>	<b>120 cm SSD</b>	<b>Total</b>
Number of dose points	80	80	80	240
Number of points meeting the criteria of DD < 2% or DTA < 2 mm	80	80	80	240
Percent of points meeting the criteria	100.0%	100.0%	100.0%	100.0%

Table 3.34: Summary of the analysis of the results based on the criteria of less than 2% or 2 mm for 6 MV x EDW (15°) Fields after EC remodeling.

<b>6 MV x EDW (15 degrees) Fields</b>	<b>85 cm SSD</b>	<b>100 cm SSD</b>	<b>120 cm SSD</b>	<b>Total</b>
Number of dose points	70	70	70	210
Number of points meeting the criteria of DD < 2% or DTA < 2 mm	70	70	70	210
Percent of points meeting the criteria	100.0%	100.0%	100.0%	100.0%

Table 3.35: Summary of the analysis of the results based on the criteria of less than 2% or 2 mm for 6 MV x EDW (60°) Fields after EC remodeling.

<b>6 MV x EDW (60 degrees) Fields</b>	<b>85 cm SSD</b>	<b>100 cm SSD</b>	<b>120 cm SSD</b>	<b>Total</b>
Number of dose points	70	70	70	210
Number of points meeting the criteria of DD < 2% or DTA < 2 mm	70	70	70	210
Percent of points meeting the criteria	100.0%	100.0%	100.0%	100.0%

Table 3.36: Summary of the analysis of the results based on the criteria of less than 2% or 2 mm for 6 MV x PW (15°) Fields after EC remodeling.

<b>6 MV x PW (15 degrees) Fields</b>	<b>85 cm SSD</b>	<b>100 cm SSD</b>	<b>120 cm SSD</b>	<b>Total</b>
Number of dose points	70	70	70	210
Number of points meeting the criteria of DD < 2% or DTA < 2 mm	70	70	70	210
Percent of points meeting the criteria	100.0%	100.0%	100.0%	100.0%

Table 3.37: Summary of the analysis of the results based on the criteria of less than 2% or 2 mm for 6 MV x for PW (30°) Fields after EC remodeling.

<b>6 MV x PW (30 degrees) Fields</b>	<b>85 cm SSD</b>	<b>100 cm SSD</b>	<b>120 cm SSD</b>	<b>Total</b>
Number of dose points	70	70	70	210
Number of points meeting the criteria of DD < 2% or DTA < 2 mm	70	70	70	210
Percent of points meeting the criteria	100.0%	100.0%	100.0%	100.0%

Table 3.38: Summary of the analysis of the results based on the criteria of less than 2% or 2 mm for 6 MV x PW (45°) Fields after EC remodeling.

<b>6 MV x PW (45 degrees) Fields</b>	<b>85 cm SSD</b>	<b>100 cm SSD</b>	<b>120 cm SSD</b>	<b>Total</b>
Number of dose points	70	70	70	210
Number of points meeting the criteria of DD < 2% or DTA < 2 mm	70	70	70	210
Percent of points meeting the criteria	100.0%	100.0%	100.0%	100.0%

Table 3.39: Summary of the analysis of the results based on the criteria of less than 2% or 2 mm for 6 MV x PW (60°) Fields after EC remodeling.

<b>6 MV x PW (60 degrees) Fields</b>	<b>85 cm SSD</b>	<b>100 cm SSD</b>	<b>120 cm SSD</b>	<b>Total</b>
Number of dose points	60	60	60	180
Number of points meeting the criteria of DD < 2% or DTA < 2 mm	60	60	60	180
Percent of points meeting the criteria	100.0%	100.0%	100.0%	100.0%

Table 3.40: Summary of the analysis of the results based on the criteria of less than 2% or 2 mm for 15 MV x Open Fields after EC remodeling.

<b>15 MV x Open Fields</b>	<b>85 cm SSD</b>	<b>100 cm SSD</b>	<b>120 cm SSD</b>	<b>Total</b>
Number of dose points	160	160	160	480
Number of points meeting the criteria of DD < 2% or DTA < 2 mm	160	160	157	477
Percent of points meeting the criteria	100.0%	100.0%	98.1%	99.4%

Table 3.41: Summary of the analysis of the results based on the criteria of less than 2% or 2 mm for 15 MV x EDW (15°) Fields after EC remodeling.

<b>15 MV x EDW (15 degrees) Fields</b>	<b>85 cm SSD</b>	<b>100 cm SSD</b>	<b>120 cm SSD</b>	<b>Total</b>
Number of dose points	84	84	84	252
Number of points meeting the criteria of DD < 2% or DTA < 2 mm	84	84	84	252
Percent of points meeting the criteria	100.0%	100.0%	100.0%	100.0%

Table 3.42: Summary of the analysis of the results based on the criteria of less than 2% or 2 mm for 15 MV x EDW (60°) Fields after EC remodeling.

<b>15 MV x EDW (60 degrees) Fields</b>	<b>85 cm SSD</b>	<b>100 cm SSD</b>	<b>120 cm SSD</b>	<b>Total</b>
Number of dose points	84	84	84	252
Number of points meeting the criteria of DD < 2% or DTA < 2 mm	84	84	84	252
Percent of points meeting the criteria	100.0%	100.0%	100.0%	100.0%

Table 3.43: Summary of the analysis of the results based on the criteria of less than 2% or 2 mm for 15 MV x PW (15°) Fields after EC remodeling.

<b>15 MV x PW (15 degrees) Fields</b>	<b>85 cm SSD</b>	<b>100 cm SSD</b>	<b>120 cm SSD</b>	<b>Total</b>
Number of dose points	84	84	84	252
Number of points meeting the criteria of DD < 2% or DTA < 2 mm	83	80	84	247
Percent of points meeting the criteria	98.8%	95.2%	100.0%	98.0%

Table 3.44: Summary of the analysis of the results based on the criteria of less than 2% or 2 mm for 15 MV x for PW (30°) Fields after EC remodeling.

<b>15 MV x PW (30 degrees) Fields</b>	<b>85 cm SSD</b>	<b>100 cm SSD</b>	<b>120 cm SSD</b>	<b>Total</b>
Number of dose points	84	84	84	252
Number of points meeting the criteria of DD < 2% or DTA < 2 mm	84	84	84	252
Percent of points meeting the criteria	100.0%	100.0%	100.0%	100.0%

Table 3.45: Summary of the analysis of the results based on the criteria of less than 2% or 2 mm for 15 MV x PW (45°) Fields after EC remodeling.

<b>15 MV x PW (45 degrees) Fields</b>	<b>85 cm SSD</b>	<b>100 cm SSD</b>	<b>120 cm SSD</b>	<b>Total</b>
Number of dose points	84	84	84	252
Number of points meeting the criteria of DD < 2% or DTA < 2 mm	84	84	84	252
Percent of points meeting the criteria	100.0%	100.0%	100.0%	100.0%

Table 3.46: Summary of the analysis of the results based on the criteria of less than 2% or 2 mm for 15 MV x PW (60°) Fields after EC remodeling.

<b>15 MV x PW (60 degrees) Fields</b>	<b>85 cm SSD</b>	<b>100 cm SSD</b>	<b>120 cm SSD</b>	<b>Total</b>
Number of dose points	72	72	72	216
Number of points meeting the criteria of DD < 2% or DTA < 2 mm	72	72	72	216
Percent of points meeting the criteria	100.0%	100.0%	100.0%	100.0%

As summarized in Tables 3.47 to 3.50 that follow, majority of the points were meeting the criteria of less than 2% or 2 mm after remodeling the electron contamination for simple as well as complex geometries for both the beam energies.

Table 3.47: Comparison of the analysis of the results based on the criteria of less than 2% or 2 mm for 6 MV photon beam (simple geometry) before and after EC remodeling.

<b>6 MV Photon Beam: Simple Geometry</b>	<b>Before EC Remodeling</b>	<b>After EC Remodeling</b>
Number of dose points	240	240
Number of points meeting the criteria of DD < 2% or DTA < 2 mm	224	240
Percent of points meeting the criteria	93.3%	100.0%

Table 3.48: Comparison of the analysis of the results based on the criteria of less than 2% or 2 mm for 6 MV photon beam (complex geometries) before and after EC remodeling.

<b>6 MV Photon Beam: Complex Geometries</b>	<b>Before EC Remodeling</b>	<b>After EC Remodeling</b>
Number of dose points	1,470	1,230
Number of points meeting the criteria of DD < 2% or DTA < 2 mm	1,379	1,230
Percent of points meeting the criteria	93.8%	100.0%

Table 3.49: Comparison of the analysis of the results based on the criteria of less than 2% or 2 mm for 15 MV photon beam (simple geometry) before and after EC remodeling.

<b>15 MV Photon Beam: Simple Geometry</b>	<b>Before EC Remodeling</b>	<b>After EC Remodeling</b>
Number of dose points	480	480
Number of points meeting the criteria of DD < 2% or DTA < 2 mm	466	477
Percent of points meeting the criteria	97.1%	99.4%

Table 3.50: Comparison of the analysis of the results based on the criteria of less than 2% or 2 mm for 15 MV photon beam (complex geometries) before and after EC remodeling.

<b>15 MV Photon Beam: Complex Geometries</b>	<b>Before EC Remodeling</b>	<b>After EC Remodeling</b>
Number of dose points	1,764	1,476
Number of points meeting the criteria of DD < 2% or DTA < 2 mm	1,691	1,471
Percent of points meeting the criteria	95.9%	99.7%

### 3.2 Discussions

For the validation measurements using GafChromic EBT 2 film, a total of 230 and 276 buildup dose measurements, performed using Attix ion PP chamber and EBT 2 film, for 6 MV and 15 MV photon beams, respectively were compared. For the 6 MV photon beam, the mean absolute difference was  $1.4\% \pm 1.5\%$  (1SD) while for 15 MV photon beam the mean absolute

difference was  $1.1\% \pm 1.0\%$  (1SD). This indicates that the buildup dose measurements performed using Attix pp ion chamber and EBT 2 film were in good agreement. This provided good confidence in the measurements using Attix pp ion chamber.

As shown in the results most of the points of measurements made using the Attix Chamber and the modeling based on the measurements using cylindrical ion chamber, not meeting the criteria are for open fields, fields with block tray, fields with physical wedges of 15 degrees and 30 degrees and for fields with shorter SSDs. This may be due the fact that the electron contamination is high for open fields. The block trays made out of low atomic number material are known to enhance the electron contamination of high energy x-ray beams. The physical wedges of 15 degrees and 30 degrees are made out of steel while the 45 degrees and 60 degrees physical wedges are made out of lead. Again the wedges made out of low atomic number material (steel) are producing more electron contamination.

As noted earlier, and as can be seen in Figures 3.13 to 3.32, the agreement between experimentally measured build up doses using Attix pp ion chamber and those calculated by P3 (before EC models remodeling) for the 15 MV photon beam is better than that of the 6 MV photon beam, especially at the surface of the phantom (0 cm depth). Also as pointed out earlier, the modeling in Pinnacle<sup>3</sup> was based on the measurements done using cylindrical chamber (Model IC 15: radius of 3 mm, outer diameter of 6.8 mm and active volume of  $0.13 \text{ cm}^3$ ), which is thought to be not a suitable chamber for these measurements in the buildup region. The thought of cylindrical chamber as not being suitable for measurements in the buildup region may be attributed to the uncertainty on the location of its effective point of measurement and the large

fluence perturbation correction required, when used in phantom (Plaetsen et al., 1994), and its overestimation of dose in the buildup region, without the application of special correction, because of its relative large volume (Zhu, 1999). On the other hand, one of the primary advantages of parallel plate ionization chambers, of which the Attix pp ion chamber is an example, is their good depth resolution, making them well suited for measurements in the high dose gradient regions or in situations where the uncertainty in the point of measurements must be minimized (Buckley & Rogers, 2006). Also, fixed-parallel plate ion chambers with the design criterion of  $w/s \geq 25$ , where  $w$  and  $s$  are the wall diameter and plate separation of the parallel plate ion chamber respectively, are considered suitable for measurements of dose in the buildup region without the need for correction factors to account for the overestimation of dose due to secondary electrons scattered into the chamber volume from the wall of the chamber; Attix pp ion chamber design criterion exceeds this as it has a  $w/s$  of 40.

The reason for the close match between Attix pp ion chamber surface dose measurements and those of P3 calculations for the 15 MV photon beams, as compared to that of the 6 MV photon beam, may be attributed to the facts that: cylindrical chambers overestimate surface and buildup dose more than fixed parallel plate ion chambers; surface dose decreases with an increase in the energy of the photon beam because as the beam energy increases, scattered electrons are more forward peaked and are less likely to add to the dose in the ionization chamber active volume (Parsai et al., 2008). The match between Attix pp ion chamber surface dose measurements and those of P3 calculations for the 6 MV photon beam was greatly improved after EC models in P3 were remodeled using Attix pp ion chamber measured data. In the research conducted by Parsai et al. (2008), surface and buildup doses of photon beams simulated using the BEAM/EGS4

Monte Carlo code system were compared with those measured using extrapolation, parallel plate, and cylindrical ionization chamber. They recommended that surface and buildup dose measured data using fixed parallel plate chamber or extrapolation chamber should be used in the buildup region in a treatment planning system as all other available chamber types tend to over-estimate the values by more than 50%.

## Chapter 4

### Conclusions

The buildup region dose calculation for the Pinnacle<sup>3</sup> (version 9.0), a commercial treatment planning system, commissioned and in use at the Saskatoon Cancer Center, has been experimentally verified using the Attix parallel plate ionization chamber. The modeling in Pinnacle<sup>3</sup>, which is based on measurements made using cylindrical ionization chamber, lead to large discrepancies in dose in the buildup region; this may support the thought that cylindrical ionization chamber is not suitable for measurements in the buildup region. The discrepancies between measured and calculated buildup doses that did not meet the criteria of less than 2% or 2 mm were mostly for open fields, block tray fields, fields with physical wedges of 15 degrees and 30 degrees and for fields with shorter source-to-surface distances. This is attributed to the high electron contamination associated with these fields.

An interesting result of close match of modeling based on cylindrical ionization chamber with the Attix parallel plate ionization chamber measurements for the 15 MV photon beam need more investigations to ensure this is indeed the case. This could be true as pointed out by some other authors (Parsai et al., 2008) that as the beam energy increases, the high energy scattered electrons produced are more forward peaked and thus, cause less perturbations.

As shown by the good agreement between measurements using Attix parallel plate ionization chamber and calculations by Pinnacle<sup>3</sup> after the remodeling of the Electron contamination models using Attix parallel plate ionization chamber measurements, the Electron Contamination

equation used by Pinnacle<sup>3</sup> treatment planning system seems to be adequate for modeling of electron contamination in the buildup dose region for a variety of clinical setups.

The disagreement between Attix parallel plate chamber and GafChromic EBT 2 buildup dose measurements was less than 3% for 89.9% of the buildup dose values compared. This is an indication that Attix parallel plate ionization chamber buildup dose measurements were in good agreement with those of Gafchromic EBT 2 film, and hence its suitability for measurements in the buildup region. It is recommended to use good parallel plate ionization chamber, such as Attix parallel plate ionization chamber, for measurements in the buildup region.

## References

- AAPM Task Group 21 (1983). A protocol for the determination of absorbed dose from high-energy photon and electron beams. American association of physicists in medicine. *Med. Phys.*, 10(6), 741-771.
- Adams, E. J., & Hounsell, A. R. (1995). Changes to dose in the build-up region when using multi-leaf collimators in place of lead blocks supported on an accessory tray. *Radiother. Oncol.*, 37, 225-229.
- Ahnesjö, A. (1989). Collapsed cone convolution of radiant energy for photon dose calculation in heterogeneous media. *Med. Phys.*, 16(4), 577-592.
- Andrés, C., del Castillo, A., Tortosa, R., & Alonso, D. (2010). A comprehensive study of the Gafchromic EBT 2 radiochromic film. A comparison with EBT. *Med. Phys.*, 37(12), 6271-6278.
- Animesh. (2005). Advantages of multiple algorithm support in treatment planning system for external beam dose calculations. *J. Cancer Res. Ther.*, 1(1), 12-20.
- Arjomandy, B., Tailor, R., Anand, A., Sahoo, N., Gillin, M., Prado, K. & Vicic, M. (2010). Energy dependence and dose response of Gafchromic EBT2 film over a wide range of photon, electron, and proton beam energies. *Med. Phys.*, 37(5), 1942-1947.
- Bäck, S. Å. J., Magnusson, P., Olsson, L. E., Montelius, A., Fransson, A., & Mattsson, S. (1998). Verification of single beam treatment planning using a ferrous dosimeter Gel and MRI (FeMRI). *Acta Oncologica* 37 (6), 561-566.
- Baird, C. T., Starkschall, G., Liu, H. H., Buchholz, T. A., & Hogstrom, K. R. (2001). Verification of tangential breast treatment dose calculations in a commercial 3D treatment planning system. *J. Appl. Clin. Med. Phys.*, 2(2), 73-84.
- Bedford, J. L, Childs, P. J., Hansen, V. N., Mosleh-Shirazi, M. A. Verhaegen, F., & Warrington, A. P. (2003). Commissioning and quality assurance of Pinnacle<sup>3</sup> radiotherapy treatment planning system for external beam photons. *Br. J. Radiol.*, 76, 163-176.
- Bentel, G. C. (1996). *Radiation Therapy Planning* (2nd ed). McGraw-Hill.
- Buckley, L. A., and Rogers, D. W. O. (2006). Wall correction factors, Pwall, for parallel-plate ionization chambers. *Med. Phys.*, 33(6), 1788-1796.
- Buston, M. J., Cheung, T., Yu, P. K. N., & Alnawaf, H. (2009). Dose and absorption spectra response of EBT 2 Gafchromic film to high energy x-rays. *Australian Physical and Engineering Sciences in Medicine*, 32(4), 196-202.
- Cadman, P., McNutt, T., & Bzdusek, K. (2005). Validation of physics improvement for IMRT with a commercial treatment-planning system. *J. Appl. Clin. Med. Phys.* 6(2), 74-86.
- Court, L. E., Tishler, R. B., Allen, A. M., Xiang, H., Makrigiorgos, M., & Chin, L. (2008). Experimental evaluation of the accuracy of skin dose calculation for a commercial treatment planning system. *J. Appl. Clin. Med. Phys.*, 9(1), 29-35.
- Desroches, J., Bouchard, H., & Lacroix, F. (2010). Technical Note: Potential errors in optical density measurements due to scanning side in EBT and EBT2 Gafchromic film dosimetry. *Med. Phys.*, 37(4), 1565-1570.
- Fontanarosa, D., Orlandini, L. C., Andriani, I., & Bernardi L. (2009). Commissioning Varian enhanced dynamic wedge in the PINNACLE treatment planning system using Gafchromic<sup>TM</sup> EBT film. *Med. Phys.*, 36(10), 4504-4510.

- Fraass, B., Doppke, K., Hunt, M., Kutcher, G., Starkschall, G., Stern, R., & Dyke, J. V. (1998). American association of physicists in medicine radiation therapy committee task group 53: Quality assurance for clinical radiotherapy treatment planning. *Med. Phys.*, 25(10), 1773-1829.
- Gerbi, B. J. (1993). The response characteristics of a newly designed plane-parallel ionization chamber in high-energy photon and electron beams. *Med. Phys.*, 20(5), 1411-1415.
- Gerbi, B. J. & Khan, F. M. (1987). The polarity effect of commercially available plane-parallel ionization chambers. *Med. Phys.*, 14(2), 210-215.
- Gerbi, B. J. & Khan, F. M. (1990). Measurement of dose in the buildup region using fixed-separation plane-parallel ionization chambers. *Med. Phys.*, 17(1), 17-26.
- Gerbi, B. J. & Khan F. M. (1997). Plane-parallel ionization chamber response in the buildup region of obliquely incident photon beams. *Med. Phys.*, 24(6), 873-878.
- Gershkevitsh, E., Schmidt, R., Velez, G., Miller, D., Korf, E., Yip, F., Wanwilairat, S., & Vatnitsky, S. (2009). Dosimetric verification of radiotherapy treatment planning systems: Results of IAEA pilot study. *Radiother. Oncol.*, 89, 338-346.
- Guan, Y., Zhou, L., Zhen, X., Lu, W., & Zhang, S. (2010). Dosimetric verification of collapsed cone convolution algorithm in heterogeneous media. *Bioinformatics and Biomedical Engineering*, 1(4), 18-20.
- Harms, W. B., Sr., Low, D. A., Wong, J. W., & Purdy, J. A. (1998). A software tool for the quantitative evaluation of 3D dose calculation algorithms. *Med. Phys.*, 25(10), 1830-1836.
- Hartmann, B., Martišíková, M., & Jäkel, O. (2010). Technical Note: Homogeneity of Gafchromic EBT2<sup>®</sup> film. *Med. Phys.*, 37(4), 1753-1756.
- Hasenbalg, F., Neuenschwander, H., Mini, R., & Born, E. J. (2007). Collapsed cone convolution and analytical anisotropic algorithm dose calculations compared to VMC++ Monte Carlo simulations in clinical cases. *Phys. Med. Biol.*, 52, 3679-3691.
- Hsu, S. H., Moran, J. M., Chen, Y., Kulasekere, R., & Roberson, P. L. (2010). Dose discrepancies in the buildup region and their impact on dose calculations for IMRT fields. *Med. Phys.* 37(5), 2043-2053.
- IAEA Technical Report Series no. 430: *Commissioning and quality assurance of computerized planning systems for radiation treatment of cancer*. (2004). International Atomic Energy Agency.
- IAEA Technical Document 1540: *Specification and acceptance testing of radiotherapy treatment planning systems*. (2007). International Atomic Energy Agency.
- ISP (2009a). EBT 2 White Paper. International Specialty Products.  
[http://online1.ispcorp.com/\\_layouts/Gafchromic/content/products/](http://online1.ispcorp.com/_layouts/Gafchromic/content/products/)
- ISP (2009b) GAFCHROMIC EBT 2 User Protocol. International Specialty Products.  
[http://online1.ispcorp.com/\\_layouts/Gafchromic/content/products/](http://online1.ispcorp.com/_layouts/Gafchromic/content/products/)
- Jayaraman, S. & Lanzl, L. (2004). *Clinical Radiotherapy Physics*. (2nd ed.). Springer-Verlag Berlin Heidelberg.
- Khan, F. M. (2010). *The Physics of Radiation Therapy* (4th ed.). Wolters Kluwer/Lippincott Williams & Wilkins.
- Lindsay, P., Rink, A., Ruschin, M., & Jaffray, D. (2010). Investigation of energy dependence of EBT and EBT-2 Gafchromic film. *Med. Phys.*, 37(2), 571-576.
- Low, D. A., Harms, W. B., Mutic, S., & Purdy, J. A. (1998). A technique for the quantitative evaluation of dose distributions. *Med. Phys.*, 25(5), 656-661.

- Lydon, J. M. (1998). Photon dose calculations in homogenous media for a treatment planning system using a collapsed cone superposition convolution algorithm. *Phys. Med. Biol.* 43, 1813-1822.
- Malhotra, H. K., Deshpande, D. D., & Salvi, S. V. (1997). Surface dose measurements using parallel plate markus chamber for  $^{60}\text{Co}$ , 6 and 10 MV photon beams. *J. Med. Phys.*, 22(4) 169-194.
- Martišiková, M., Ackermann, B., & Jäkel, O. (2008). Analysis of uncertainties in Gafchromic EBT<sup>®</sup> film dosimetry of photon beams. *Phys. Med. Biol.* 53, 7013-7027.
- Nilsson, B. & Montelius, A. (1986). Fluence perturbation in photon beams under nonequilibrium conditions. *Med. Phys.*, 13(2), 191-195.
- O'Shea, E. & McCavana, P. (2003). Review of surface dose detectors in radiotherapy. *J. Radiother. Prac.*, 3(2), 69-76.
- Paelinck, L., Wagter, C. D., Esch, A. V., Duthoy, W., Depuydt, T., & Neve, W. D. (2005). Comparison of build-up dose between Elekta and Varian linear accelerators for high-energy photon beams using radiochromic film and clinical implications for IMRT head and neck treatments. *Phys. Med. Biol.*, 50, 413-428.
- Panettieri, V., Barsoum, P., Westermark, M., Brualla, L., & Lax, I. (2009). AAA and PBC calculation accuracy in the surface build-up region in tangential beam treatments. Phantom and breast case study with the Monte Carlo code PENELOPE. *Radiother. Oncol.*, 93, 94-101.
- Parsai, E. I., Shvydka, D., Pearson, D., Gopalakrishnan, M., and Feldmeier, J. J. (2008). Surface and build-up region dose analysis for clinical radiotherapy photon beams. *Appl. Radiat. Isot.* 66, 1438-1442.
- Plaetsen, A. V., Seuntjens, J., and Thierens, H. (1994). Verification of absorbed doses determined with thimble and parallel-plate ionization chambers in clinical electron beams using ferrous sulphate dosimetry. *Med. Phys.*, 21(1), 37- 44.
- Podgorsak, E. (2005). *Radiation Oncology Physics: A Handbook for Teachers And Students*. International Atomic Energy Agency.
- Ramsey, C. R., Cordrey, I. L., Spencer, K. M., & Oliver, A. L. (1999). Dosimetric verification of two commercially available three-dimensional treatment planning systems using TG 23 test package. *Med. Phys.*, 26(7), 1188-1195.
- Rawlinson, J. A., Arlen, D., & Newcombe, D. (1992). Design of parallel plate ion chambers for buildup measurements in megavoltage photon beams. *Med. Phys.*, 19(3), 641-648.
- Richley, L., John, A. C., Coomber, H., & Fletcher, S. (2010). Evaluation and optimization of the new EBT2 radiochromic film dosimetry system for patient dose verification in radiotherapy. *Phys. Med. Biol.*, 55, 2601-2617.
- Roland, T. F., Stathakis, S., Ramer, R., & Papanikolaou, N. (2008). Measurements and comparison of skin dose for prostate and head-and-neck patients treated on various IMRT delivery systems. *Appl. Radiat. Isot.* 66, 1844-1849.
- Sankar, A., Kurup, P. G. G., Murali, V., Ayyangar, K. M., Nehru, R. M., & Velmurugan, J. (2006). Evaluation of gafchromic EBT film for intensity modulated radiation therapy dose distribution verification. *J. Med. Phys.*, 31(2), 78-82.
- Shih, R., Li, X. A., & Chu, J. C. H. (2000, July). Dynamic wedge versus physical wedge: a Monte Carlo study. In *Proceedings of the 22<sup>nd</sup> Annual Engineering in Medicine and Biology Society International Conference, Chicago* (p. 1676-1678).

- Shimono, T., Koshida, K., Nambu, H., Matsubara, K., Takahashi, H., & Okuda, H. (2009). Polarity effect in commercial ionization chambers used in photon beams with small fields. *Radiol. Phys. Technol.*, 2, 97-103.
- Starkschall, G., Steadham, R. E., Popple, R. A., Ahmad, S., & Rosene, I. I. (2000). Beam-commissioning methodology for a three-dimensional convolution/superposition photon dose algorithm. *J. Appl. Clin. Med. Phys.* 1(1), 8-27.
- Tannous, N. B. J., Gagnon, W. F., & Almond, P. R. (1981). Buildup region and skin-dose measurements for the Therac 6 Linear Accelerator for radiation therapy. *Med. Phys.*, 8(3), 378-381.
- Todorovic, M., Fischer, M., Cremers, F., Thom, E., & Schmidt, R. (2006). Evaluation of GafChromic EBT prototype B for external beam dose verification. *Med. Phys.*, 33(5), 1321-1328.
- Venselaar, J. & Welleweerd, H. (2001). Application of a test package in an intercomparison of the photon dose calculation performance of treatment planning systems used in a clinical setting. *Radiother. Oncol.*, 60, 203-213.
- Venselaar, J., Welleweerd, H., & Mijnheer, B. (2001). Tolerances for the accuracy of photon beam dose calculations of treatment planning systems. *Radiother. Oncol.*, 60, 191-201.
- Weber, L. & Nilsson, P. (2002). Verification of dose calculations with a clinical treatment planning system based on a point kernel dose engine. *J. Appl. Clin. Med. Phys.*, 3(2), 73-87(2002).
- Wickman, G. & Holmström, T. (1992). Polarity effect in plane-parallel ionization chambers using air or a dielectric liquid as ionization medium. *Med. Phys.*, 19(3), 637-640.
- Yokoyama, S., Roberson, P. L., Litzenberg, D. W., Moran, J. M., & Fraass, A. B. (2004). Surface buildup dose dependence on photon field delivery technique for IMRT. *J. Appl. Clin. Med. Phys.*, 5(2), 71-81.
- Zhu, C. T. (1999, July). *Dosimetric Pitfalls for Relative Dosimetry in Electron Disequilibrium Region*. American association of physicists in medicine refresher course. [www.aapm.org/meetings/99AM/pdf/2816-18115.pdf](http://www.aapm.org/meetings/99AM/pdf/2816-18115.pdf)
- Zhu, J. (2005). Generation of wedge-shaped dose distributions through dynamic multileaf collimator dose delivery. *J. Appl. Clin. Med. Phys.*, 6(3), 37-45.